NACA RM L52E26

NACA

RESEARCH MEMORANDUM

INVESTIGATION OF INTERFERENCE LIFT, DRAG, AND PITCHING MOMENT OF A SERIES OF RECTANGULAR WING AND BODY COMBINATIONS AT MACH NUMBERS OF 1.62, 1.93, AND 2.41

By Donald E. Coletti

Langley Aeronautical Laboratory
Langley Field, Va.

NATIONAL ADVISORY COMMITTEE
FOR AERONAUTICS
WASHINGTON

August 13, 1952
Declassified February 26, 1958

NATIONAL ADVISORY COMMITTEE FOR AERONAUTICS

RESEARCH MEMORANDUM

INVESTIGATION OF INTERFERENCE LIFT, DRAG, AND PITCHING MOMENT OF A SERIES OF RECTANGULAR WING AND BODY COMBINATIONS AT MACH NUMBERS OF 1.62, 1.93, AND 2.41

By Donald E. Coletti

SUMMARY

An investigation was made of a series of rectangular wing and body combinations at Mach numbers 1.62, 1.93, and 2.41 to determine the effects of aspect ratio, incidence angle, and forebody length on the interference lift, drag, and pitching moment. Also, a limited investigation was made to determine the effect of Reynolds number on the wings in the presence of the body.

The models consisted of a series of 6-percent biconvex circular-arc rectangular wings of aspect ratio 2, 3, and 4 with incidence angles of approximately 0° and 3° on bodies of fineness ratio 9.13 and 10.27.

The results of the investigation indicated no effect of forebody length on the interference quantities. The values of interference lift, pitching moment, and drag were found to be functions of both Mach number and aspect ratio. In addition, Reynolds number was found to have appreciable effect upon the wings in the presence of the body. The method of Tucker gave the best prediction of the interference lift on the wing due to the body. A modified slender-body theory was in favorable agreement with the experimental lift of the wing in the presence of the body at the higher Reynolds numbers at all Mach numbers. The methods of Tucker and of Nielsen and Kaattari gave good predictions of the experimental lift on the body due to the wing.

INTRODUCTION

For some time it has been realized that the interference between a wing and body may be of such magnitude that it would have considerable

effect on the aerodynamic characteristics of supersonic aircraft and missiles. Consequently, a great deal of effort is being devoted both to obtaining experimental information on this interference and to the development of theoretical methods which will predict its magnitude reliably.

Numerous analytical approaches have been made towards the solution of the problem (refs. 1 to 14). One of the first attempts to make an approximation of wing-body interference was made by Spreiter (ref. 1). On the assumption that the wing-body combination to be very slender and of very low aspect ratio, the flow was approximated by considering it to be two dimensional in planes perpendicular to the body center line. The high-aspect-ratio problem was considered by Ferrari (ref. 3), who devised an iteration procedure for solving it. First-order approximations of the pressure field acting on the wing were obtained by assuming the wing to be acting in the field of the body alone. By assuming the body to be acting in the field of the wing alone, the pressure field acting on the body was approximated. Continuing the calculations beyond the first approximation becomes increasingly long and difficult. Lagerstrom and Graham (ref. 8) used the slender-body theory of Spreiter as a basis for applying corrections for both planar and nonplanar systems. The corrections for these systems were "estimated from considerations of planar systems where exact linearized solutions exist and from a general theorem about low-aspect-ratio configurations." Nielsen, Katzen, and Tang (ref. 12) also used slender-body theory as a basis for applying corrections to nonslender wings of wing-body combinations. They have shown that the ratio of the lift of the wing-body combination to that of the "wing alone" is accurately predicted by slender-body theory. This method is limited to triangular wing-body combinations. However, Nielsen and Kaattari (ref. 13) extended this method to include other wing plan forms. In addition to this, a prediction of the interference lift on the body due to the wing was obtained by the use of several simplifying assumptions as to the process by which the lift is carried over from the wing onto the body. In reference 14, Tucker presents an approximate method for obtaining the lift components of wing-body combinations for rectangular and triangular wings. The principal assumption is that the body is flat and the various components of lift may be calculated by standard linearized theory methods. Some experimental work has been performed in obtaining interference characteristics (refs. 15 to 19); however, a portion of the work was somewhat isolated in that it was done for the purpose of correlation with a particular theory.

The purpose of the present investigation was to provide force data from tests of a systematic series of rectangular wing-body configurations over a range of supersonic Mach numbers in order to assess the various theoretical estimates and to determine the relative importance of various interference quantities. This test program investigated at Mach numbers

of 1.62, 1.93, and 2.41 the interference effects of configurations consisting of wings with aspect ratio 2, 3, and 4 at incidence angles of approximately 0° and 3° using two different forebody lengths. In addition, an investigation was made on the wings in the presence of the body at the three Mach numbers over a range of Reynolds numbers.

SYMBOLS

A aspect ratio, b/c

α angle of attack of body

b total wing span

c wing chord

C_L lift coefficient, Lift/qS

C_D drag coefficient, Drag/qS

C_m pitching-moment coefficient about 50-percent chord, Moment/qSc

C_X longitudinal force coefficient for total wing in presence of body, X/qS

$C_{L_\alpha} = \frac{dC_L}{d\alpha}$ at $C_L = 0$

$C_{L_i} = \frac{dC_L}{di}$ at $C_L = 0$

$C_{m_\alpha} = \frac{dC_m}{d\alpha}$ at $C_L = 0$

d body diameter

i angle of wing incidence

L total body length

M Mach number

n fineness ratio, L/d_{max}

q	dynamic pressure, $\rho V^2/2$
ρ	stream density
R	Reynolds number, $\rho V c/\mu$
S	total wing area including portion submerged in body
t	maximum wing thickness
t/c	thickness ratio
X	longitudinal force, positive rearward
x	longitudinal coordinate from nose of body
μ	coefficient of viscosity
A.C.	aerodynamic-center position relative to 50-percent chord, positive forward

Subscripts:

min	minimum
max	maximum

Configuration identification:

Direct measurements

B	body alone
W	total wing alone
W_e	exposed wing alone excluding portion submerged in body
WB	total wing and body in combination
W(B)	total wing in the presence of the body

Derived measurements

b(w)	interference on body due to wing = WB - [W(B) + B]
w(b)	interference on wing due to body = W(B) - W_e

APPARATUS AND TESTS

Tunnel.- The Langley 9-inch supersonic tunnel is a closed-throat, single-return, continuous operating tunnel in which the test section is approximately 9 inches square. The Mach number may be changed by means of removable two-dimensional nozzle blocks which form the top and bottom walls of the test section. The pressure and humidity can be controlled at all times during the tunnel operation.

Models.- The basic models consisted of a body having interchangeable noses to give fineness ratio of 9.13 and 10.27 and a series of biconvex circular-arc rectangular wings having design aspect ratio of 2, 3, and 4 with each aspect ratio consisting of two wings with two incidence angles (approximately 0° and 3°). Table I gives the body coordinates and wing-shape parameters. A sketch of the models is shown in figure 1.

A change from one model configuration to another is readily provided as illustrated in figure 2. The wing was mounted on a three-component strain-gage balance located in a hollow chamber of the body. A cover, forming the outside body surface, was placed over the balance and the rectangular center section of the wing. Two rectangular slots, 180° apart, were cut through the body shell to accommodate the wing. An average gap of about 0.007 inch was maintained around the wing in the slot to prevent fouling.

Internal balance.- The internal strain-gage balance was designed to obtain the lift, drag, and pitching-moment of any type wing in the presence of the body. The balance was comprised of three strain-gage beams, the wing carriage, and the flexure pivots. (See figs. 1 and 2.) Each beam had four strain-gage grids mounted near the point of maximum bending moment of the beam. The beams were then wired into a full bridge circuit independently of one another. The forces were indicated by an SR-4 indicator. The summation of the forces of the two beams labeled L_1 and L_2 (fig. 1) obtained the normal force, and the beam labeled D obtained the longitudinal force in the direction of the body axis. The pitching moment was obtained by resolving the forces of L_1, L_2, and D about the reference point of the wing. In order to minimize the interaction between the normal and longitudinal forces, the flexure pivots were made as thin as possible - in fact, no interaction was detected on the normal-force beam due to a longitudinal force. However, a longitudinal force was detected due to a normal force. This one-way interaction was found to be a small percentage of the total force and was taken into account in the final calibration. Preliminary tests made with pressure outlets installed at various positions in the balance chamber indicated no pressure gradients in the chamber between $\pm 6^{\circ}$ angle of attack with the 0.007-inch gap. Calibration was made of the small temperature effects in the balance and account of these effects was made in the data.

External balance.- The lift, drag, and pitching-moment of the wing-body combination, of the two bodies alone, and of the wings alone were obtained by an external balance system. The configurations were sting-mounted to a system of self-balancing beam scales. A windshield was used to cover the sting so that all unnecessary external forces could be eliminated. For a more detailed description of the windshield in relation to the body, see reference 20. The nose of the windshield was made flush with the rear of the body, and the pressure within was adjusted to free-stream static pressure. Consequently, all the data presented are for the case of zero base drag. For the case of the wings alone, a special sting and windshield were required. The sting was rectangular in shape and very small in proportion to the wing size. Other geometric parameters between the sting and windshield plus effects due to tare may be found in reference 21.

Tests, general.- Tests were conducted at Mach numbers of 1.62, 1.93, and 2.41. Measurements were made of lift, drag, and pitching moment about the wing 50-percent chord for the wings alone, bodies alone, wings in the presence of the bodies, and the wing-body combinations. Reynolds numbers of the tests based on the wing chord are 0.46×10^6 at $M = 1.62$; 0.42×10^6, and $M = 1.93$; 0.33×10^6 and at $M = 2.41$. A limited series of tests were made with the internal balance to obtain the forces on the wings in the presence of the body at Reynolds numbers of 1.05×10^6 and 1.40×10^6 at $M = 1.62$; 1.28×10^6 at $M = 1.93$; 1.02×10^6 at $M = 2.41$. The angle of attack of each configuration was indicated on a scale, graduated in degrees, by means of a light reflected from a small mirror mounted flush on the rear of the body and on the sting in the case of the wing alone. The range of angle of attack was approximately $\pm 6^\circ$.

Throughout the tests, the dew point in the tunnel was maintained at a level where condensation effects would be negligible.

PRECISION OF DATA

The precision of the various quantities involved in the testing is listed in table II. The estimated uncertainties in a given quantity obtained from the strain-gage balance were combined by the method which follows from the theory of least squares outlined in reference 22. For the case where the precision varies with the lift, the accuracy was determined at the approximate end of linearity of the lift. The uncertainties of both the strain-gage and scale data are presented as averages of all wings and bodies since there was a random variation of inaccuracies due to varying wing plan form, body length, Mach number, and Reynolds number. As stated previously, the pressure at the base of the model was

held approximately at the free-stream static pressure. The maximum difference encountered between the two pressures gave an error of ±0.0002 in C_D. This inaccuracy was a part of the total uncertainty given in table II.

The inaccuracy of the slopes of the lift and pitching-moment curves for all the configurations is approximately ±0.0002. By use of the theory of least squares, the precision of the interference lift and pitching-moment curve slopes on the body due to the wing, b(w), is ±0.00035. The resulting precision of the aerodynamic center is ±11 percent. The interference drag is ±0.0012. The precision of the interference lift and pitching-moment curve slopes on the wing due to the body, w(b), is ±0.00028 and for the aerodynamic center it is ±13 percent. The precision of the interference drag is ±0.0012.

The incidence angles of the wings were obtained from repeated measurements at various spanwise positions on all the wings. The inaccuracy in the measurement of these wings was of a random nature and the total uncertainty was evaluated by using the theory of least squares. A special test was made to determine whether the angle of attack of the wing in the presence of the body changed relative to the body when the forces increased with increasing angles of attack. This angle was indicated by means of a small mirror mounted flush in the wing. It was found that the relative angle increased to a maximum of 0.02° at 7° body angle of attack. This effect was believed to be negligible; therefore, no correction was applied to the data.

The accuracy of stream Mach number represents a maximum variation about a mean Mach number throughout the test section.

PRESENTATION OF DATA

In figures 3 to 33, the aerodynamic characteristics C_L, C_D, C_X, and C_m of the wings alone, bodies alone, wings and bodies in combination, and wings in the presence of the bodies are presented as a function of angle of attack. All the coefficients are based on the total wing area of the particular configuration. The Reynolds number is equal to 0.46×10^6 for the data in figures 3 to 11, 0.42×10^6 in figures 12 to 20, and 0.33×10^6 in figures 21 to 29. The Reynolds numbers for the data in figures 30 to 33 are given on those figures.

In the discussion, all of the wings will be referred to by the design aspect ratio and nominal incidence angles of 0° and 3° rather than by the actual values (see table I) for reasons of brevity; however, the actual values were used in all of the plotting and data reduction.

It will be noted that several of the configurations were not tested at all three Mach numbers. This was due primarily to lack of time since the major part of the test program was to be completed before repowering of the tunnel. The 9-inch supersonic wind tunnel originally had only sufficient power to obtain a maximum Reynolds number corresponding to a stagnation pressure of approximately 30 inches of mercury. The repowered tunnel is capable of attaining a Reynolds number equivalent to 120 inches of mercury stagnation pressure. In addition, considerable difficulty was encountered in achieving satisfactory operation of the internal balance, resulting in a decrease of the allotted time for testing. It was thus decided that where no major differences could be detected in the lift and moment curve slopes due to varying incidence angle and forebody length, a portion of the test program would be eliminated. The moment data for the wings at $M = 1.93$ and $M = 2.41$ were obtained but were in error from undetermined causes; consequently, these results are not presented but are estimated indirectly. The data for the curve of C_D against α at $M = 1.62$ for the rectangular wing of $i \approx 3^{\circ}$ on the short body were incorrect and are therefore not included in figure 11.

With the above omissions, it was necessary in some cases to extrapolate for the necessary values in order to obtain the interference effects. This procedure will be covered in more detail under the Discussion of Results.

The aerodynamic characteristics for the wings in the presence of the body in figures 30 to 33 were obtained after the tunnel was repowered, at which time no external balance was available. These results were obtained at higher Reynolds numbers than those used in figures 3 to 29. Sufficient data were not obtained for the evaluation of interference quantities; however these results will be used for a comparison with those of like configurations.

DISCUSSION OF RESULTS

Wing Lift, General

A comparison between the theoretical and experimental values of the lift-curve slopes at $\alpha = 0^{\circ}$ of the rectangular wings alone is given in figure 34. Since the wings of aspect ratio 2, 3, and 4 were not tested at $M = 1.62$, the curves were extrapolated to that Mach number as represented by the dashed lines. It is believed that the values of the lift-curve slopes at $M = 1.62$ arrived at in this manner are sufficiently accurate to be used in obtaining the interference quantities. Indications are that the theoretical predictions are slightly high, possibly because of the low Reynolds numbers of these tests.

To determine the effect the body has on the lift of a wing, a comparison is made between the exposed wing alone and the exposed wing in the presence of the body due to varying incidence angle. The exposed wing alone, W_e, is defined herein as that portion of the wing outside the body, and its characteristics are those of a wing of reduced aspect ratio made by putting the two exposed halves together. This configuration is in contrast to the total wing alone, which includes that portion of the wing enclosed by the body. In figures 35, 36, and 37 are shown the incremental lift-curve slopes of the exposed rectangular wings in the presence of the body due to varying the incidence angle as a function of the angle of attack at the three Mach numbers. All of the values, except those at $\alpha = 0^{\circ}$, were obtained from the faired curves of lift coefficient, and the symbols are used merely to distinguish between the two body lengths. The incremental lift-curve slope at a given angle of attack was obtained as the difference of the lift coefficients for the two incidence angles divided by the difference of the incidence angles. It should be mentioned here that the incidence angles of the wings were changed by "rotating" about the 50-percent-chord point. Also included on these figures are the theoretical lift-curve slopes of the exposed wings alone obtained from the theory shown in figure 34. The effect of interference is the difference between the values of the exposed wing alone lift-curve slope and that of the incremental lift-curve slope. This loss in lift, shown by the incremental lift-curve slopes, is due to the effective wing area being reduced at the wing-body juncture. Furthermore, it can be assumed that identical body upwash prevails at the small incidence angles at any given angle of attack.

Also presented in figures 35, 36, and 37 are the theoretical estimates of the lifts of the wings in the presence of the body due to varying incidence angle obtained by Tucker in reference 14. In most instances, the agreement with the experimental results is excellent.

The exposed wing alone halves might also be considered to be mounted in free stream on two infinite reflection planes, one body diameter apart. Comparison of the experimental lift of the exposed wings alone with that of the exposed wings due to varying incidence angle (figs. 35, 36, and 37) as a function of both the Mach number and aspect ratio is shown in figure 38. Experimentally, the characteristics of the exposed wings alone were obtained from figure 34 in the same manner as were the theoretical estimates previously mentioned. Thus a true picture is obtained with the body at $\alpha = 0^{\circ}$ regarding the effect of the wing-root pressures bleeding over the body as compared to the case of a reflection plane at the wing root. It is seen that, as the Mach number and aspect ratio increase, the effect of the wing-root-pressure bleed-off decreases, particularly for increasing aspect ratio. Figure 39 shows that the region of influence behind the Mach line emanating from the root of the wing leading edge decreases as the Mach number increases. It may be said that

the region of influence behind this Mach line decreases in proportion with increasing Mach number and aspect ratio. As an example, the configuration of aspect ratio 2 has about 15 to 20 percent less lift than the same configuration assumed to have a reflection plane at the wing root; however, at aspect ratio 4, the lift reduction is almost negligible.

Basic Quantities for Interference Evaluation

Figures 40(a), (b), and (c) show, for the various aspect ratios, the variation of lift-curve slope, pitching-moment slope, and the minimum drag values with Mach number for the wing and body in combination WB, wing in the presence of the body W(B), body alone B, and the exposed wing alone W_e. A summary of these quantities is given in table III. The quantities are taken directly from the curves in figures 3 to 29, where no corrections have been made for the drag due to the variable wing thicknesses. Since the forebody length has negligible effect on the values of C_{L_α} and C_{m_α}, the average values for the two forebody lengths are presented. A similar situation exists for these parameters at the two incidence angles; therefore, the data were treated in the same manner. Since the direct measurement of pitching moment for the total wing alone was incorrect, an indirect method was used in obtaining these values. They were constructed from the interference value of the pitching moment for the wing in the presence of the body; however, a more detailed explanation will be given under the section dealing with interference quantities.

The drag correction given below was applied to all of the wing data in order to account for the small differences in thickness ratios (see table I). A value of $\frac{t}{c} = 0.06$ was selected as the correct thickness.

$$C_{D_{min(corrected)}} = \left[C_{D_{min(actual)}} - C_{D_{lam}}\right]\left(\frac{\left(\frac{t}{c}\right)_{correct}}{\left(\frac{t}{c}\right)_{actual}}\right)^2 + C_{D_{lam}} \tag{1}$$

The corrected values reduced the difference exhibited between the two incidence angles for both the wings of aspect ratio 2 and 3, so that an average curve could be drawn. For the aspect-ratio-4 wing, the situation required further examination. The correction reduced the differences but not sufficiently to allow average values to be substituted. Upon closer examination of the aspect-ratio-4 wing with a 3° incidence, the leading edge was found to be quite blunt in comparison with that of the other wings. It is believed that this condition could be the cause for the differences shown in figure 40(c). As for C_{L_α} and C_{m_α}, the

forebody length had no measurable effect on the $C_{D_{min}}$ values for the wing in the presence of the body.

Interference Quantities

General.- Included in figure 40 is a dashed curve representing the summation of the values for the wing in the presence of the body and the values for the body alone $\left(W(B) + B\right)$. The difference between this addition and the value for the wing-body combination WB is the interference on the body due to the wing b(w). In like manner, the interference on the wing due to the body, w(b), is the difference between the forces on the wing in the presence of the body, W(B), and on the exposed wing alone, W_e, in free stream.

A summation of the interference quantities for the body due to the wing, b(w), and the wing due to the body, w(b), is presented in figure 41 for all Mach numbers and aspect ratios. The values for the exposed wing alone were obtained indirectly (as explained in a previous section), the symbols for the values in figure 41(b) are used only to differentiate between the three curves. Since there was no effect of forebody length on the basic quantities, there is naturally no effect on the interference quantities. In figures 41(a) and (b), the values are again based on the total wing area, whereas in figures 41(c) and (d) the values are based on the maximum cross-sectional body area. Unless so stated, the following discussions pertain to the values based upon the total wing area.

Lift, b(w).- With reference to figure 39, it is seen that as both the Mach number and aspect ratio increase, the induced downwash on the body, created by the wing tip, would decrease as the region of influence is farther removed from the tips. If this were the case, the results of the interference lift of the body due to the wing would, when based upon a common reference area, show a decreasing spread between the curves in going from a low to a high aspect ratio, and the curves would tend to converge in going to the higher Mach numbers. As seen in figure 41(c), a slight convergence of the curves is noted, but the decreasing spread with increasing aspect ratio is not apparent. This result is probably due to the fact that the wing-tip-induced negative lift on the body is a small percentage of the total interference.

Presented in figure 42 is a comparison of theoretical estimates with the experimental values of the lift-curve slopes for the body due to the wing as a function of both aspect ratio and Mach number. Spreiter's slender-body theory (ref. 1) is not altogether applicable to the configurations under discussion; however, as was pointed out by Nielsen and Kaattari in reference 13, the ratio of the lift carried by the body of

the combination to the lift on the wing alone may be accurately predicted by slender-body theory. By applying the linear theory lift-curve slope of the exposed wing alone to this ratio, the lift on the body due to the wing is obtained and is presented as modified slender-body theory in figure 42. For the most part, the lift is overestimated by this theory.

Nielsen's and Kaattari's method for estimating this interference lift (represented by ref. 13) agrees very well with the experimental results at $M = 1.62$ and is in fair agreement at the higher Mach numbers. The method is inapplicable wherever the wing-tip cone intersects the body in the region of the wing-root chord; this occurs for the aspect-ratio-2 wing at Mach number 1.62 (see fig. 39). In obtaining the lift carry-over onto the body from the wing, this method makes use of assumptions in slender-body theory that the straight portion of a body develops no lift and that the interference lift is due primarily to lift carried over from the wing onto the body. The body is collapsed to a plane and the Mach helixes become Mach lines. Another assumption is that the lift from a point on the wing does not decrease as it is carried downstream within its Mach cone regardless of body cross section. The interference lift is obtained only in the region of the body bounded by the Mach lines emanating from the leading- and trailing-edge root-chord juncture. The theory does not take into account tip effects.

The method presented by Tucker (ref. 14) is seen to be in as good agreement with the experimental values as that of Nielsen and Kaattari. Tucker has broken the problem down into a superposition scheme proposed by Lagerstrom and Van Dyke (ref. 7). Assumptions are made that the body is replaced by a flat plate, and that the lift on the body is confined between the Mach lines emanating from the wing-root leading and trailing edges. The wing-body combination is represented by a source distribution, and the velocity potential is obtained in the various appropriate areas of the combination. By numerically integrating over the wing and over the body, the net lift on each component is obtained.

A model similar to the configurations of this report was tested by Moskowitz and Maslen (ref. 15). The model had a rectangular wing of aspect ratio 2.33 mounted on the cylindrical section of a body; however the ratio of wing chord to body diameter was 2 compared to 1.43 for the present tests. The ratio of body diameter to wing span was 0.214. The tests were made at a Mach number of 1.90 and consisted of detailed pressure measurements on both the wing and the body. By integrating the lifting pressures on the body in the region between the Mach planes emanating from the wing leading and trailing edges, a value of 0.006 was obtained for $C_{L_{\alpha_{b(w)}}}$, based on the total wing area. This did not take into account the tip effects. The value does not agree too well with the present data; however, by considering that this lift is a function

of the ratio of body diameter to wing span and βA, where $\beta = \sqrt{M^2 - 1}$, a value may be obtained that agrees favorably with that of the aspect-ratio-3 wing at Mach number 1.62.

Pitching moment, b(w).- Figure 41(a) shows that the interference pitching moment on the body due to the wing is a function of both Mach number and aspect ratio. With reference to the sketches of figure 39, the wing-root lift carry-over onto the body acts behind the midchord point, so that a negative pitching moment is obtained. The tip-induced negative lift would give a positive moment, but as was mentioned previously, this lift is perhaps a small percentage of the total interference lift and would be difficult to isolate unless a program varying afterbody length were undertaken. As the Mach number is increased, the lift carry-over moves rearward along the body, giving a larger pitching moment, as shown in figure 41(a). It is noticed in figure 39(c) that the nose shocks cross the tips of the aspect-ratio-4 wing. This fact was not discovered until completion of the tests and is the result of an error in body design. The effect of this phenomenon is believed to be negligible since no effect of forebody length could be found in the lift and moment curve slopes for the wing in the presence of the body.

Aerodynamic centers, b(w).- The combined effects of the two components of wing-induced body lift and their aerodynamic-center locations give the interference aerodynamic-center variation (fig. 41(a)). The location of the aerodynamic center of the lift on the body due to the wing moves back with both increasing aspect ratio and Mach number.

Drag, b(w).- The interference drag values were obtained in the same manner as those of the lift and moment. These variations with Mach number and aspect ratio are small. It appears quite clear that the differences in minimum drag as affected by forebody length both for the body-alone curves and the curves for the wing-body combination (fig. 40) are predominantly wave-drag effects. An approximation was made of the skin friction on the body of $n = 10.27$ with and without a wing. First, it is known that the boundary layer is laminar on the body alone at this Reynolds number. Also, it was assumed that the wave drag was constant regardless of the type of boundary layer, and that for the wing-body combination the boundary layer changed from laminar to turbulent at a station on the body coincident with the wing midchord. The results of this approximation for the increase in body drag due to increase in skin friction indicated, within the experimental accuracy of the drag measurements, that the interference effects of the wing upon the minimum body drag are predominantly skin-friction effects.

Lift, w(b).- The lift of the wing due to the body decreases with increasing Mach number, and aspect ratio appears to have little or no

effect. The latter result simply indicates that the body upwash effects on wing lift are predominantly confined to the wing-root sections.

Presented in figure 43 is a comparison of various theoretical estimates with the experimental values of the lift-curve slopes for the wing in the presence of the body, W(B), and of the interference lift-curve slopes for wing due to the body, w(b), as a function of both aspect ratio and Mach number. For comparison, theoretical estimates are included for the exposed wing alone (zero interference). Also shown are some effects of Reynolds number variation. It is seen that as the Reynolds number is increased for the case of the wing in the presence of the body at any one Mach number, the value of the lift-curve slope increases. The lower Reynolds numbers probably lead to more separation at the wing trailing edge and body juncture than would be the case for higher Reynolds numbers; consequently, the experimental incremental lift on the wing due to the body is reduced by a greater amount than would be the case for the isolated wing. It is further seen that as both the aspect ratio and Mach number increase, the values tend to converge. This convergence may be attributed to the root effects becoming a relatively decreasing part of the total lift.

The most common estimate of the lift of a straight wing mounted on a body of cylindrical or near-cylindrical section is made by assuming that the wing is in the upwash field generated by an infinite cylinder ahead of the wing. The lift of the wing is then summed over the span on the assumption that the local lift change is proportional to the local change in angle of attack at each spanwise station. Such an assumption yields the correct linear theory value only when the spanwise variation of angle of attack is linear. The result of such a calculation is shown by the upper solid curve, and it is apparent that the simple strip integration overestimates the effects of the presence of the body.

The dashed curve was obtained from a linear-theory calculation in which the cylindrical upwash was used, but spanwise gradients in angle of attack were accounted for. It was assumed in this case that the wing was mounted from a reflection plane at the body intersection and that the flow-angle distribution ahead of the wing was retained. Such a calculation gives the correct boundary condition at the intersection of the wing leading edge and body and out along the Mach line on the wing from this point. However, the pressures obtained are too high in the region of the trailing edge and body juncture. In other words, the pressures which would normally "bleed-off" around the body surface are restricted by the reflection plane. As seen from figure 43(a), at Mach number 1.62, the results of this calculation are identical with that of the simple strip integration. However, at a Mach number of 1.93, the linear theory gives a better answer but still too much interference lift.

The opposite extreme in boundary conditions is illustrated in the first step in Ferrari's iteration procedure in which the body is assumed to be replaced with a flat plate or a continuation of the wing, still with the spanwise angle-of-attack distribution ahead of the wing. This case gives pressures at the wing root which are too low by allowing complete "bleed off," so to speak; consequently, less interference lift is predicted than is actually the case. This is shown more clearly by comparing the experimental values of the lift of the wing due to the body with Ferrari's theory at the bottom of figure 43. The theoretical curves were obtained as the difference between the theoretical lift of the wing in the presence of the body and the theoretical lift of the exposed wing alone. It would be expected that in the limit of increasing chord for a given body diameter, Ferrari's first-step solution would be correct and that the reflection-plane boundary estimate would be correct in the limit of decreasing chord for a given body diameter. As the aspect ratio is increased indefinitely, both solutions should of course converge to a common curve as the root effects become a relatively small part of the total.

Also presented in figure 43 is the modified slender-body theory for the lifts of the wing in the presence of the body and the lifts on the wing due to the body. The same method of application of the theory was made here as was made for the lift on the body due to the wing (ref. 13). The prediction of the lift of the wing in the presence of the body by this method is in good agreement with the experimental results obtained at the higher Reynolds numbers at $M = 1.62$ and 1.93. Tucker's method (ref. 14) is in very good agreement with the experimental results of the lift on the wing due to the body at Mach numbers of 1.93 and 2.41. However, it should again be pointed out that the interference lift on the wing will probably be altered as the Reynolds number is increased because of reduced separation, thus, the agreement between experiment and the various theoretical estimates may be altered somewhat at still higher test Reynolds numbers.

Pitching moment and aerodynamic centers, $w(b)$.- The interference pitching moment and aerodynamic center on the wing due to the body are presented jointly in the following discussion since the pitching-moment values were obtained indirectly. It was necessary to resort to a somewhat roundabout method since the moment data for the exposed wing alone were found to be incorrect, as mentioned in connection with figure 40. Presented in figure 44 are the aerodynamic centers of the wings in the presence of the bodies due to varying angle of attack and varying incidence. It is seen that the values obtained by varying angle of attack alone are approximately the same as those obtained by varying angle of incidence. From this, the conclusion may be reached that the interference aerodynamic center of the lift of the wing due to the body is essentially the same as the aerodynamic center of the lift of the wing

in the presence of the body. From the above analogy, the interference pitching moment resulting from the interference lift of the wing due to the body is then obtained as the product of the aerodynamic center and the interference lift and is presented in figure 41(b) with the other interference quantities. The pitching moment of the exposed wing alone was then obtained as the difference of the wing in the presence of the body and the interference of the wing due to the body. This method for obtaining the pitching moment of the exposed wing alone is supported by unpublished test data from the 9-inch supersonic tunnel. Rectangular wings of aspect ratio approximately 2 were investigated and the pitching moments (known to be correct) agreed very well with the pitching moments obtained by the method described above. The interference aerodynamic center of the wing due to the body shown in figure 41(b) is, of course, the same as that in figure 44, but is added here in order that all of the interference quantities may be readily compared. Also presented in figure 44 are the theoretical aerodynamic centers of the exposed wings alone. The experimental centers are about 10 percent ahead of the theoretical centers.

Drag, w(b).- The drag of the wing due to the body (fig. 41(b)) indicates a thrusting force on the aspect ratio 2 and the zero incidence, aspect-ratio-4 wings; however, the accuracy constitutes about one-quarter of the maximum spread between all the curves. As a result the interference drag may be considered negligible for all wings except the aspect-ratio-2 wing. The thrusting interference shown by this wing may be due to the interference created at the wing-body juncture, since there is indication of a decreasing thrust as the aspect ratio increases. Also, it should be mentioned that the low Reynolds numbers of this portion of the tests probably led to more extensive separation at the wing trailing edge and body juncture than would be the case for high Reynolds numbers.

Contributions of the Basic and Interference Components

In order to assess the relative effects of each component on the complete configuration, all of the basic and interference components of lift, pitching moment, and drag are shown in figure 45 as a fraction of these totals. The individual components are then added graphically to one another rather than referenced to zero so that they can be separated and their effects indicated. Presented in parts (a), (b), and (c) are the fractional breakdowns of the various elements for the configurations involving the wings of aspect ratio 2, 3, and 4, respectively, and the body of fineness ratio 10.27. There was no change in the lift and pitching moment due to the different incidence angles for any one configuration. The minimum drag values for the various configurations of the body of fineness ratio 9.13 are plotted in figures 45(d), (e), and (f). The values of the lifts and pitching moments are the same for this reduced body length as for those of the longer body; consequently, they are not presented.

As seen in figure 45(a), about one-half of the total lift of the wing of aspect ratio 2 is contributed by the exposed wing alone. Adding the lift on the wing due to the body gives the lift of the wing in presence of the body. This interference lift constitutes about 8 percent of the total lift. The next lift increments are those for the body alone and the lift on the body due to the wing. It is seen that the interference lift on the body is about one-half the total body lift and constitutes about 20 percent of the total lift. In like manner the interference lift on the wing due to the body for the wings of aspect ratio 3 and 4 is about 10 percent of the total lift of the wing-body combination, whereas, the interference lift on the body due to the wing is approximately 12 percent.

The moment contribution of the various lift elements for the three wings (figs. 45(a), (b), and (c)) illustrates clearly that the lift on the body due to the wing acts well behind the midchord of the wing and is a function of both Mach number and aspect ratio. Both the exposed wing alone and the lift on the wing in presence of the body contribute positive moment, that is, the aerodynamic center of both is ahead of the midchord point. The moment contribution of the body is by far the largest positive moment since its aerodynamic center is in the region of the nose of the body. The interference moment of the body due to the wing generally has a greater negative moment as the aspect ratio increases. It is seen from figure 39 that the region of influence of the wing tips on the body is farther removed from the tips for the higher aspect ratio than would be the case for the lower aspect ratio and, also, this region of tip influence is moving off of the body as the Mach number increases. The amount of interference the tips contribute decreases as both the Mach number and aspect ratio increases so that the positive lift at the wing root is left to predominate; this effect has caused the proportionate increase in body interference.

For the case of the wing configuration of aspect ratio 2, the thrust interference on the wing due to the body is approximately 5 to 15 percent of the total drag at the three Mach numbers.

Concept of Wing-Lift Carry-Over

Presented in figure 46 are curves illustrating to what extent the use of the "rule of thumb" concept of wing lift carry-over may be justified within the range of Mach numbers and aspect ratios investigated. This concept assumes that the lift of the portion of the wing enclosed by the body is preserved. The curves at the top of the figure show the summation of the lifts of the total wing alone and body, as if wing lift carried over the body and no interference existed, in terms of the lift of the wing-body combination. As seen from these curves, the values of

lift carry-over vary considerably with Mach number and aspect ratio. To obtain interference values for configurations similar to the ones tested, the curves at the bottom of the figure have been included. These curves show the carry-over concept in terms of the absolute value of ΔC_{L_α} which (as shown by the equation) gives the algebraic sum of the gain in body lift (as a result of the wings' presence) and the loss of wing lift (as a result of the body's presence). Thus a value of zero for ΔC_{L_α} indicates that the wing lift carry-over concept is exact. Values greater (or less) than zero indicate the absolute value of the gain (or loss) in lift-curve slope, based on total wing area, for the complete configuration. It is seen that for certain conditions of Mach number and aspect ratio, the "rule of thumb" concept holds; however, for most of the cases, the concept is not too reliable.

General Remarks

From the results obtained in this test program, indications are that the Reynolds number has appreciable effect on the wing in the presence of the body and may have appreciable effect on the body due to the wing; consequently, the obtainment of higher test Reynolds numbers should be given serious consideration as an important factor in planning future investigations of the type reported herein. An investigation of low-aspect-ratio wings with variable afterbody length seems desirable in order to separate the effects of wing-root and tip interference; or, conversely, to assess interference forces on the afterbody.

CONCLUSIONS

An investigation of interference effects was made on a series of rectangular wings having aspect ratio of 2, 3, and 4 mounted on a slender body having two different forebody lengths. The ratio of wing-chord to body-diameter was 1.43, and the ratios of body-diameter to wing-span were 0.35, 0.23, and 0.18. Basic measurements of lift, drag, and pitching moment were obtained for the wing-body combinations, wing in presence of the body, wing alone, and body alone at Mach numbers 1.62, 1.93, and 2.41. Interference lifts, drags, and pitching moments were obtained from the basic measurements. The results indicate that:

1. Changing the forebody length so that the fineness ratio of the body changed from 9.13 to 10.27 had no effect on the interference quantities.

2. The interference lift, drag, and pitching-moment quantities were functions of both Mach number and aspect ratio.

3. The method by Tucker best predicted the interference lift on the wing due to the body while a modified slender-body theory agreed favorably with the lift of the wing in the presence of the body.

4. The interference lift on the body due to the wing was favorably predicted by the method of Nielsen and Kaattari and by the method of Tucker. The interference lifts and pitching-moments were influenced by the wing tips as well as the wing-root pressures; thus the need for including consideration of the afterbody is indicated.

5. The lift of the wing in presence of the body was increased as much as 13 percent for the aspect-ratio-2 wing at Mach number 1.62 by increasing the Reynolds number from 0.46×10^6 to 1.40×10^6; thus that viscous effects are indicated to be an important factor in wing-body interference.

6. The drag interferences on the wings due to the body were small. The wing of aspect ratio 2 indicated a thrust interference of the order of 5 to 15 percent of the total drag for all Mach numbers. However, it appears likely that this effect may not be present at higher Reynolds numbers.

7. The method of Tucker for predicting the incremental lift-curve slopes of the wings in presence of the body due to varying incidence angle agrees well with the experimental results.

Langley Aeronautical Laboratory
National Advisory Committee for Aeronautics
Langley Field, Va.

REFERENCES

1. Spreiter, John R.: Aerodynamic Properties of Slender Wing-Body Combinations at Subsonic, Transonic, and Supersonic Speeds. NACA TN 1662, 1948.

2. Spreiter, John R.: Aerodynamic Properties of Cruciform-Wing and Body Combinations at Subsonic, Transonic, and Supersonic Speeds. NACA TN 1897, 1949.

3. Ferrari, Carlo: Interference Between Wing and Body at Supersonic Speeds - Theory and Numerical Application. Jour. Aero. Sci., vol. 15, no. 6, June 1948, pp. 317-336.

4. Ferrari, Carlo: Interference Between Wing and Body at Supersonic Speeds - Note on Wind Tunnel Results and Addendum to Calculations. Jour. Aero. Sci., vol. 16, no. 9, Sept. 1949, pp. 542-546.

5. Ferrari, Carlo: Interference Between Wing and Body at Supersonic Speeds - Analysis by the Method of Characteristics. Jour. Aero. Sci., vol. 16, no. 7, July 1949, pp. 411-434.

6. Browne, S. H., Friedman, L., and Hodes, I.: A Wing-Body Problem in a Supersonic Conical Flow. Jour. Aero. Sci., vol. 15, no. 8, 1948, pp. 443-452.

7. Lagerstrom, P. A., and Van Dyke, M. D.: General Considerations About Planar and Non-Planar Lifting Systems. Rep. No. SM-13432, Douglas Aircraft Co., Inc., June 1949.

8. Lagerstrom, P. A., and Graham, M. E.: Aerodynamic Interference in Supersonic Missiles. Rep. No. SM-13743, Douglas Aircraft Co. Inc., July 1950.

9. Morikawa, George: The Wing-Body Problem for Linearized Supersonic Flow. Progress Rep. No. 4-116, Jet Propulsion Lab., C.I.T., Dec. 19, 1949.

10. Morikawa, George: Supersonic Wing-Body Lift. Jour. Aero. Sci., vol. 18, no. 4, Apr. 1951.

11. Nielsen, Jack N., and Matteson, Frederick H.: Calculative Method for Estimating the Interference Pressure Field at Zero Lift on a Symmetrical Swept-Back Wing Mounted on a Circular Cylindrical Body. NACA RM A9E19, 1949.

12. Nielsen, Jack N., Katzen, Elliott D., and Tang, Kenneth K.: Lift and Pitching-Moment Interference Between a Pointed Cylindrical Body and Triangular Wings of Various Aspect Ratios at Mach Numbers of 1.50 and 2.02. NACA RM A50F06, 1950.

13. Nielsen, Jack N., and Kaattari, George E.: Method for Estimating Lift Interference of Wing-Body Combinations at Supersonic Speeds. NACA RM A51J04, 1951.

14. Tucker, Warren A.: A Method for Estimating the Components of Lift of Wing-Body Combinations at Supersonic Speeds. NACA RM L52D22, 1952.

15. Moskowitz, Barry, and Maslen, Stephen H.: Experimental Pressure Distributions Over Two Wing-Body Combinations at Mach Number 1.9. NACA RM E50J09, 1951.

16. Cramer, R. H.: Some Theoretical and Experimental Results for Wing-Body Interference at Supersonic Velocities. Paper presented in the Bumblebee Aerodynamics Symposium. APL/JHU TG-10-4, The Johns Hopkins Univ., Appl. Phys. Lab., Nov. 4-5, 1948, pp. 267-276 and Supp. TG-10-4B.

17. Uddenberg, R. C.: Summary of Supersonic Wind Tunnel Tests on GAPA Models in Aberdeen Tunnel. Part I - Lift, Drag, and Center of Pressure Comparison for Fixed Wings of Various Planforms. Tech. Rep. III-5 (Doc. D-8231), Boeing Aircraft Co., June 1947.

18. Harshman, J., and Uddenberg, R. C.: Supersonic Wind Tunnel Tests of GAPA Models at a Mach Number of 1.28 in the Aberdeen Tunnel. Doc. No. D-7817, Boeing Aircraft Co., Aug. 2, 1946.

19. Uddenberg, R. C.: Supersonic Wind Tunnel Tests of GAPA Models at a Mach Number of 1.72 in the Aberdeen Tunnel. Doc. No. D-7818, Boeing Aircraft Co., Dec. 1946.

20. Rainey, Robert W.: Langley 9-Inch Supersonic Tunnel Tests of Several Modifications of a Supersonic Missile Having Tandem Cruciform Lifting Surfaces. Three-Component Data Results of Models Having Ratios of Wing Span to Tail Span Equal to 1. NACA RM L9L30, 1951.

21. Love, Eugene S.: Investigations at Supersonic Speeds of 22 Triangular Wings Representing Two Airfoil Sections for Each of 11 Apex Angles. NACA RM L9D07, 1949.

22. Michels, Walter C.: Advanced Electrical Measurements. Second ed., D. Van Nostrand Co., Inc., 1941.

TABLE I

BODY COORDINATES AND WING-SHAPE PARAMETERS

[See fig. 1]

Body		
x, in.	Diameter, in.	
	n = 10.27	n = 9.13
0	0.002	-----
.500	.154	-----
1.000	.296	0
1.500	.430	.262
2.000	.552	.462
2.500	.660	.620
3.000	.746	.728
3.500	.820	.814
3.750	.846	.846
4.000	.860	↑
4.625	.872	
5.000	.876	Same as
5.500	.874	n = 10.27
6.000	.872	
6.500	.866	
7.250	.794	
8.000	.692	
8.375	.628	
9.000	.500	↓

	6-percent-thick biconvex circular-arc rectangular wings						
Type	A_{design}	A_{actual}	i (deg)	b (in.)	c (in.)	t (in.)	t/c
Wing in presence of body	2	2.00	0.11	2.500	1.249	0.0738	0.0591
	3	2.99	.04	3.752	1.254	.075	.0598
	4	3.92	-.06	4.930	1.259	.075	.0596
	2	1.99	3.16	2.504	1.259	.075	.0596
	3	2.99	3.12	3.755	1.257	.0745	.0593
	4	3.98	3.02	4.977	1.250	.083	.0664
Wing alone	2	1.99	----	2.505	1.258	.0745	.0592
	3	2.98	----	3.753	1.259	.075	.0596
	4	3.97	----	4.985	1.257	.072	.0573

NACA

TABLE II

SUMMARY OF TOTAL UNCERTAINTIES

Configuration	Quantity	Accuracy for $C_L = 0$	Accuracy at approx. end of linearity
All wings in the presence of the body (strain gage)	C_L	±0.0009	±0.0012
	C_m	±.0006	±.0009
	C_D	±.0003	------
Wing-body in combination, wings alone, and bodies alone (scales)	C_L	±.0002	------
	C_m	±.0009	------
	C_D	±.0007	------
All	Initial angle of attack	±.03°	------
All	Relative angle of attack	±.01°	------
All	Incidence angle of wings	±.03°	------
All	Mach numbers	±.01	------
All	Reynolds numbers	±15,000	------
All	Stream pressure	$\pm 1\frac{1}{2}$ percent	------

NACA

TABLE III

SUMMARY OF LIFT AND PITCHING-MOMENT CURVE SLOPES, AND MINIMUM

DRAG VALUES AT ZERO LIFT FROM FIGURES 3 TO 29

M	Wing aspect ratio	i, deg (nominal)	Wing-body in combination, WB				Wing in presence of body, W(B)			Wing, W			Body, B			
			C_{L_α}	C_{m_α}	$C_{D_{min}}$		C_{L_α}	C_{m_α}	$C_{D_{min}}$	C_{L_α}	C_{m_α}	$C_{D_{min}}$	C_{L_α}	C_{m_α}	$C_{D_{min}}$	
					n = 10.27	n = 9.13									n = 10.27	n = 9.13
1.62	2	0 3	0.0420	0.0249	0.383	0.0437	0.0273 .0270	0.0054 .0056	0.0130 .0110				0.0062	0.0199	0.0171	0.0226
	3	0 3	.0489	.0170	.0334	.0370	.0368 .0365	.0057 .0053	.0153 .0144				.0042	.0132	.0113	.0151
	4	0 3	.0512	.0135	.0350	.0375	.0410 .0413	.0057 .0055	.0151 .0195				.0031	.0097	.0095	.0112
1.93	2	0 3	.0389	.0192	.0337	.0391	.0226 .0230	.0036 .0036	.0102 .0102	0.0338		0.0181	.0067	.0190	.0150	.0202
	3	0 3	.0413	.0130	.0294	.0329	.0290 .0290	.0040 .0036	.0137 .0127	.0351		.0174	.0045	.0125	.0100	.0134
	4	0 3	.0416 .0418	.0094 .0097	.0255 .0303	.0285 .0335	.0329 .0329	.0040 .0040	.0135 .0177	.0365		.0165	.0035	.0094	.0075	.0101
2.41	2	0 3	.0346	.0169	.0335	.0383	.0195 .0199	.0029 .0034	.0103 .0098	.0277		.0170	.0075	.0181	.0163	.0218
	3	0 3	.0351	.0100	.0281	.0319	.0236 .0238	.0028 .0031	.0127 .0114	.0281		.0160	.0051	.0121	.0111	.0146
	4	0 3	.0341	.0090	.0291	.0312	.0259 .0263	.0030 .0028	.0120 .0176	.0285		.0158	.0038	.0090	.0085	.0110

NACA

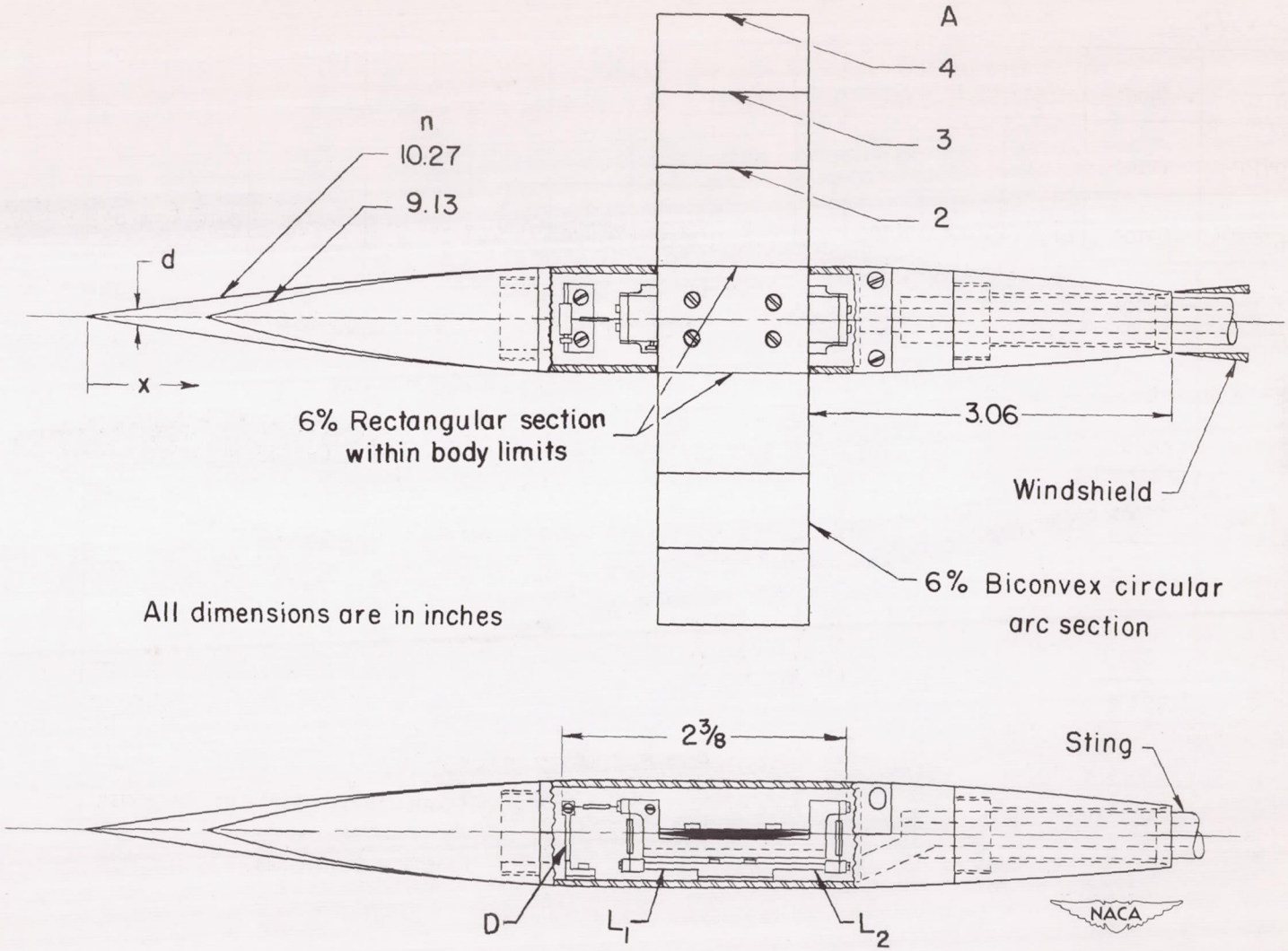

Figure 1.- Sketch of models. Body coordinates and wing-shape parameters are listed in table I.

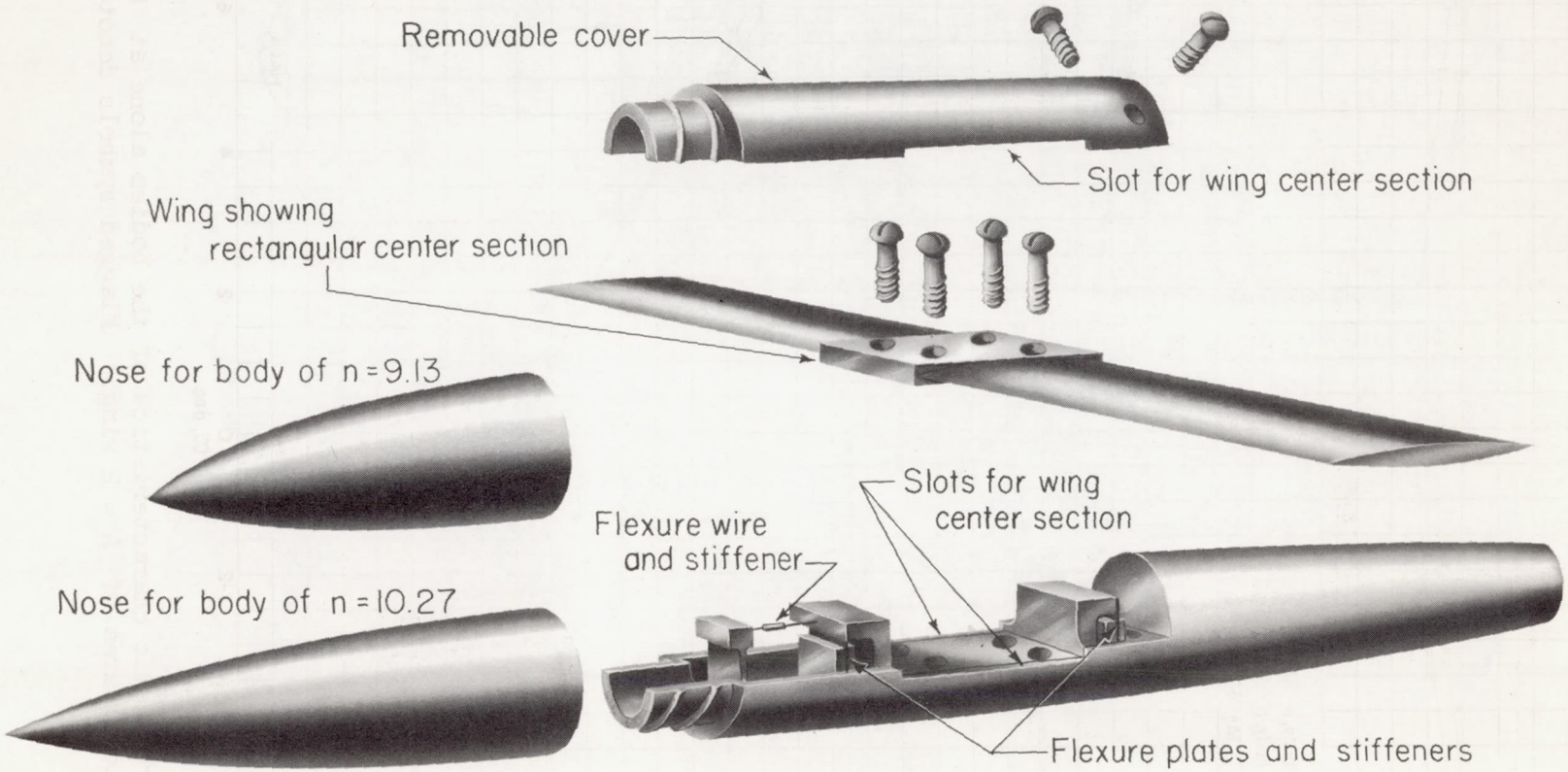

Figure 2.- Detail of model assembly.

NACA
L-76142

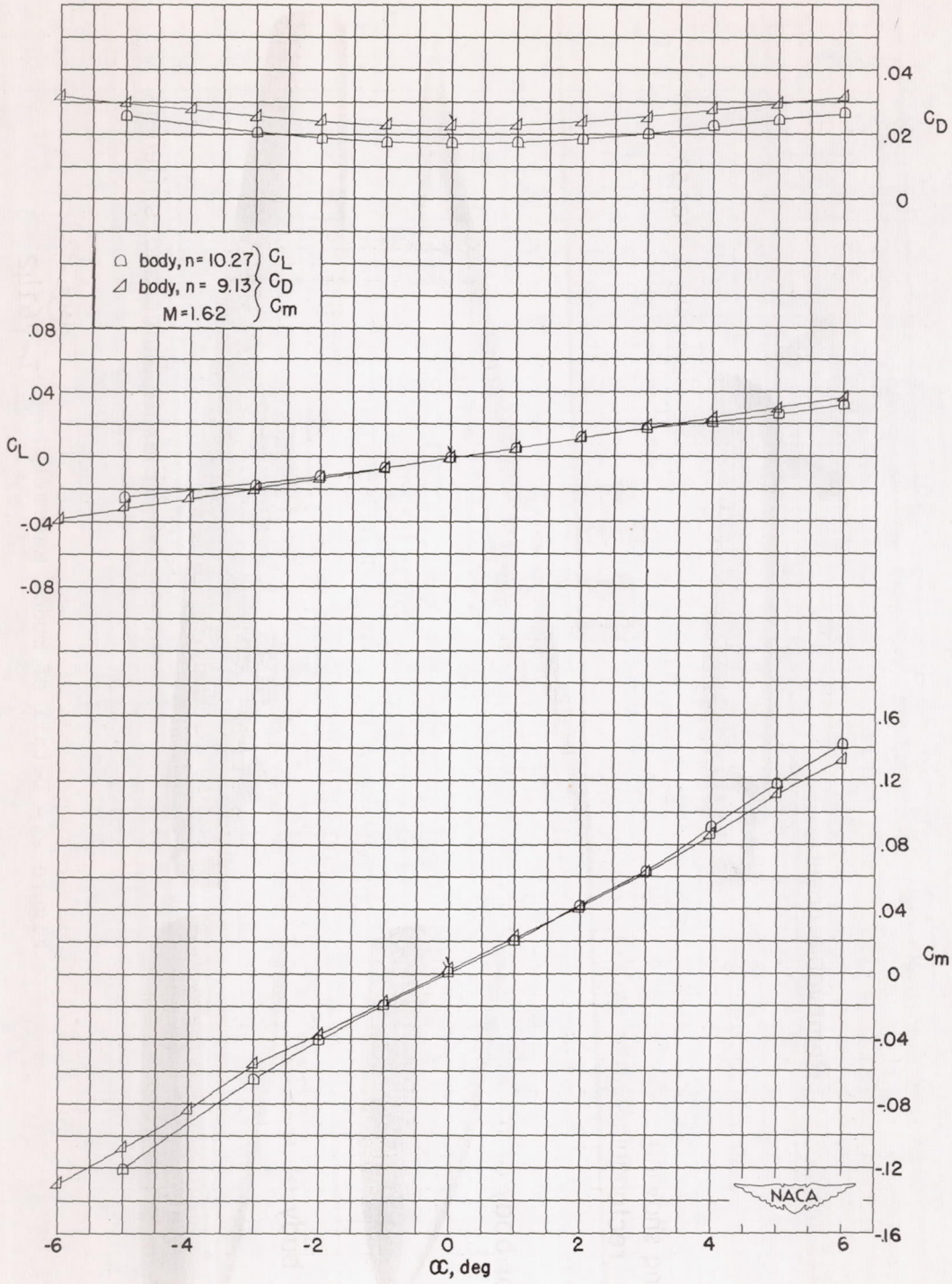

Figure 3.- Aerodynamic characteristics of the bodies alone at $M = 1.62$. (Based on total area of $A = 2$ wing.) Flagged symbols denote check points.

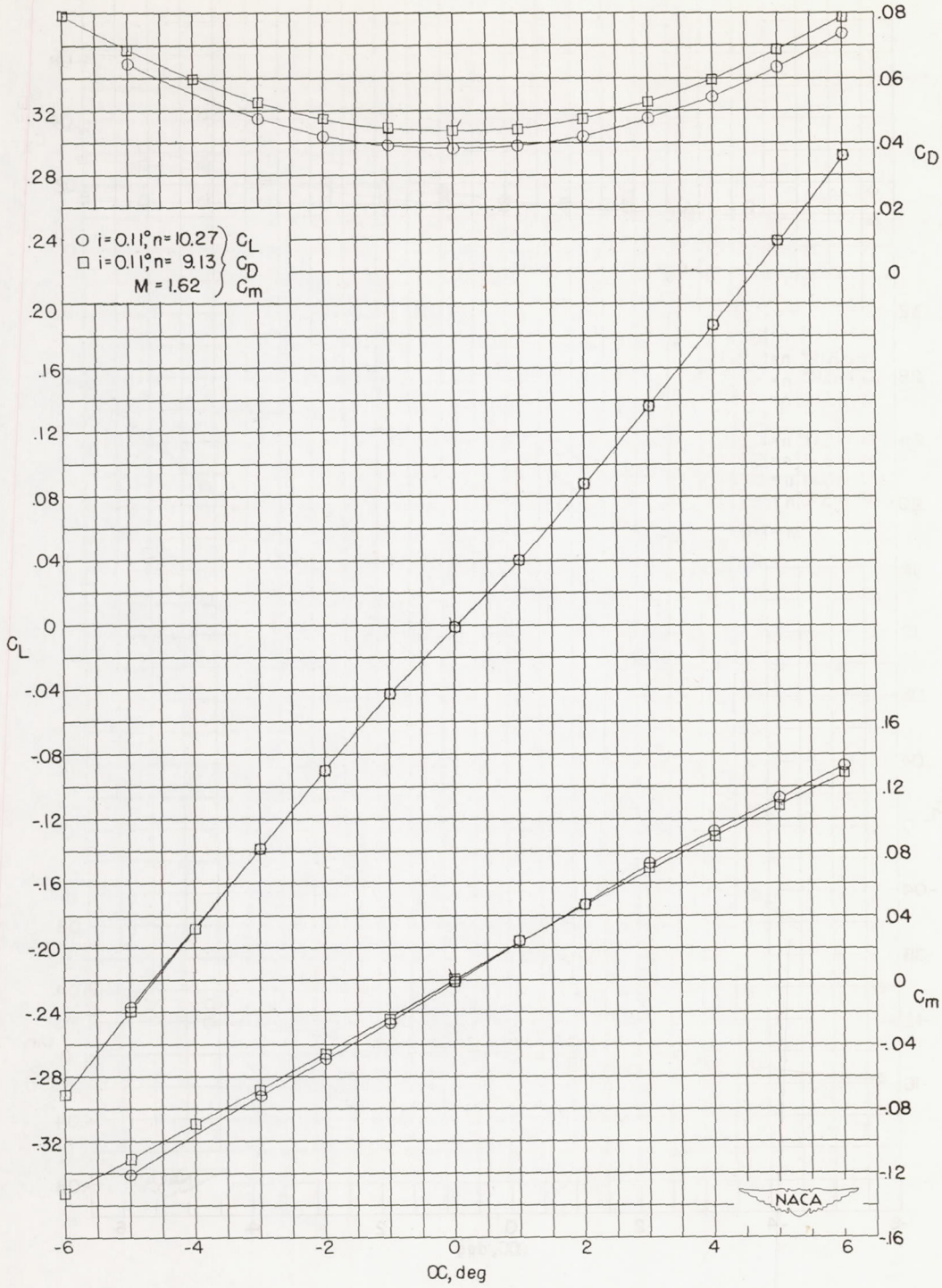

Figure 4.- Aerodynamic characteristics of the wing and body in combination for A = 2 rectangular wing at M = 1.62. Flagged symbols denote check points.

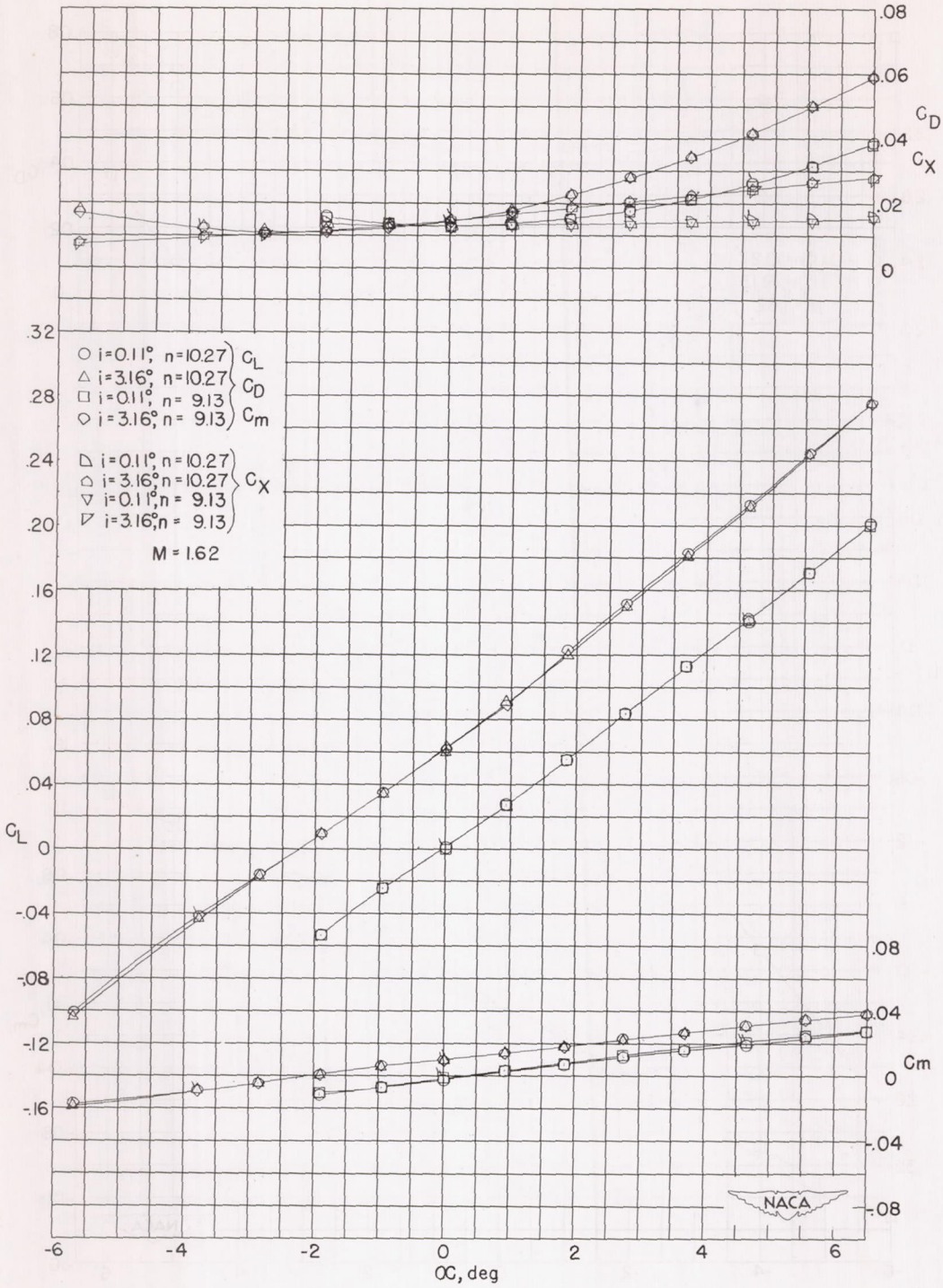

Figure 5.- Aerodynamic characteristics of the wing in the presence of the body for A = 2 rectangular wing at M = 1.62. Flagged symbols denote check points.

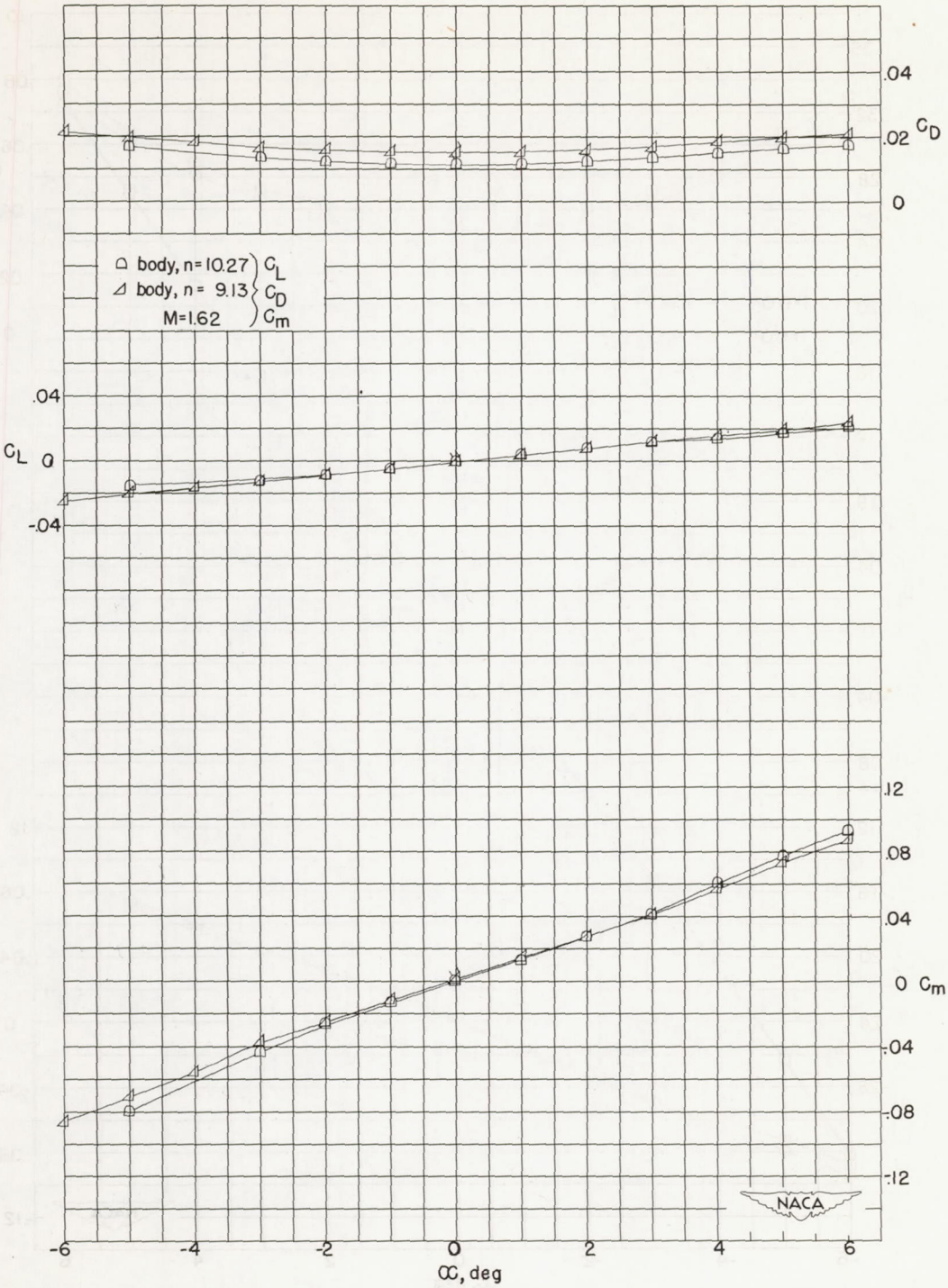

Figure 6.- Aerodynamic characteristics of the bodies alone at M = 1.62. (Based on total area of A = 3 wing.) Flagged symbols denote check points.

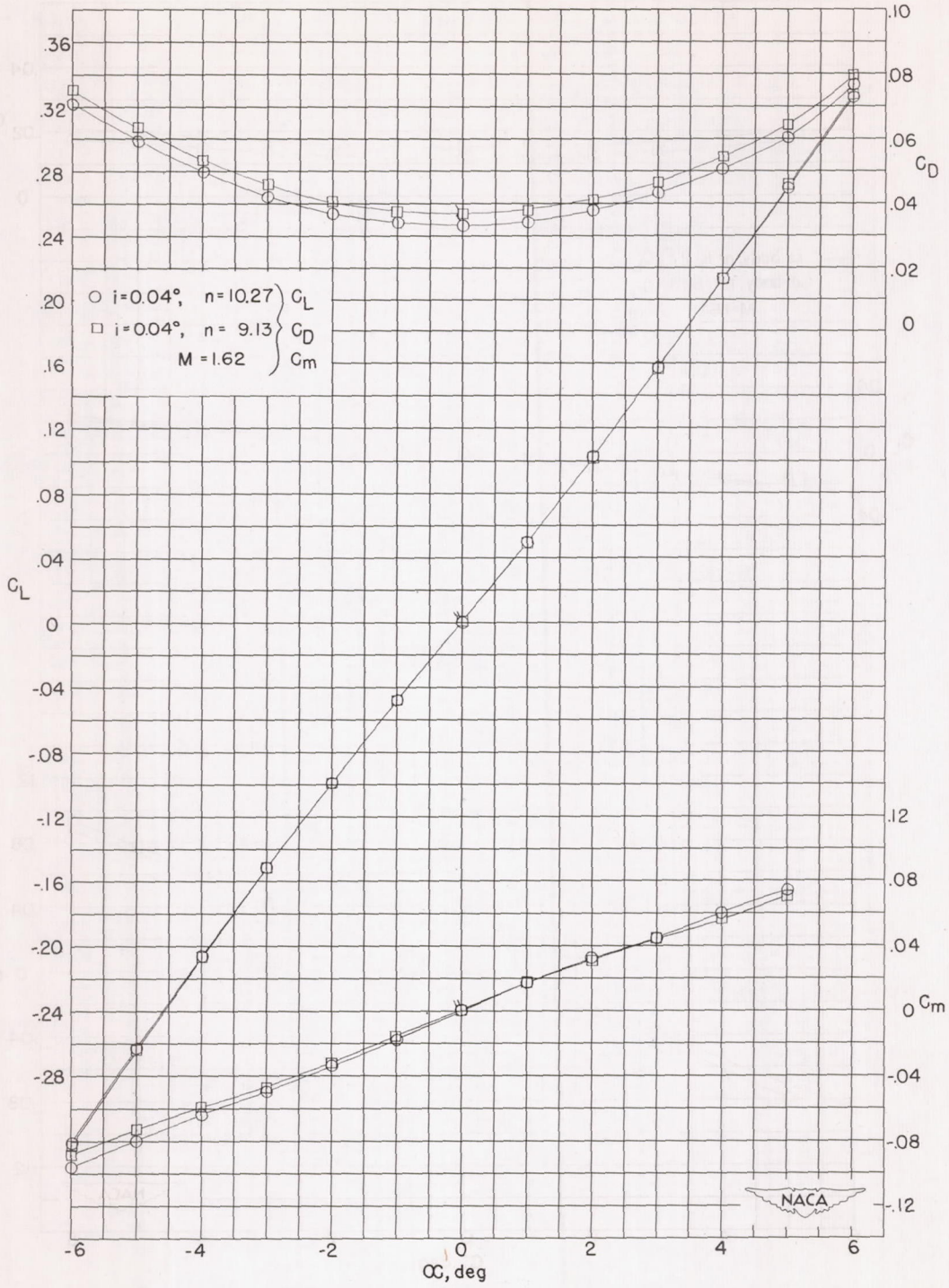

Figure 7.- Aerodynamic characteristics of the wing and body in combination for A = 3 rectangular wing at M = 1.62. Flagged symbols denote check points.

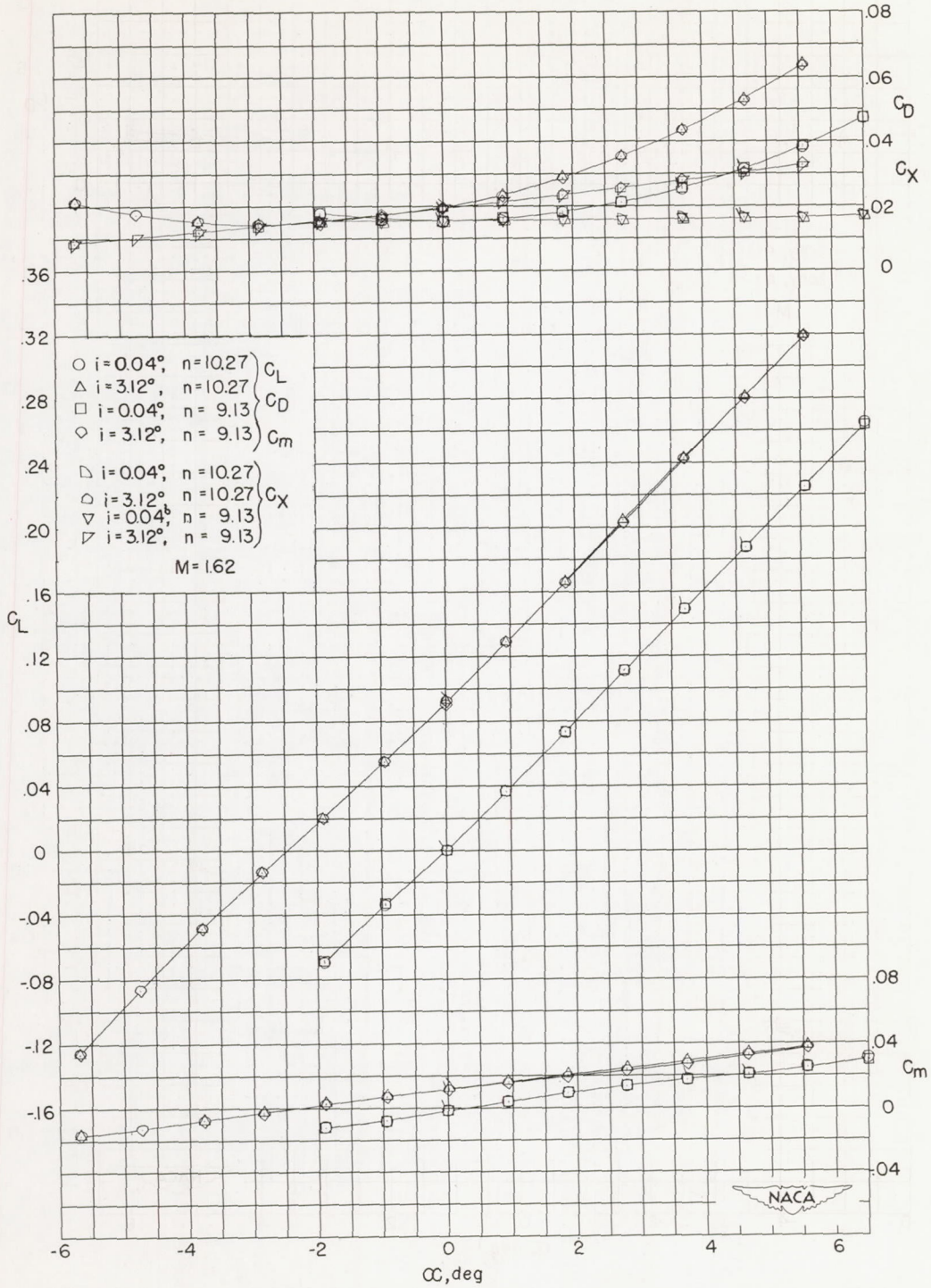

Figure 8.- Aerodynamic characteristics of the wing in the presence of the body for A = 3 rectangular wing at M = 1.62. Flagged symbols denote check points.

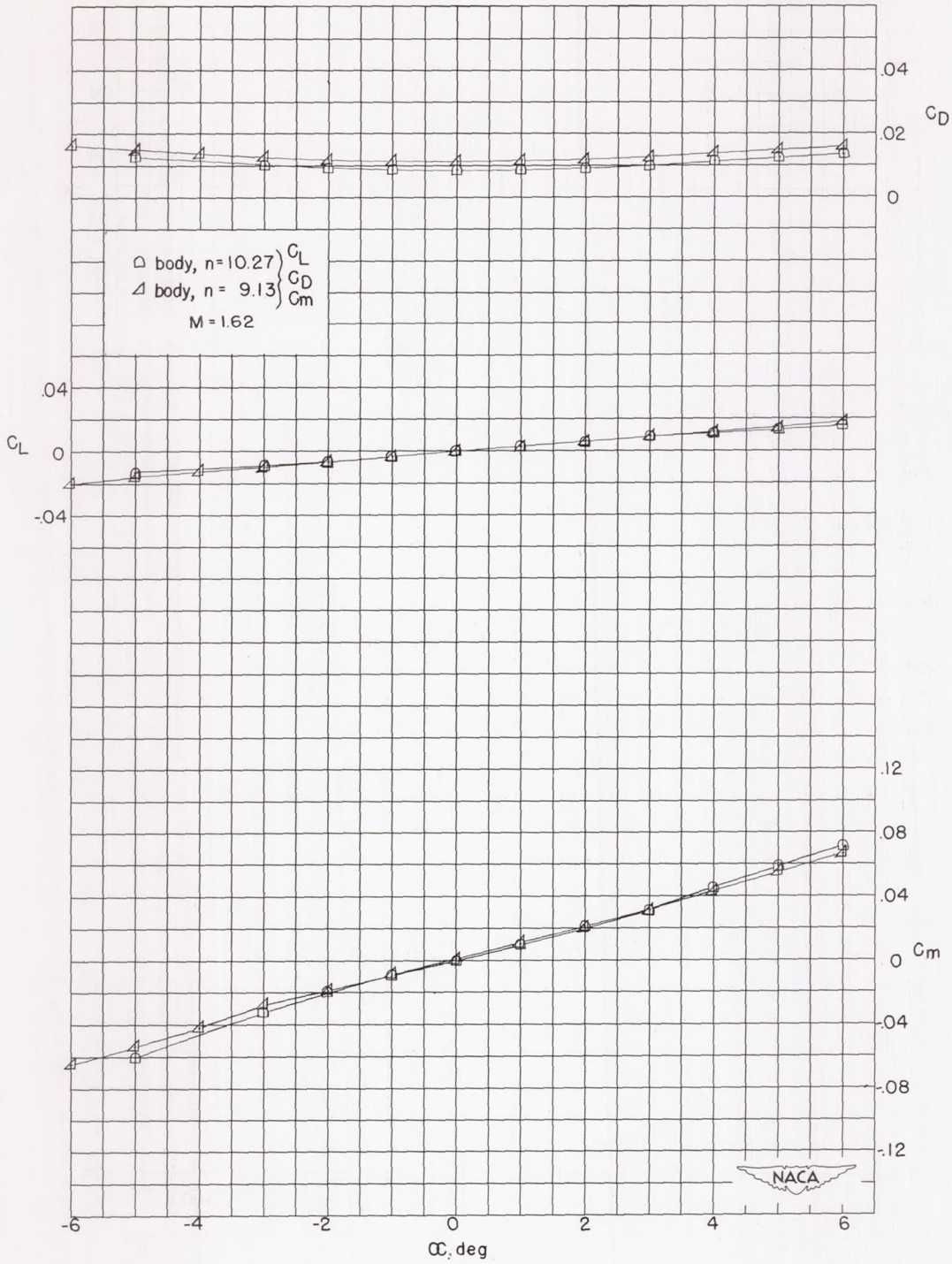

Figure 9.- Aerodynamic characteristics of the bodies alone at M = 1.62. (Based on total area of A = 4 wing.) Flagged symbols denote check points.

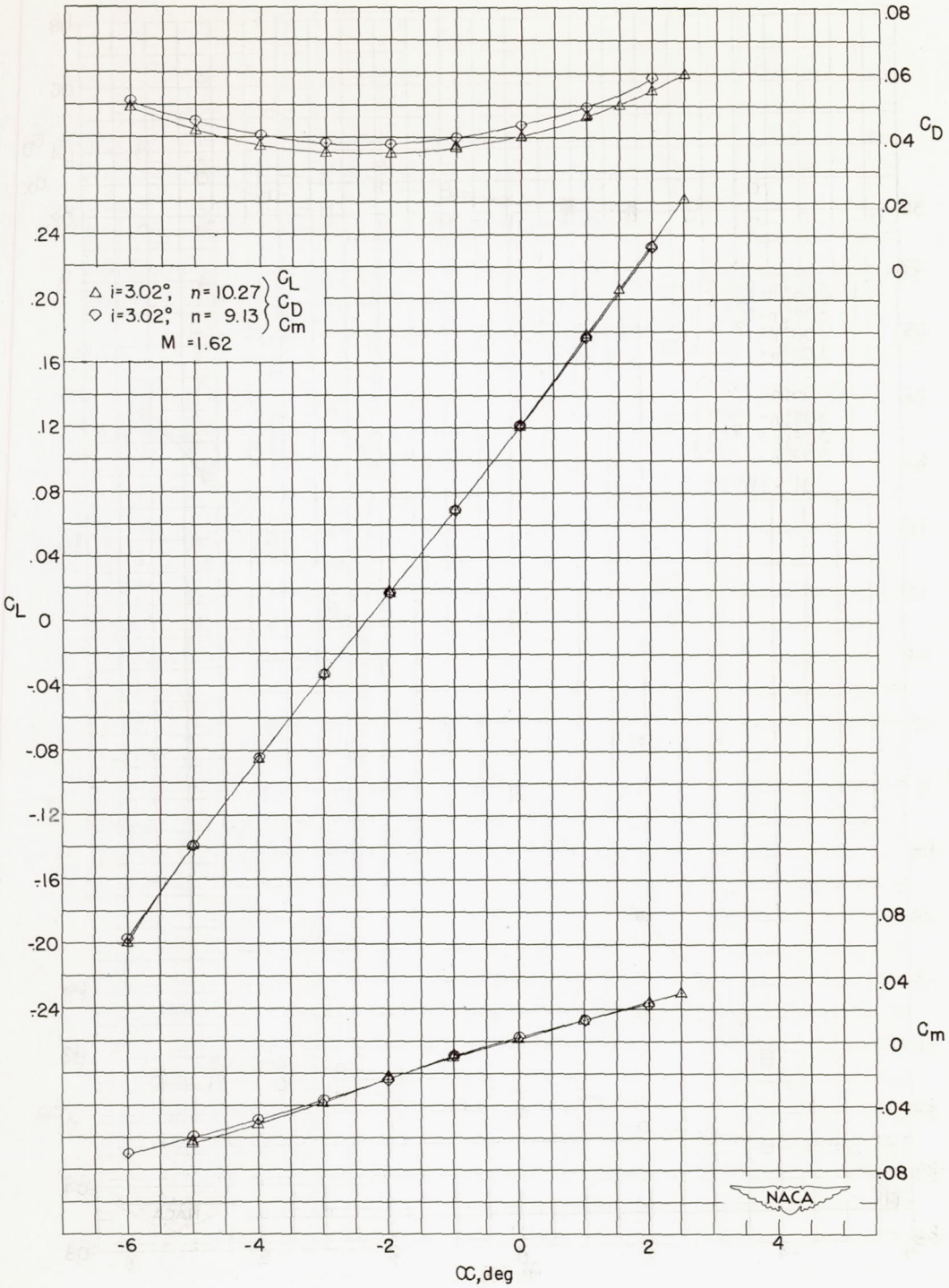

Figure 10.- Aerodynamic characteristics of the wing and body in combination for A = 4 rectangular wing at M = 1.62. Flagged symbols denote check points.

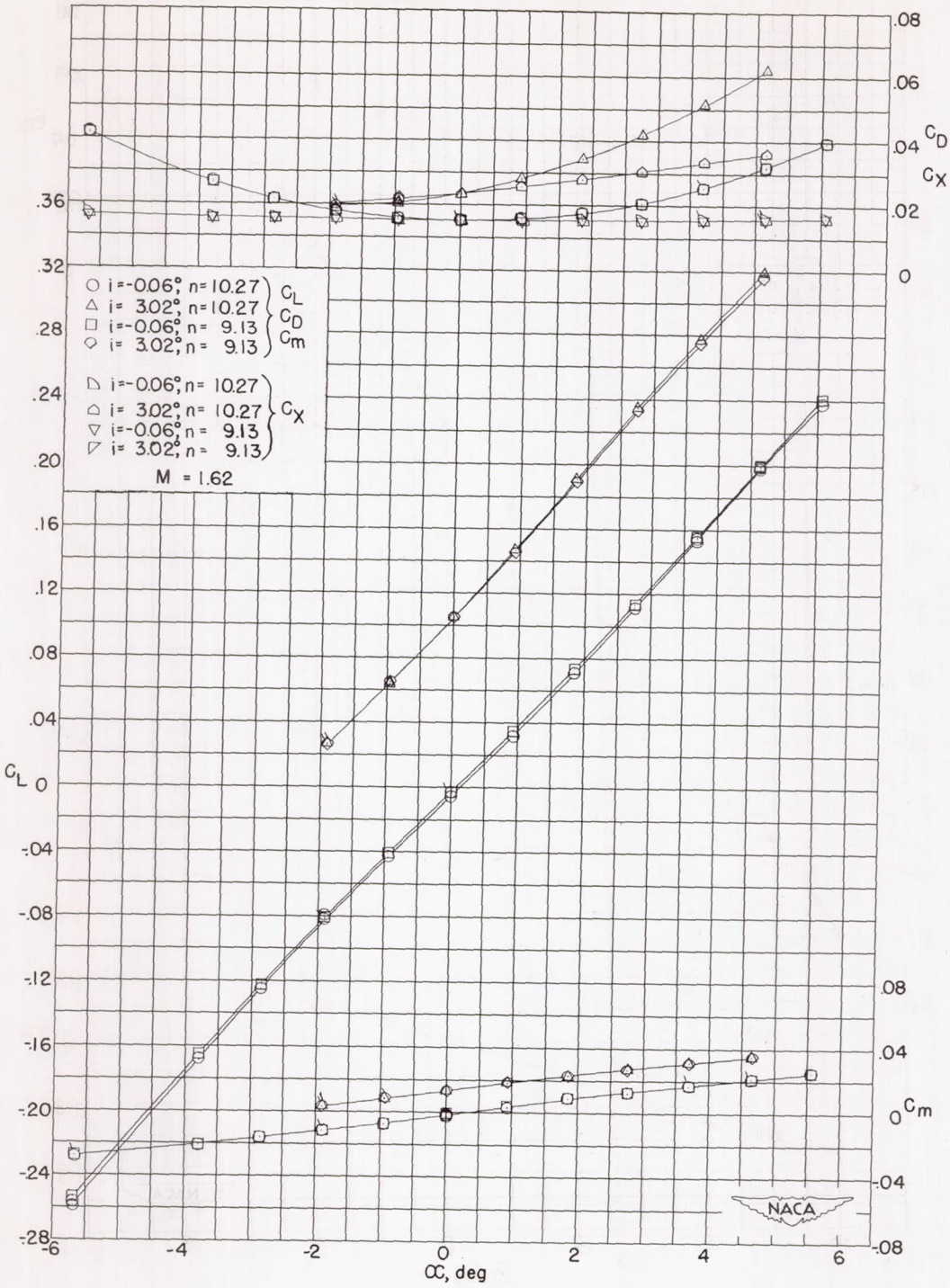

Figure 11.- Aerodynamic characteristics of the wing in the presence of the body for A = 4 rectangular wing at M = 1.62. Flagged symbols denote check points.

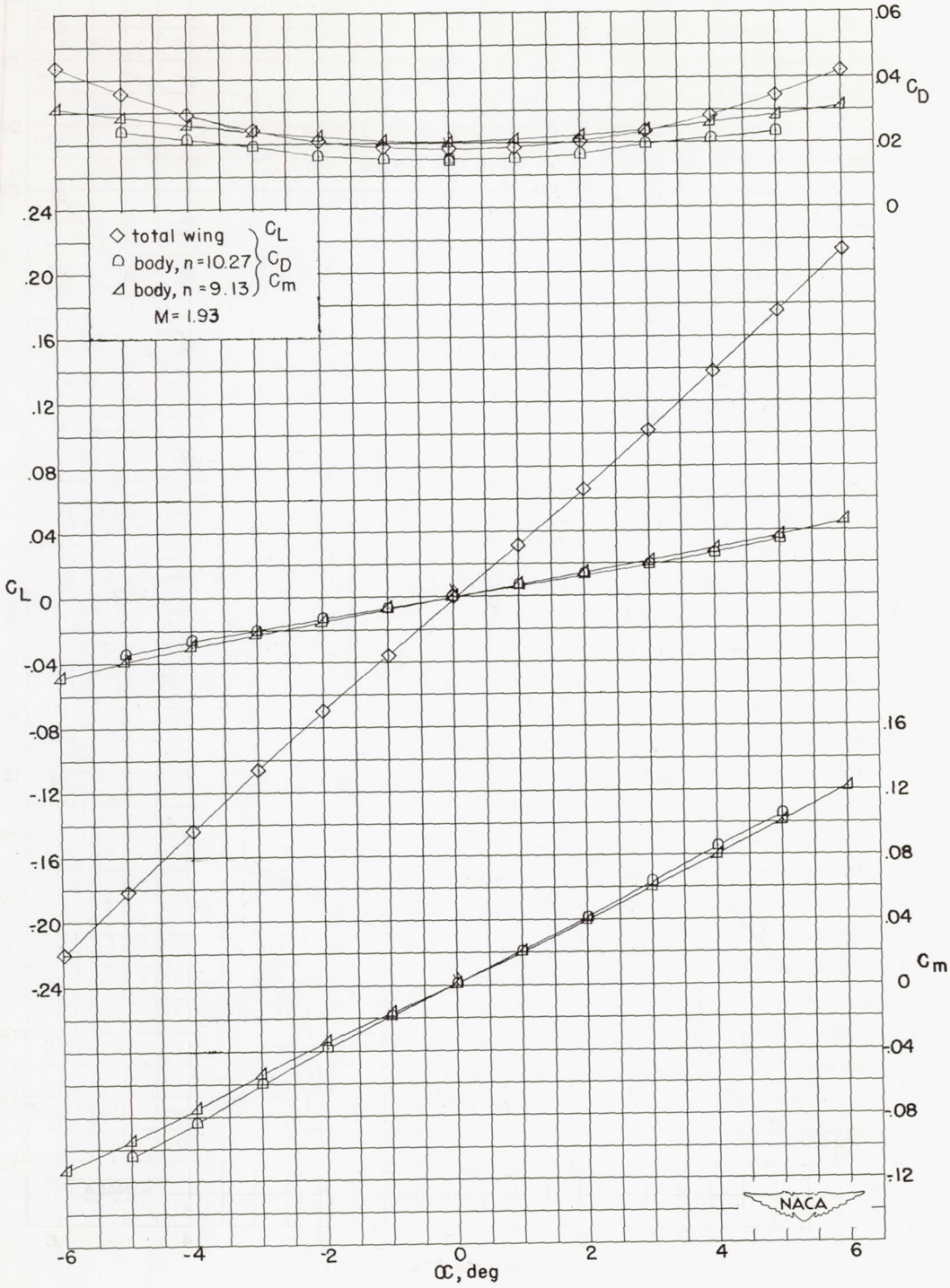

Figure 12.- Aerodynamic characteristics of the bodies alone and A = 2 rectangular wing alone at M = 1.93. (Based on total area of A = 2 wing.) Flagged symbols denote check points.

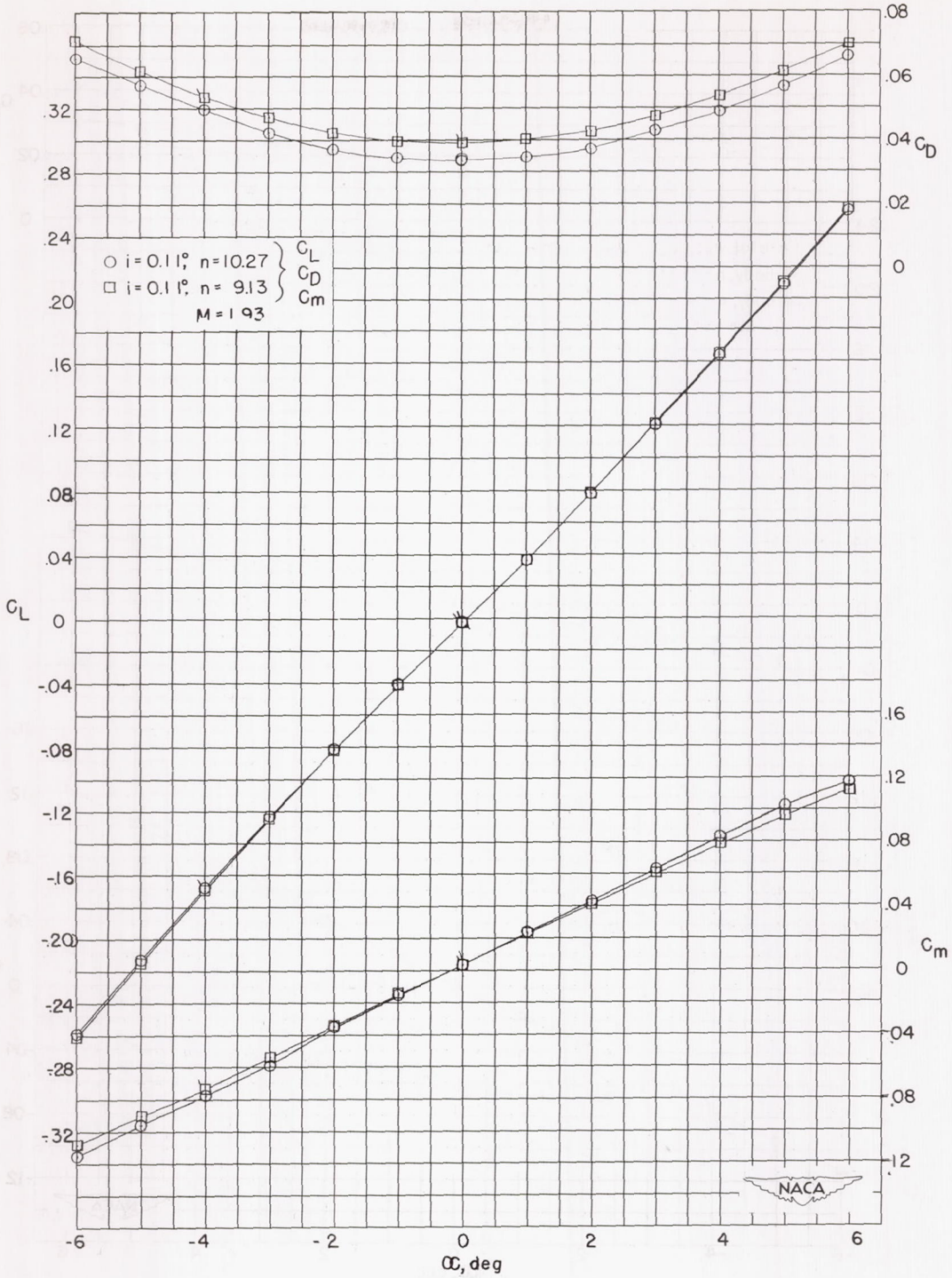

Figure 13.- Aerodynamic characteristics of the wing and body in combination for A = 2 rectangular wing at M = 1.93. Flagged symbols denote check points.

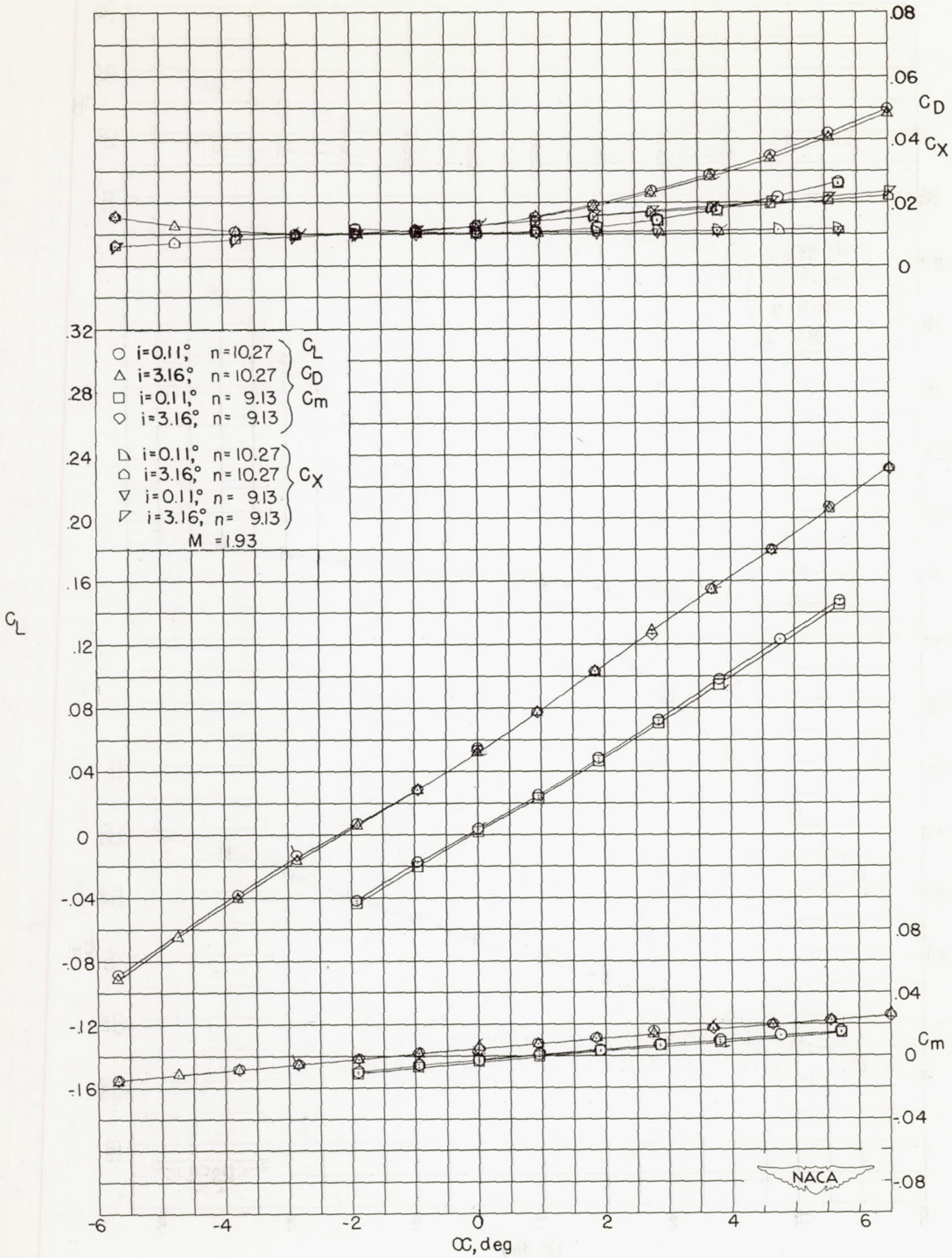

Figure 14.- Aerodynamic characteristics of the wing in the presence of the body for A = 2 rectangular wing at M = 1.93. Flagged symbols denote check points.

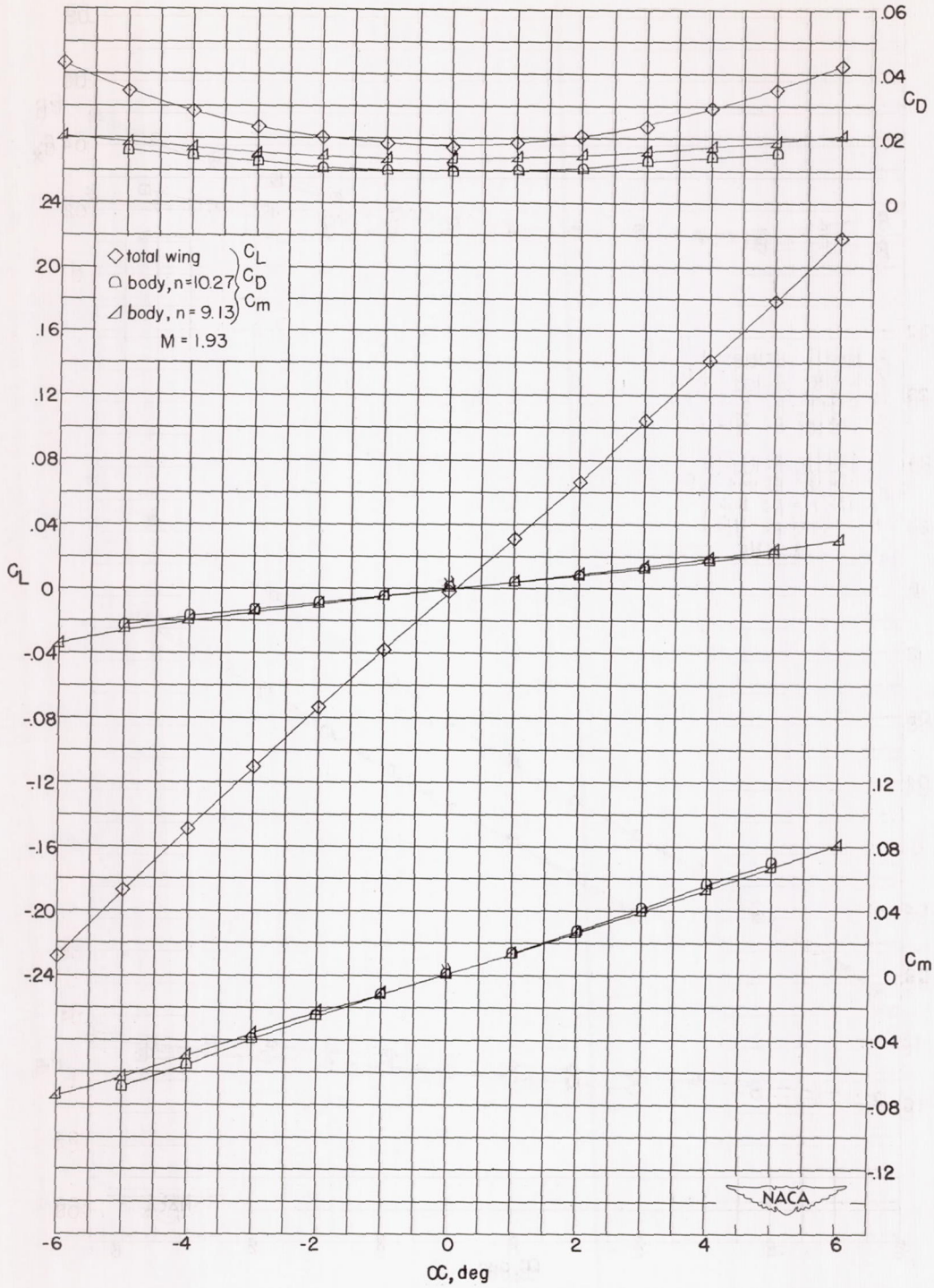

Figure 15.- Aerodynamic characteristics of the bodies alone and A = 3 rectangular wing alone at M = 1.93. (Based on total area of A = 3 wing.) Flagged symbols denote check points.

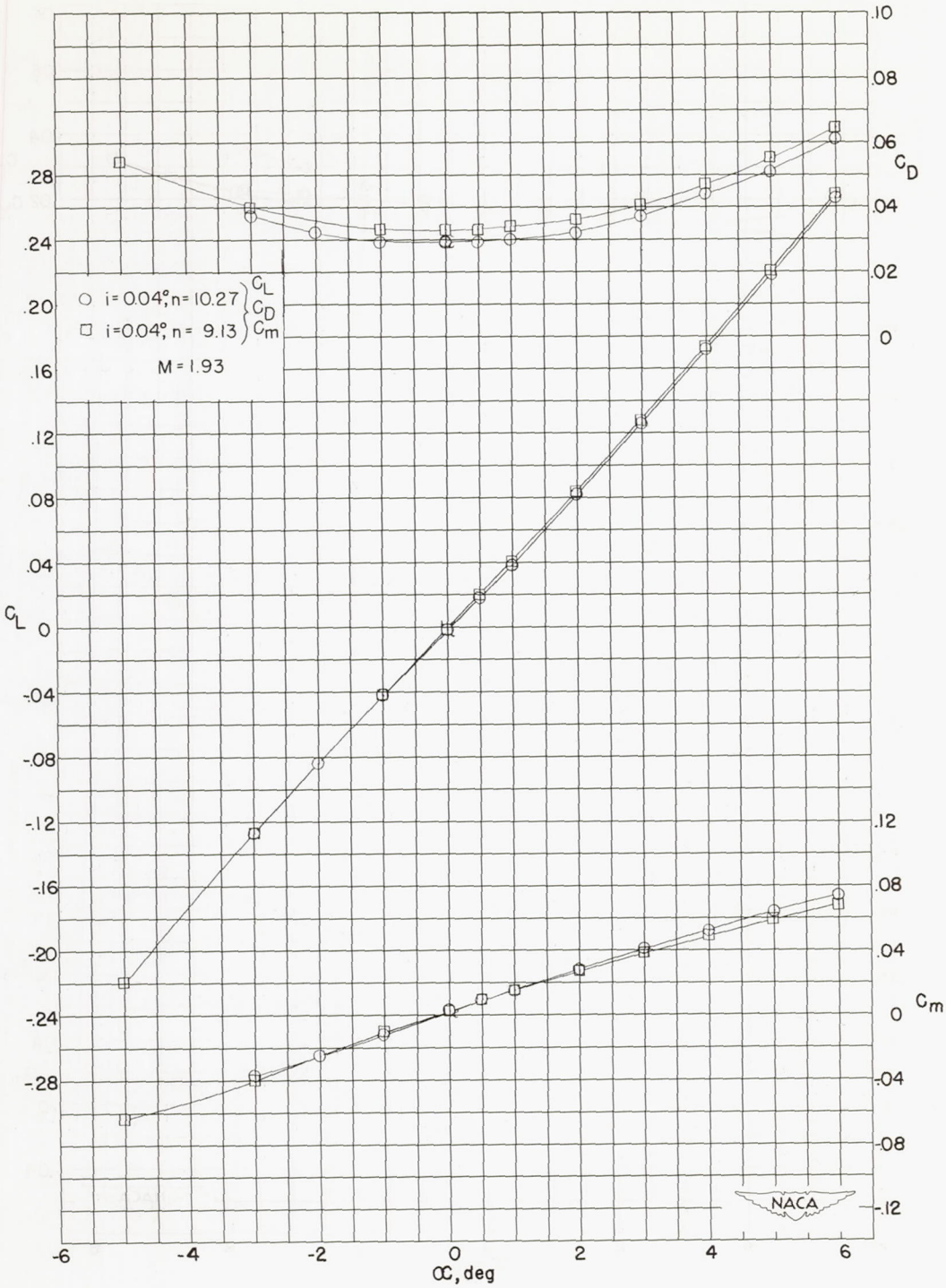

Figure 16.- Aerodynamic characteristics of the wing and body in combination for A = 3 rectangular wing at M = 1.93. Flagged symbols denote check points.

6D

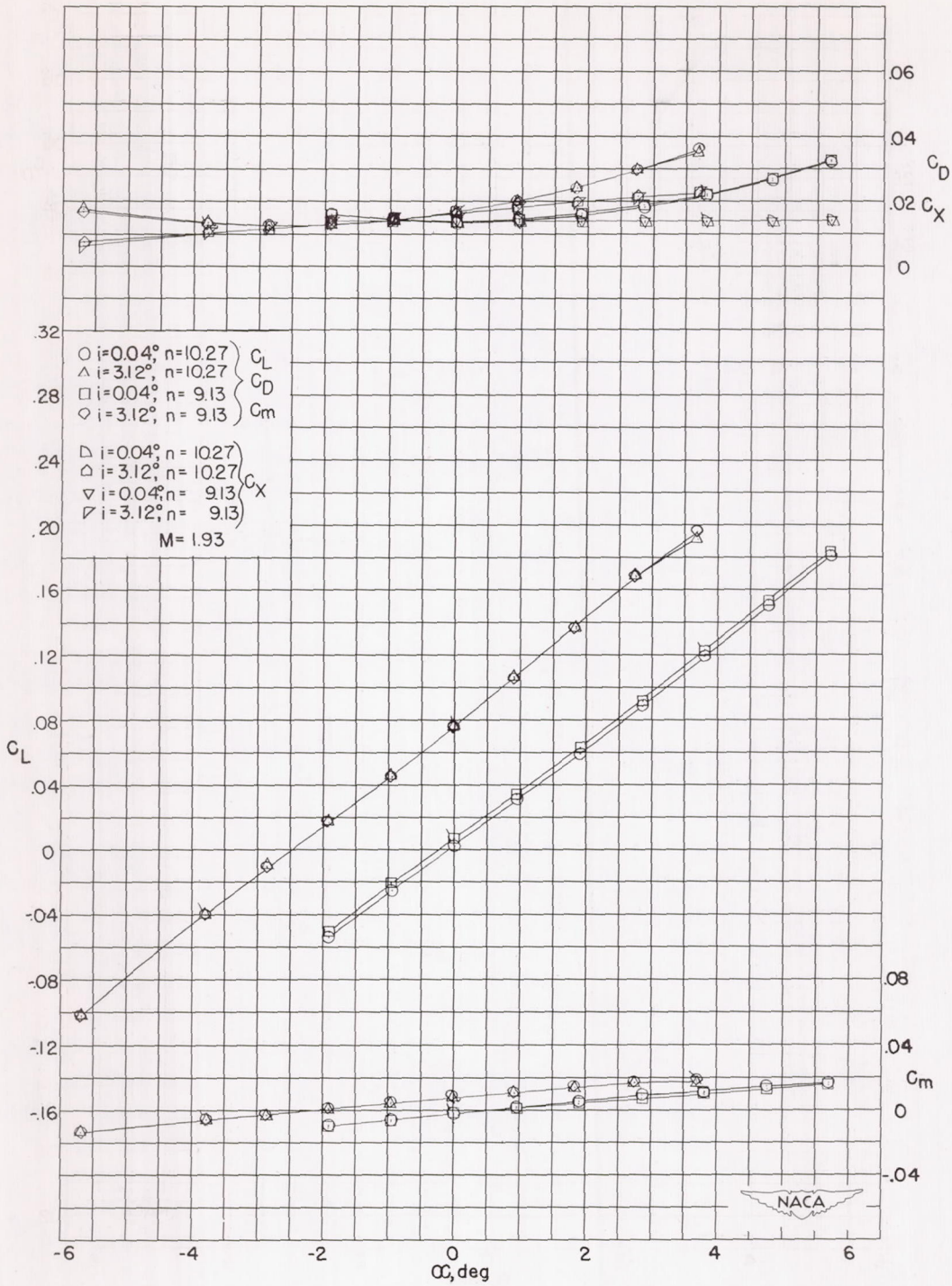

Figure 17.- Aerodynamic characteristics of the wing in the presence of the body for A = 3 rectangular wing at M = 1.93. Flagged symbols denote check points.

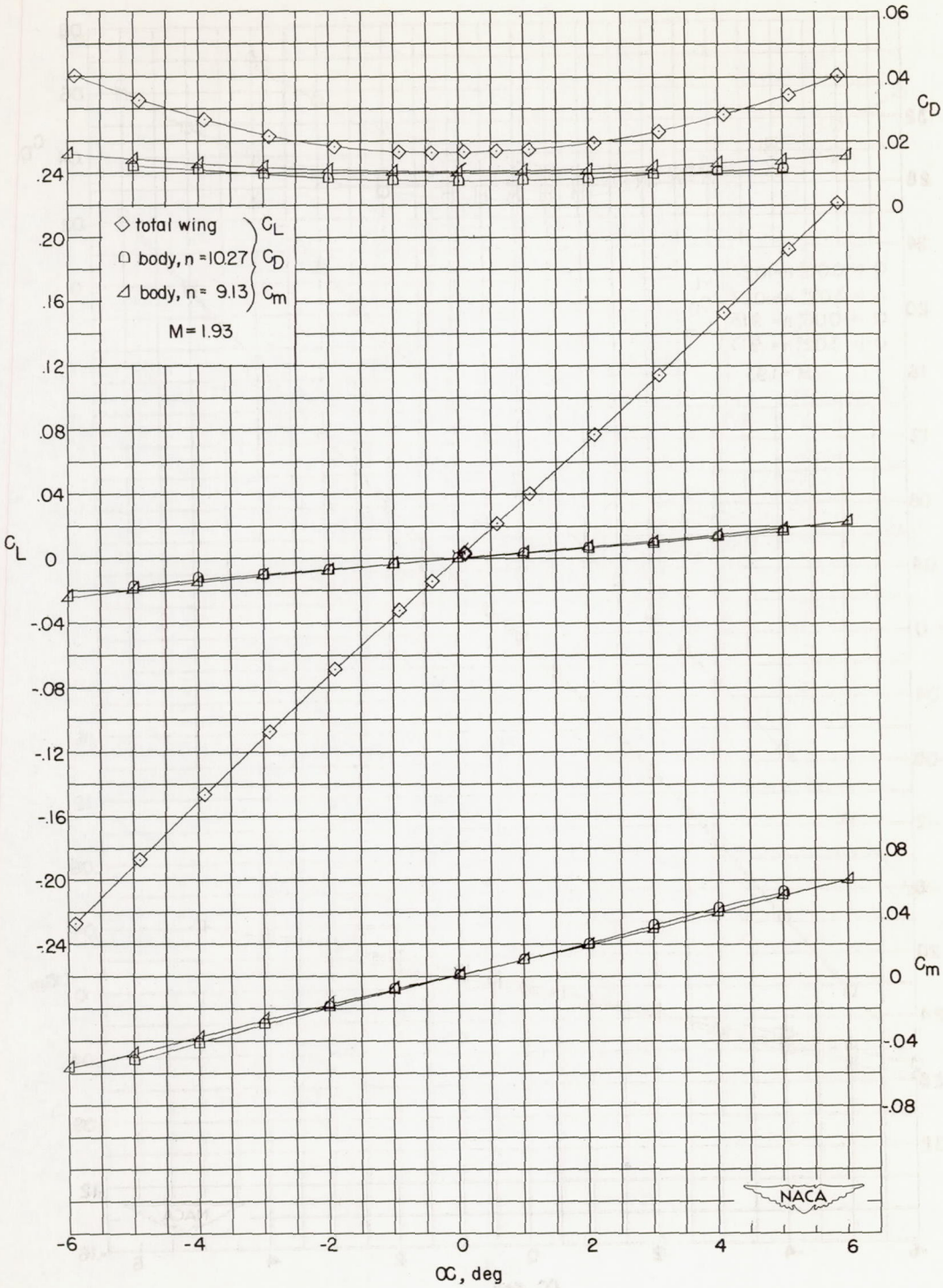

Figure 18.- Aerodynamic characteristics of the bodies alone and A = 4 rectangular wing alone at M = 1.93. (Based on total area of A = 4 wing.) Flagged symbols denote check points.

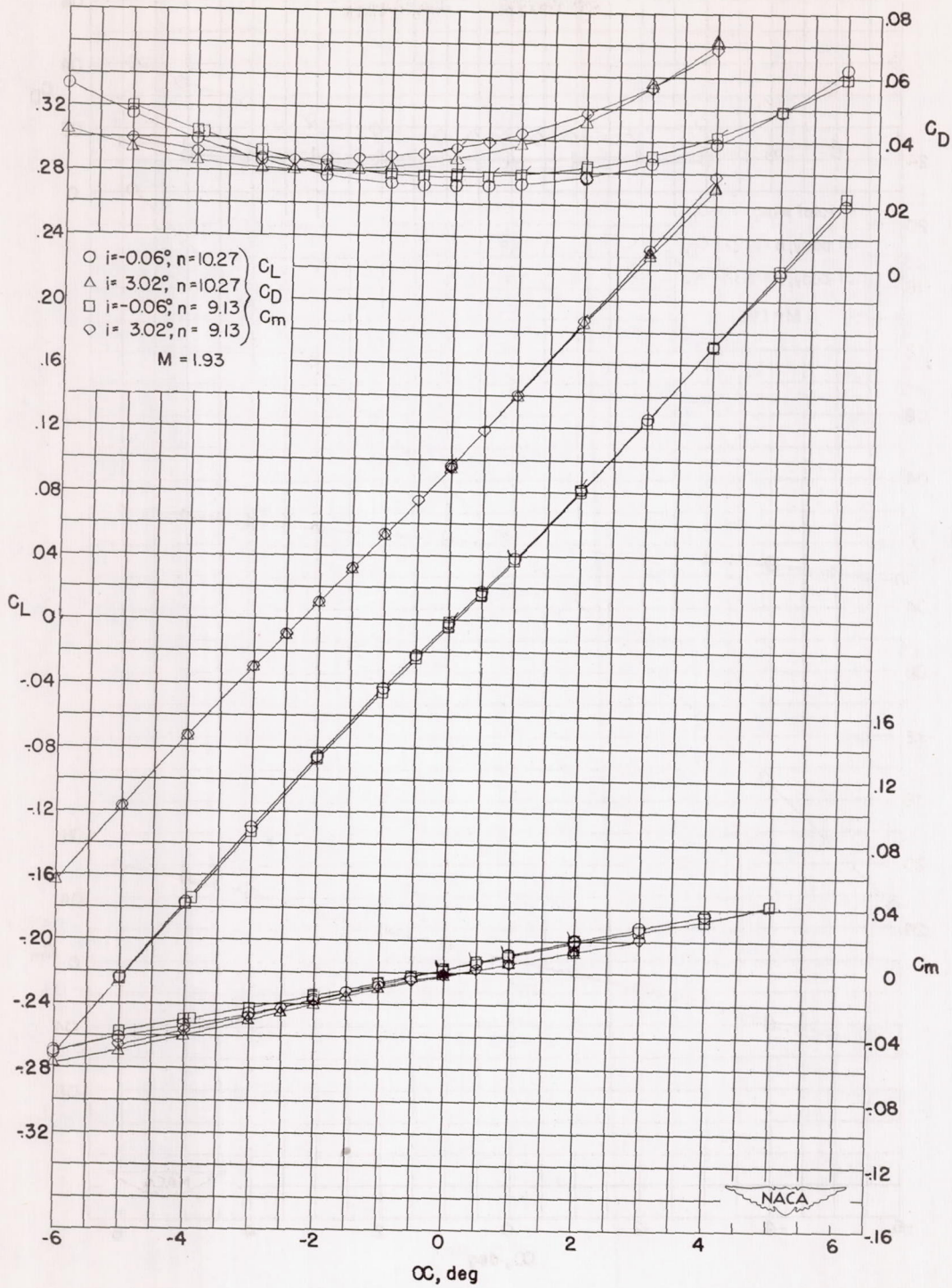

Figure 19.- Aerodynamic characteristics of the wing and body in combination for A = 4 rectangular wing at M = 1.93. Flagged symbols denote check points.

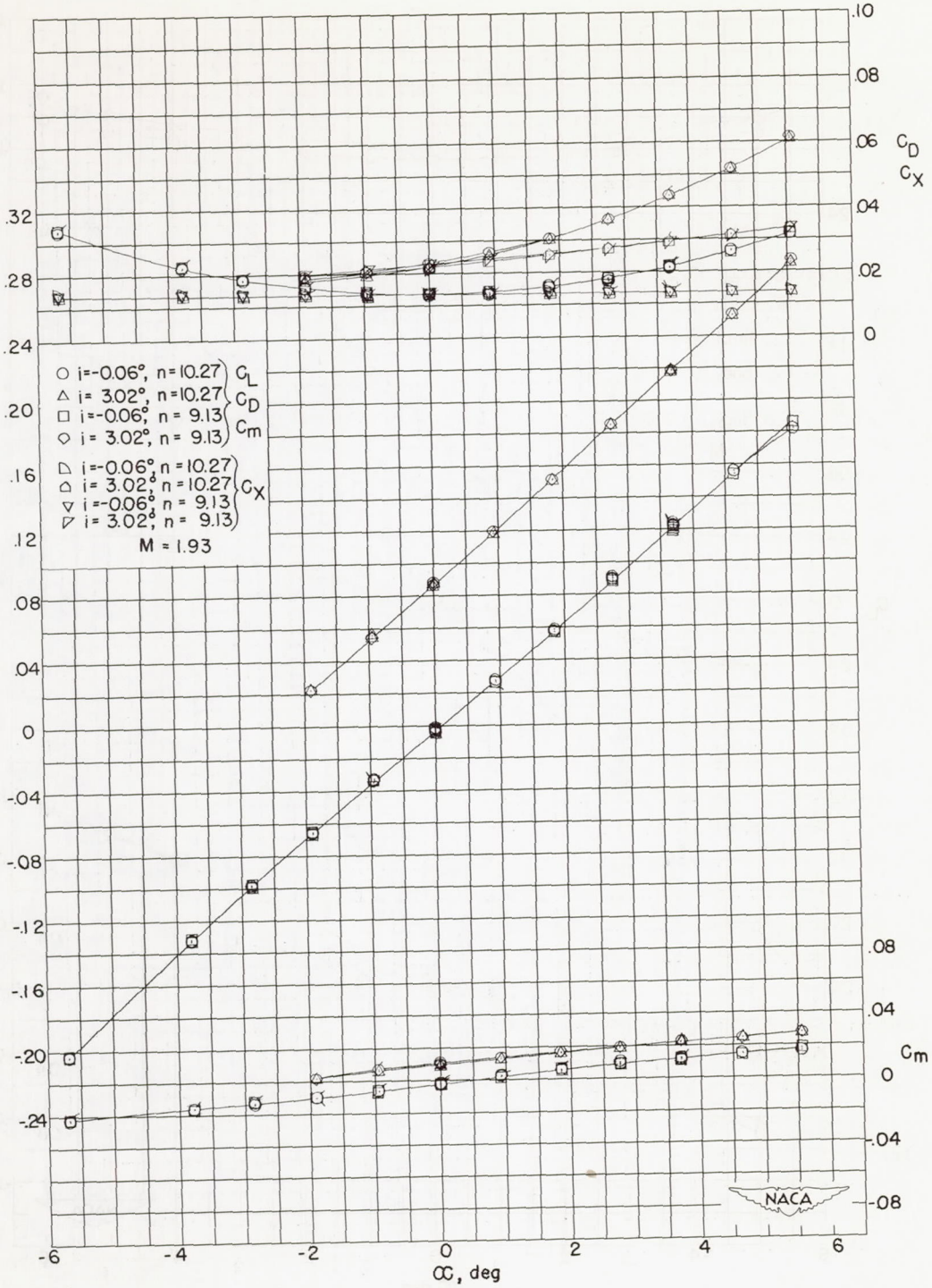

Figure 20.- Aerodynamic characteristics of the wing in the presence of the body for A = 4 rectangular wing at M = 1.93. Flagged symbols denote check points.

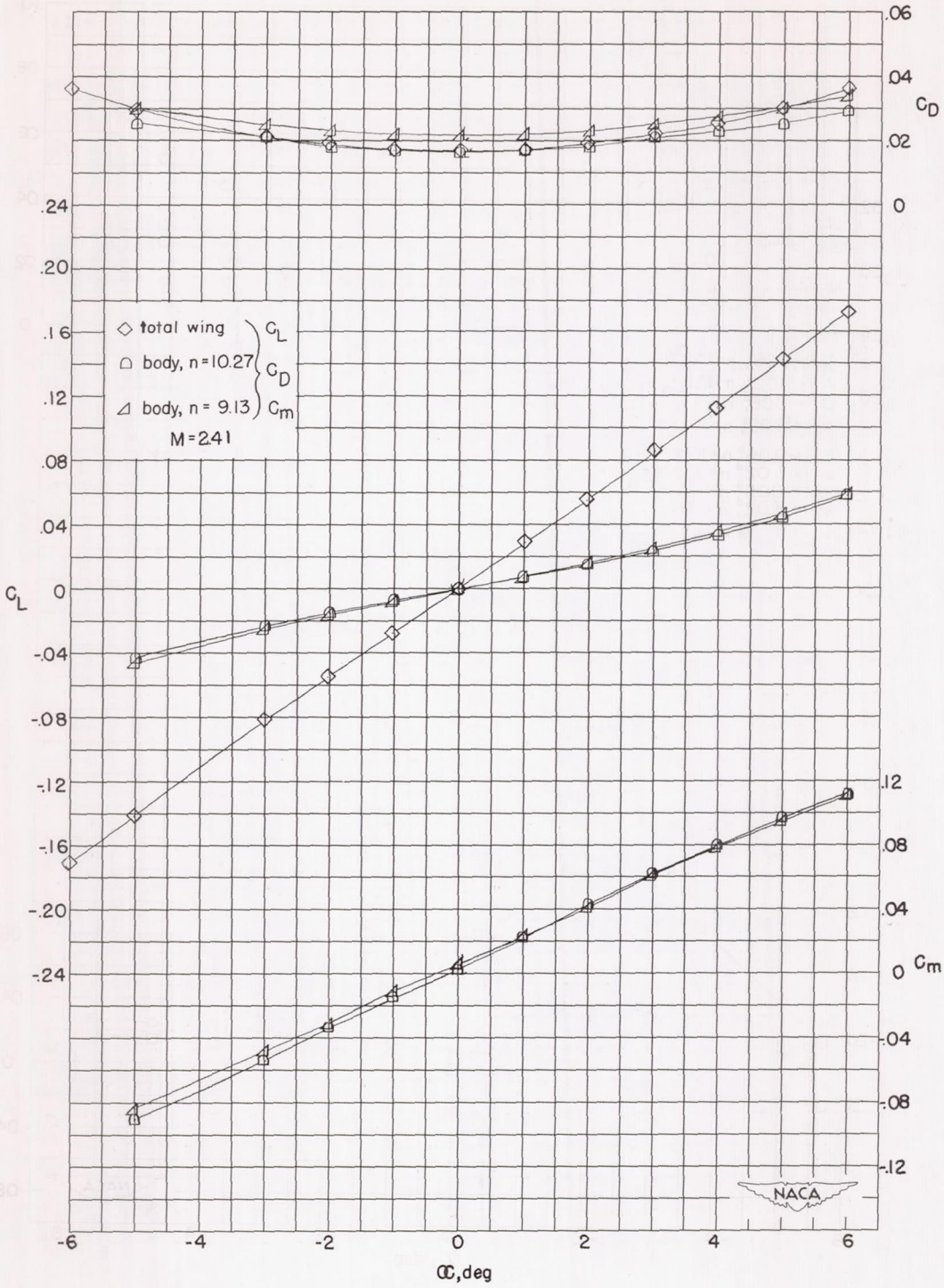

Figure 21.- Aerodynamic characteristics of the bodies alone and A = 2 rectangular wing alone at M = 2.41. (Based on total area of A = 2 wing.) Flagged symbols denote check points.

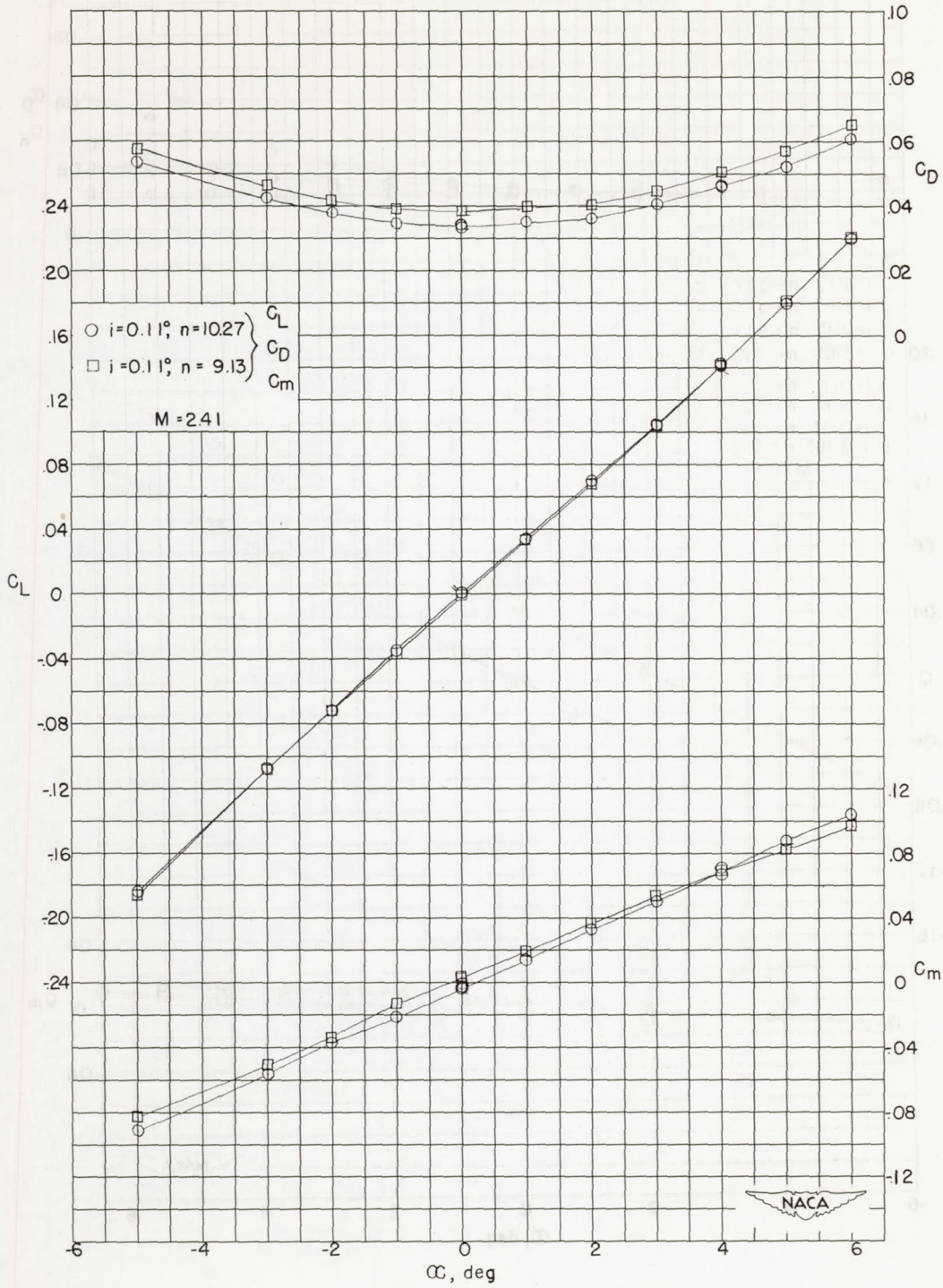

Figure 22.- Aerodynamic characteristics of the wing and body in combination for A = 2 rectangular wing at M = 2.41. Flagged symbols denote check points.

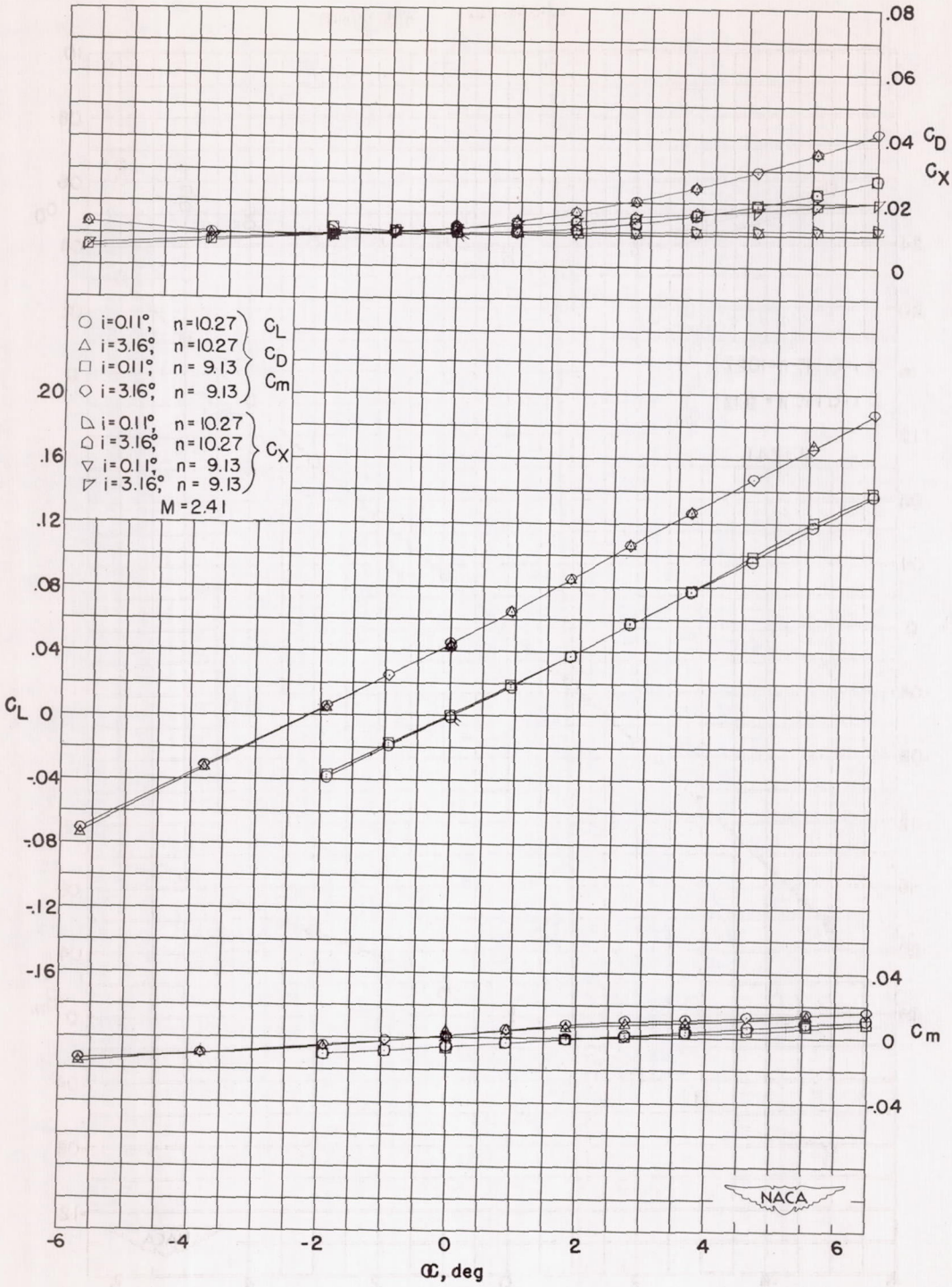

Figure 23.- Aerodynamic characteristics of the wing in the presence of the body for A = 2 rectangular wing at M = 2.41. Flagged symbols denote check points.

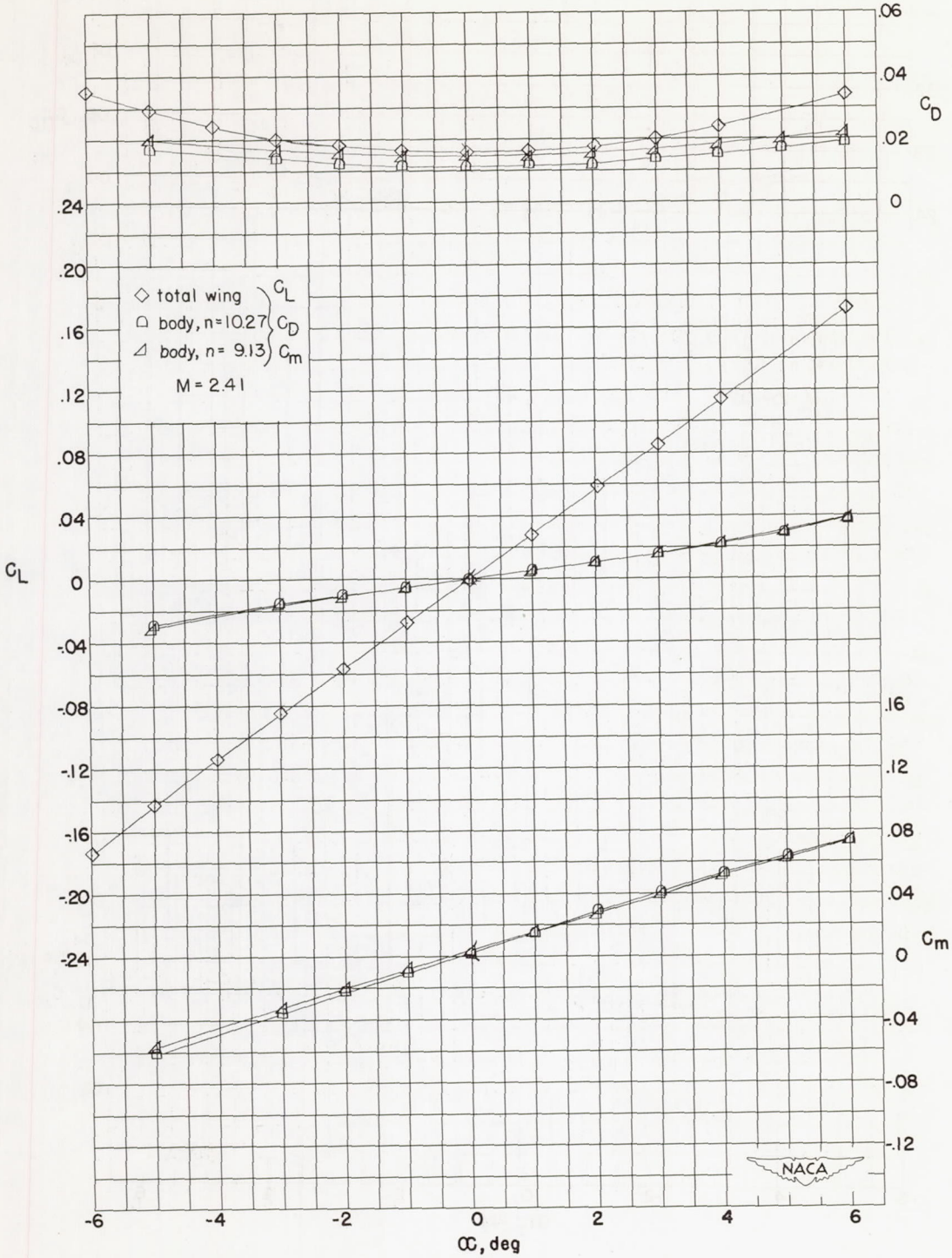

Figure 24.- Aerodynamic characteristics of the bodies alone and A = 3 rectangular wing alone at M = 2.41. (Based on total wing area of A = 3 wing.) Flagged symbols denote check points.

7D

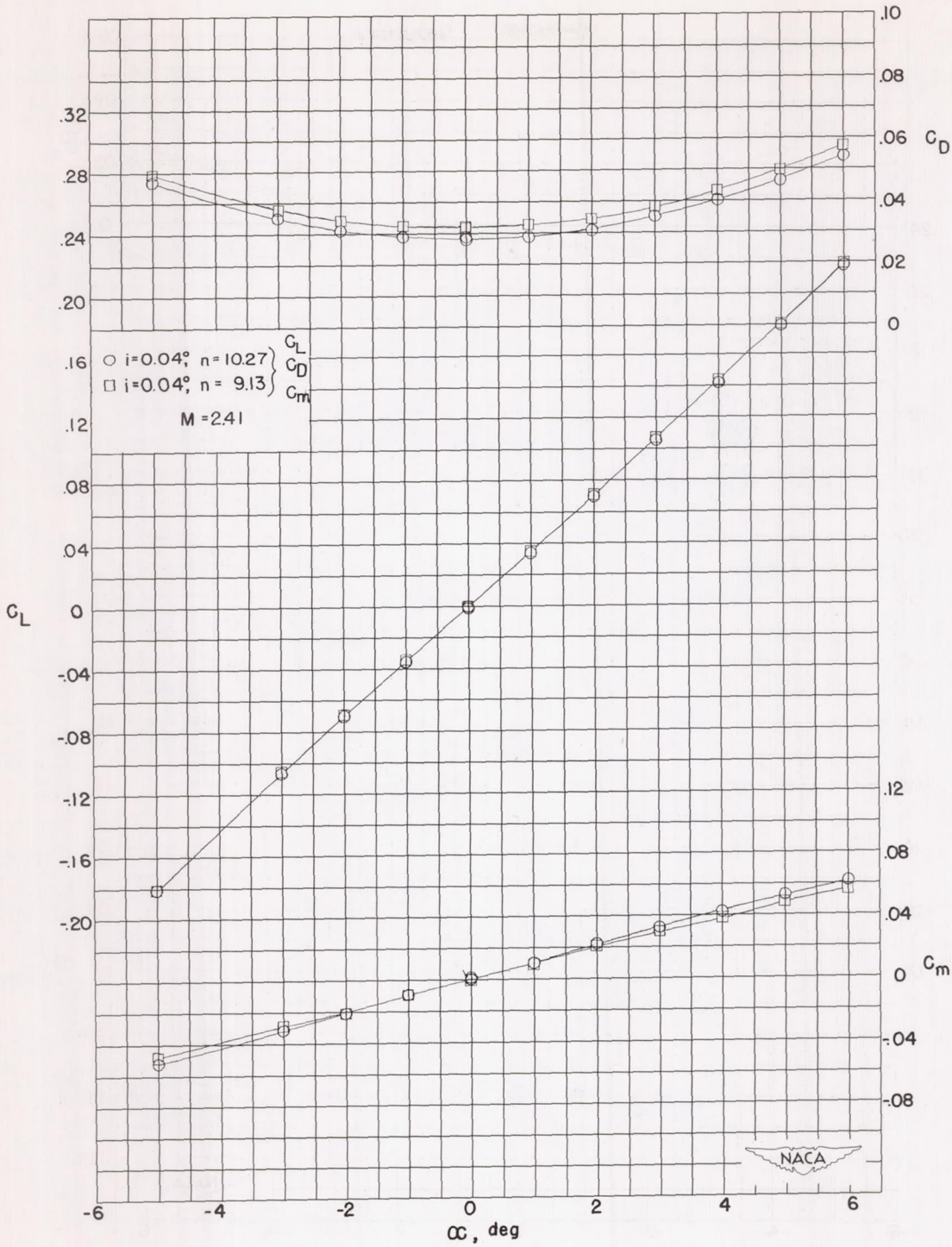

Figure 25.- Aerodynamic characteristics of the wing and body in combination for A = 3 rectangular wing at M = 2.41. Flagged symbols denote check points.

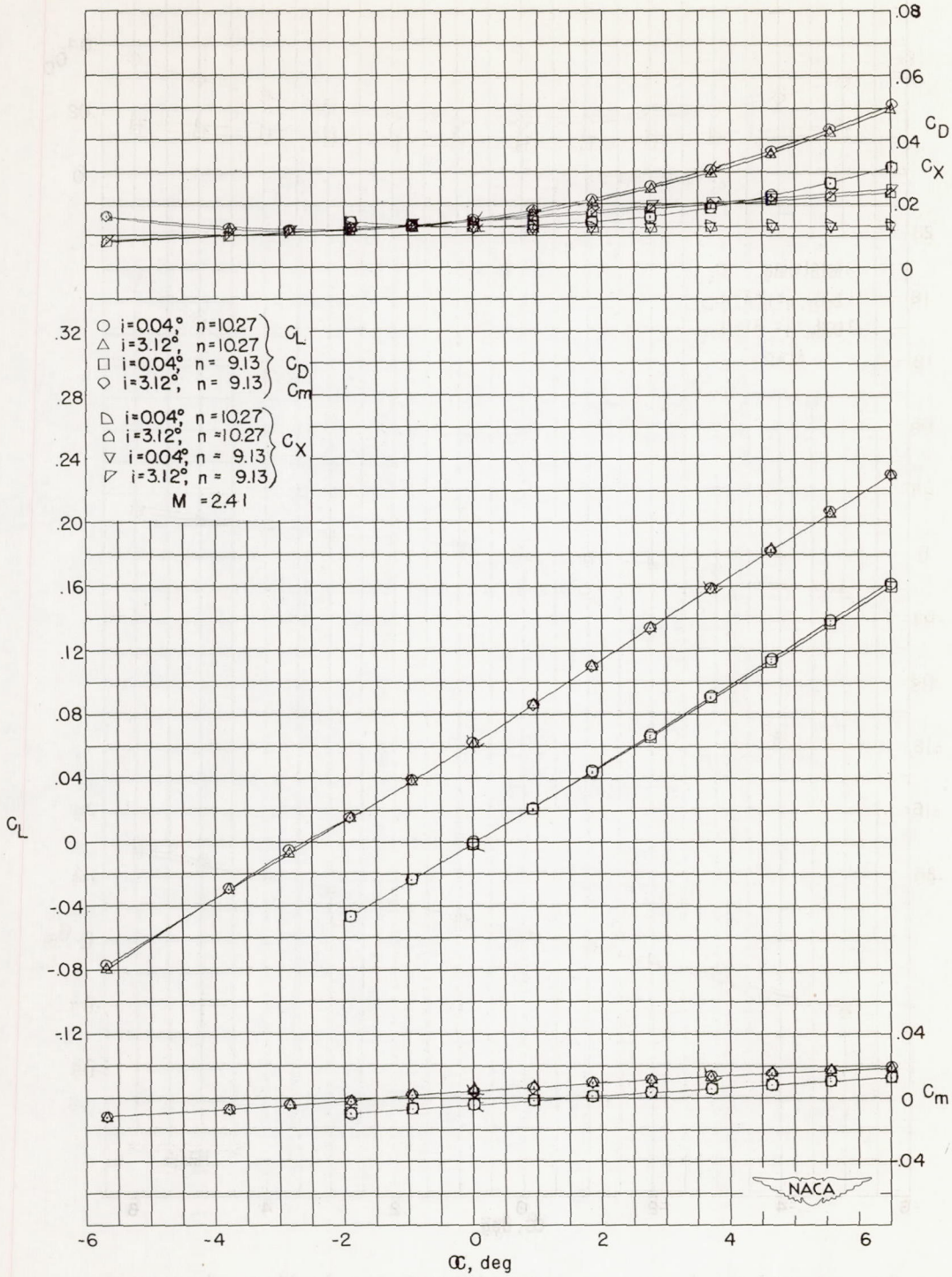

Figure 26.- Aerodynamic characteristics of the wing in the presence of the body for A = 3 rectangular wing at M = 2.41. Flagged symbols denote check points.

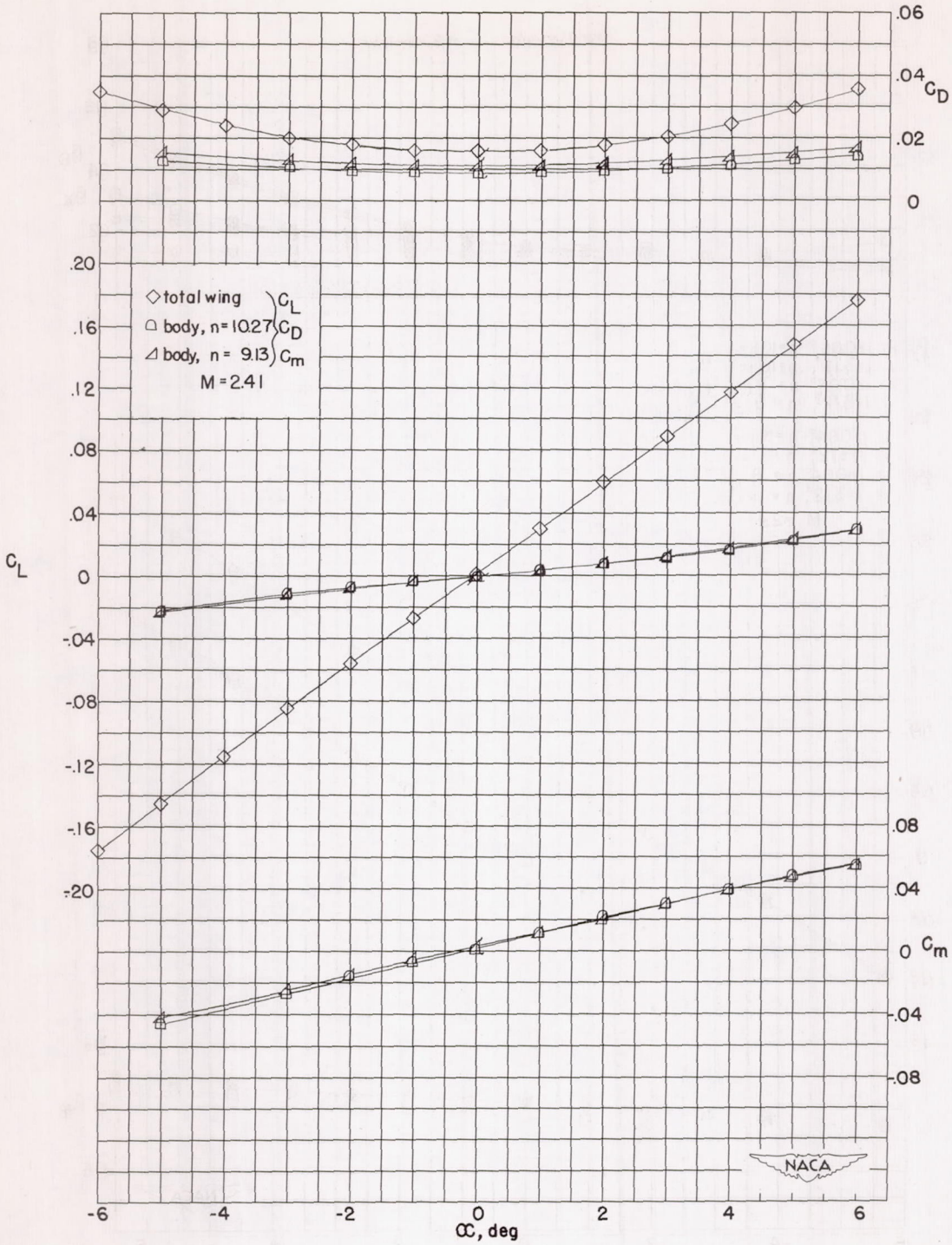

Figure 27.- Aerodynamic characteristics of the bodies alone and A = 4 rectangular wing alone at M = 2.41. (Based on total area of A = 4 wing.) Flagged symbols denote check points.

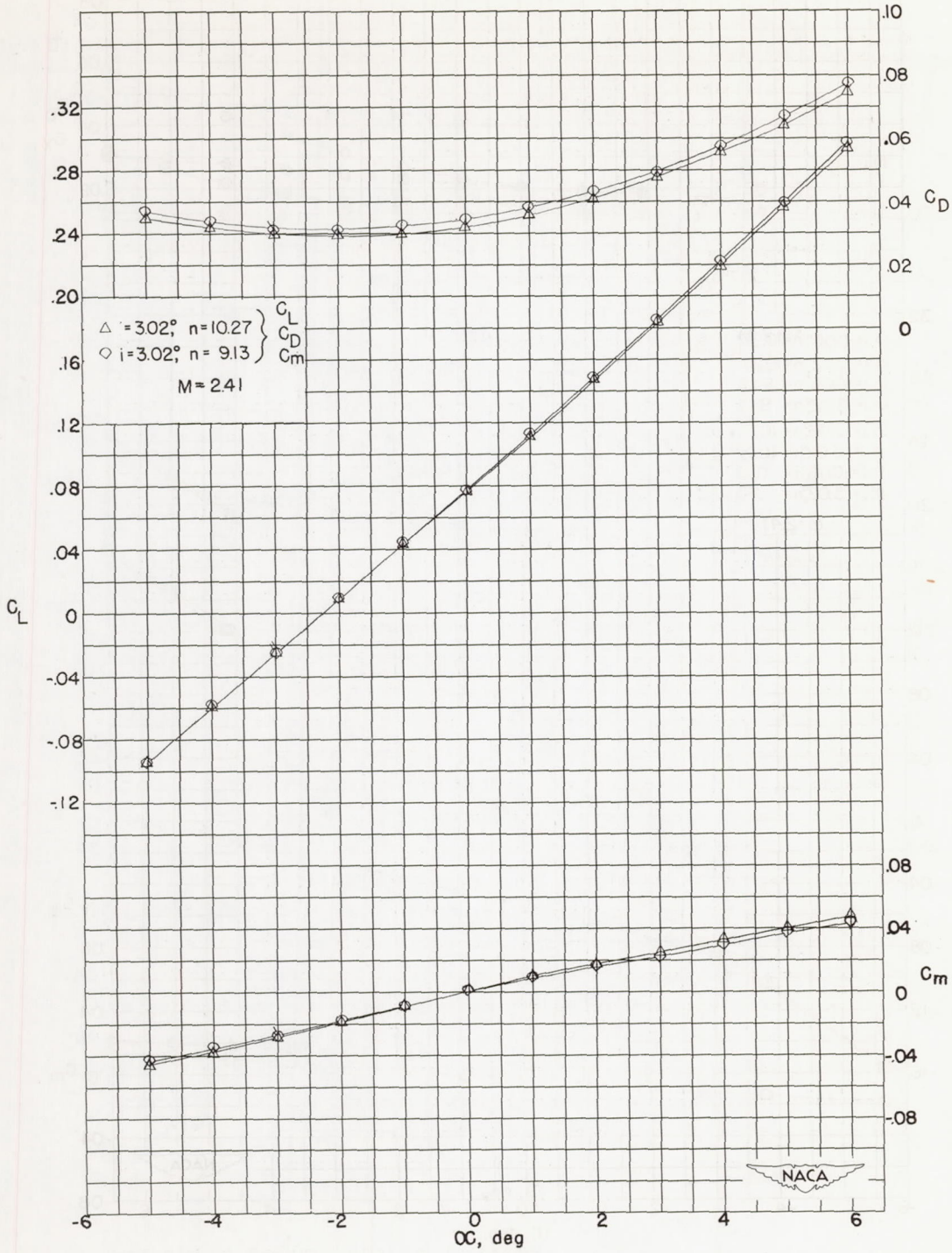

Figure 28.- Aerodynamic characteristics of the wing and body in combination for A = 4 rectangular wing at M = 2.41. Flagged symbols denote check points.

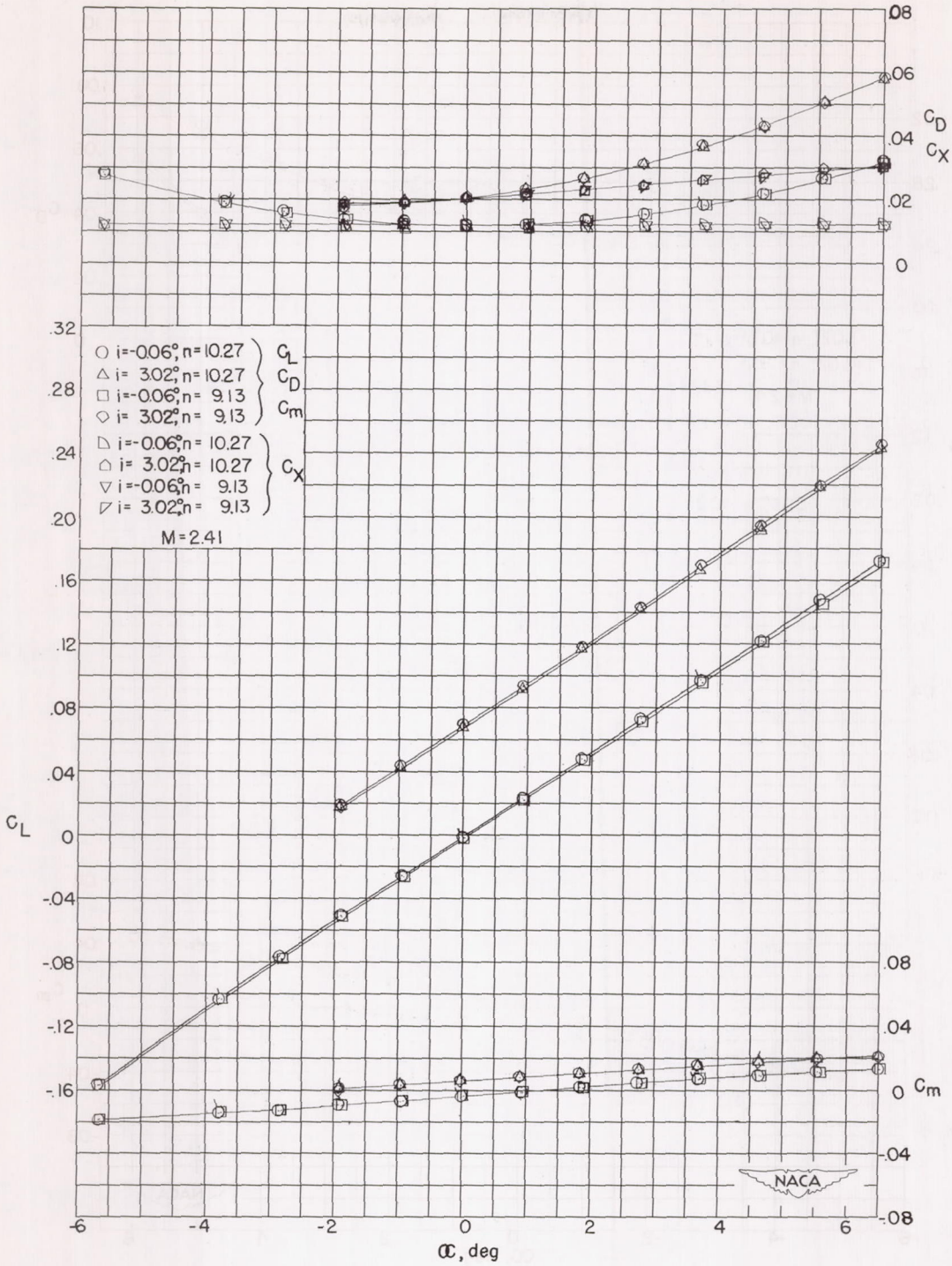

Figure 29.- Aerodynamic characteristics of the wing in the presence of the body for A = 4 rectangular wing at M = 2.41. Flagged symbols denote check points.

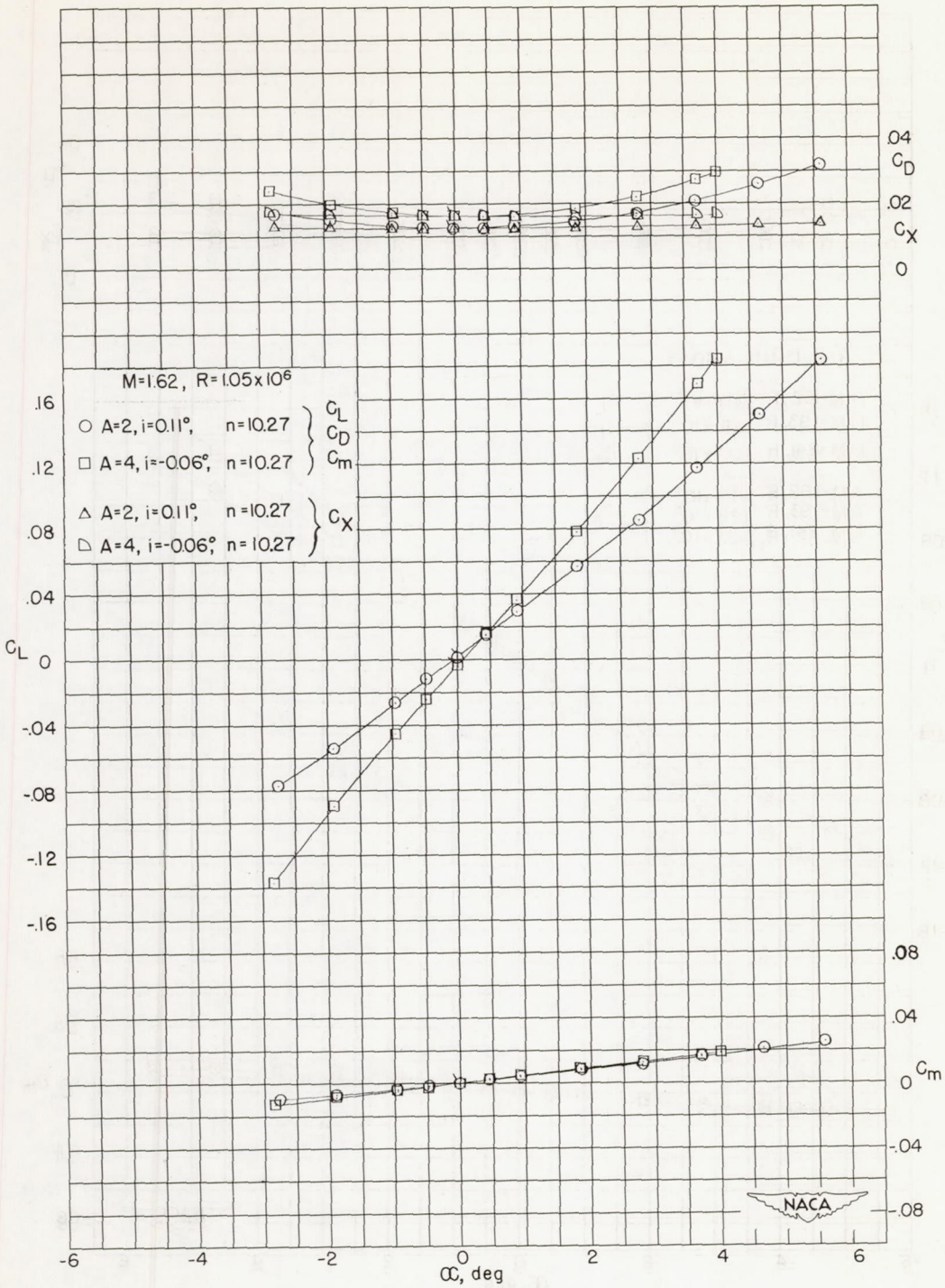

Figure 30.- Aerodynamic characteristics of the wing in the presence of the body for $A = 2$ and $A = 4$ rectangular wings at $M = 1.62$ and $R = 1.05 \times 10^6$. Flagged symbols denote check points.

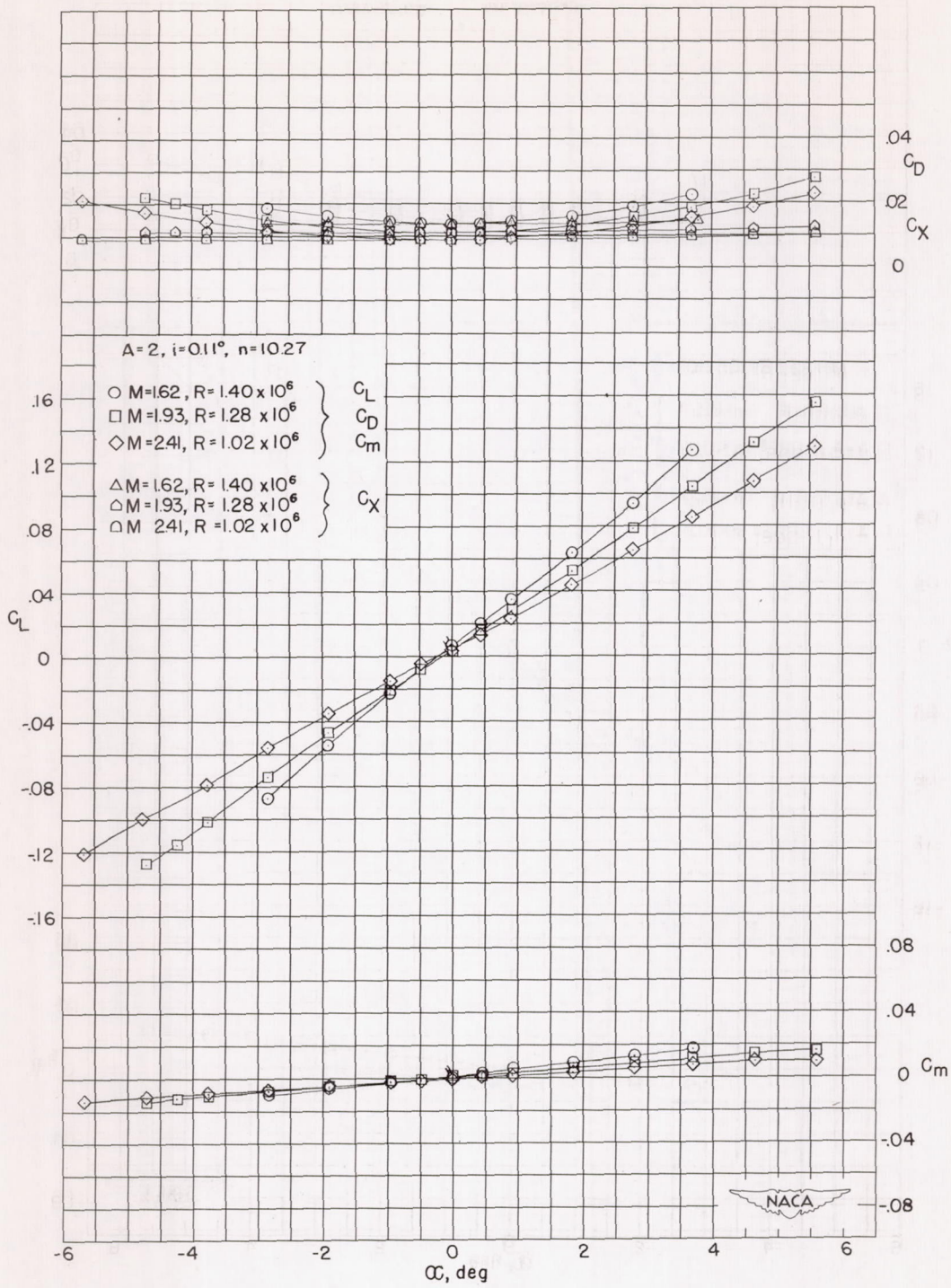

Figure 31.- Aerodynamic characteristics of the wing in the presence of the body for $A = 2$ rectangular wing at $M = 1.62$ and $R = 1.40 \times 10^6$, $M = 1.93$ and $R = 1.28 \times 10^6$, $M = 2.41$ and $R = 1.02 \times 10^6$. Flagged symbols denote check points.

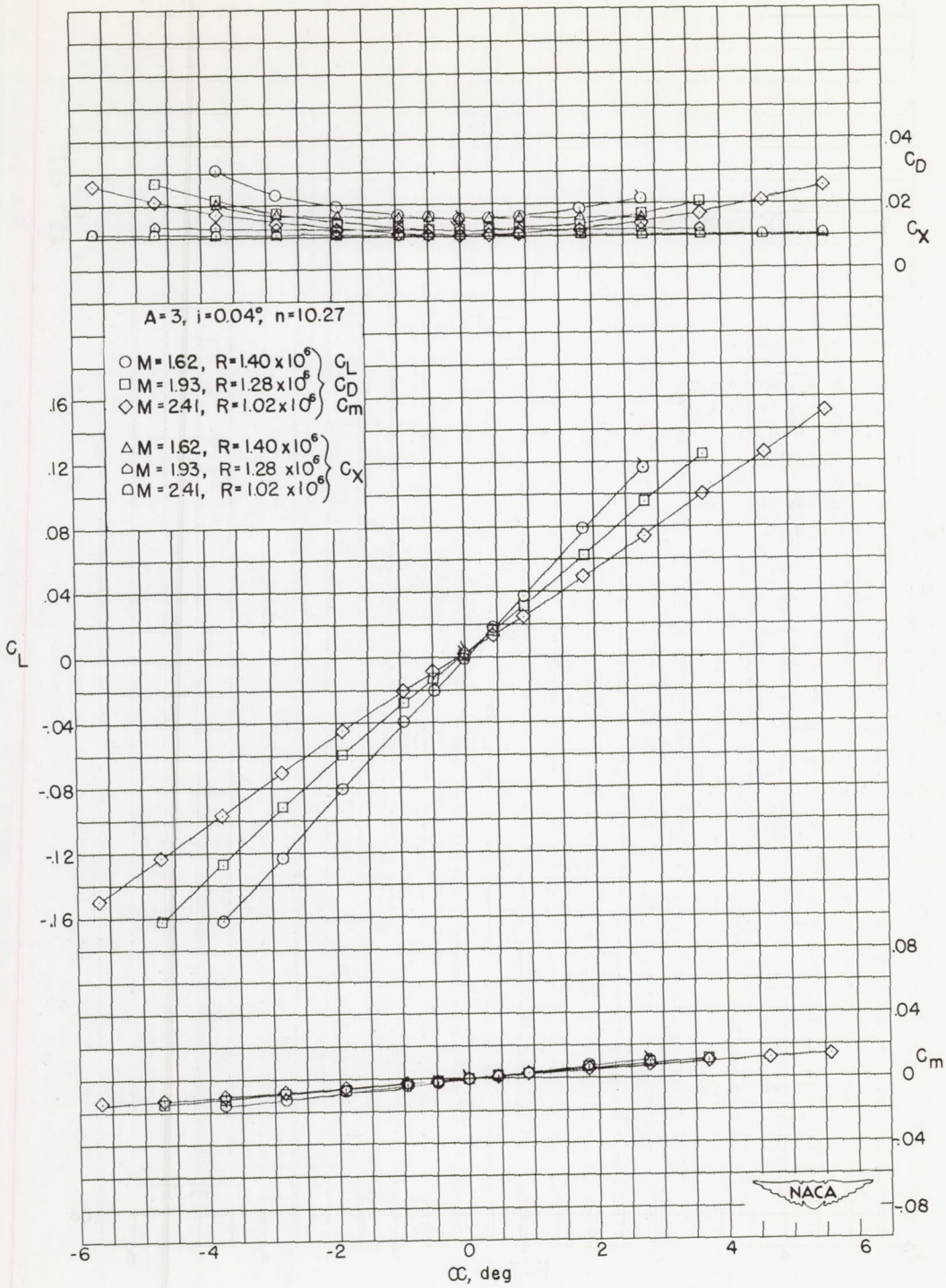

Figure 32.- Aerodynamic characteristics of the wing in the presence of the body for $A = 3$ rectangular wing at $M = 1.62$ and $R = 1.40 \times 10^6$, $M = 1.93$ and $R = 1.28 \times 10^6$, $M = 2.41$ and $R = 1.02 \times 10^6$. Flagged symbols denote check points.

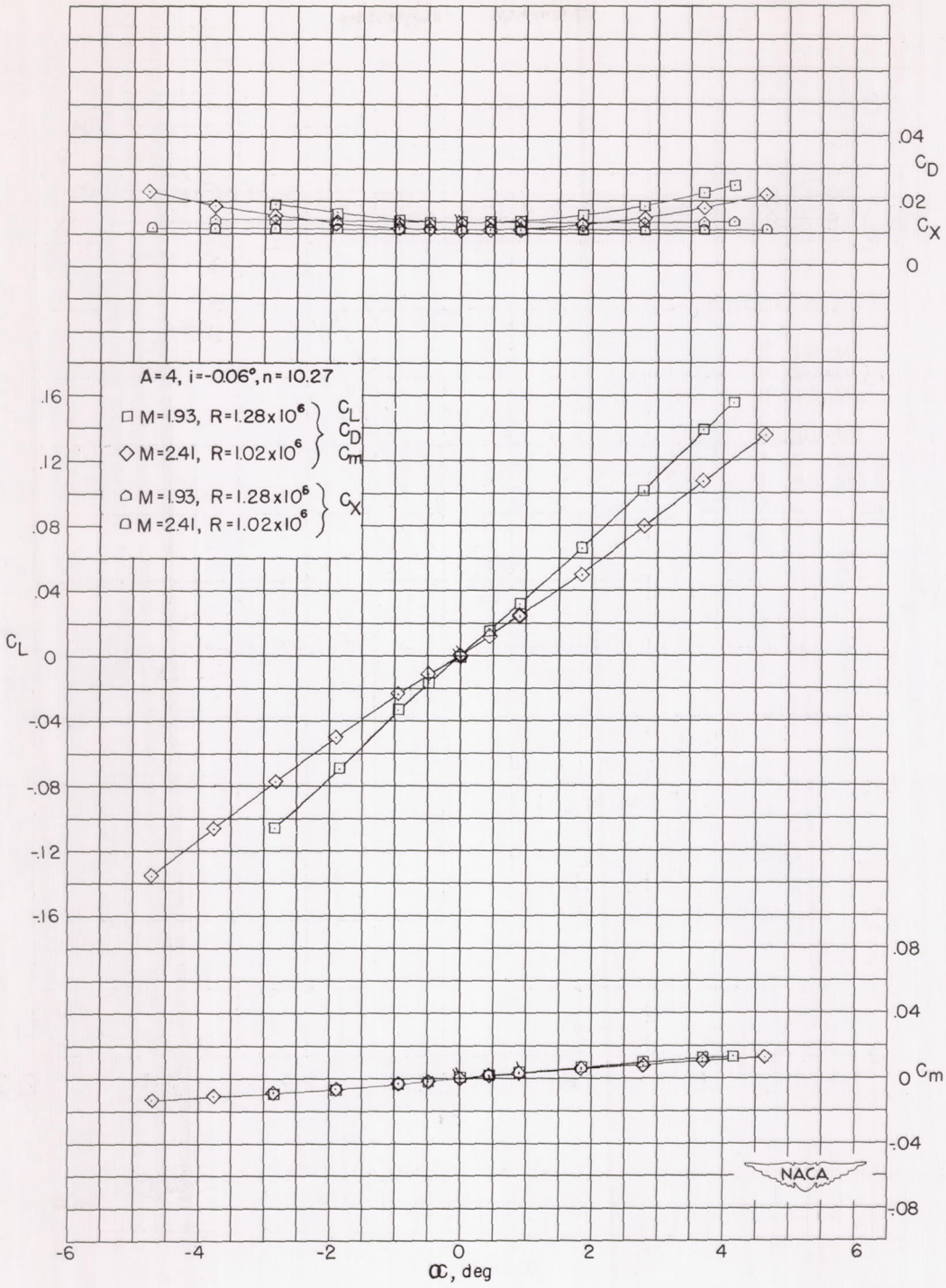

Figure 33.- Aerodynamic characteristics of the wing in the presence of the body for $A = 4$ rectangular wing at $M = 1.93$ and $R = 1.28 \times 10^6$, $M = 2.41$ and $R = 1.02 \times 10^6$. Flagged symbols denote check points.

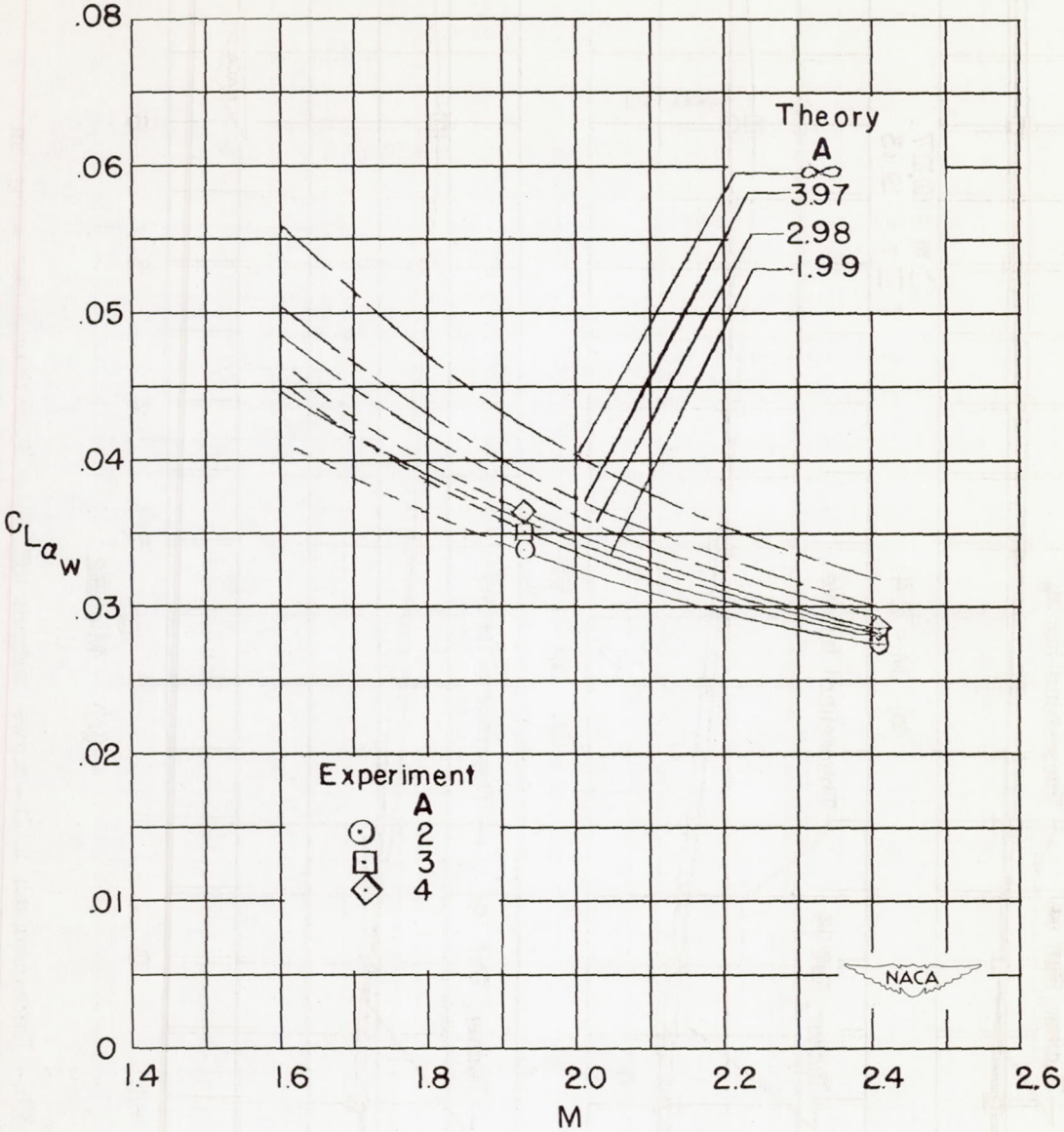

Figure 34.- Lift-curve slopes of rectangular wings alone.

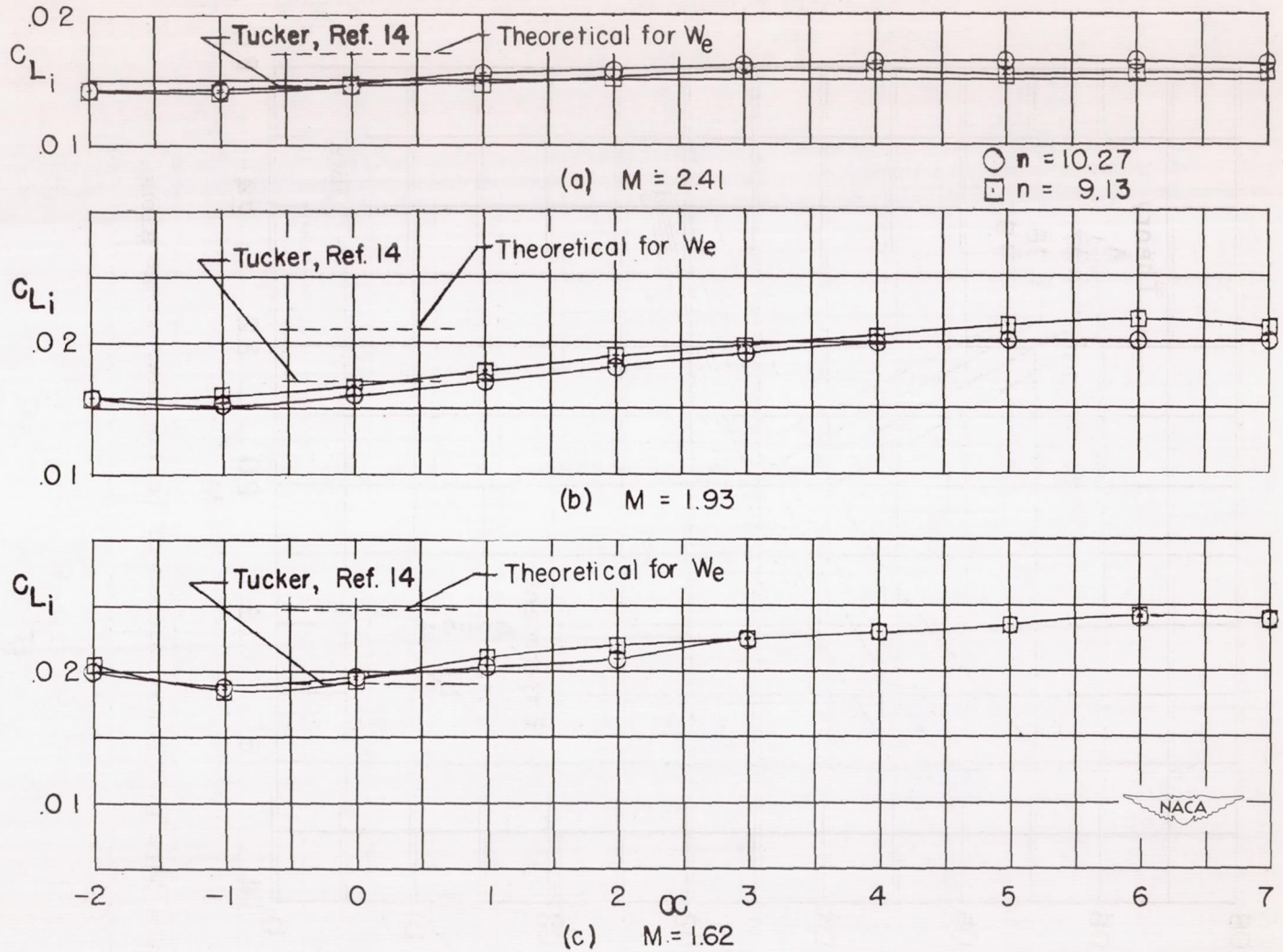

Figure 35.- Incremental lift-curve slopes of A = 2 rectangular wing in the presence of the body due to varying angle of incidence.

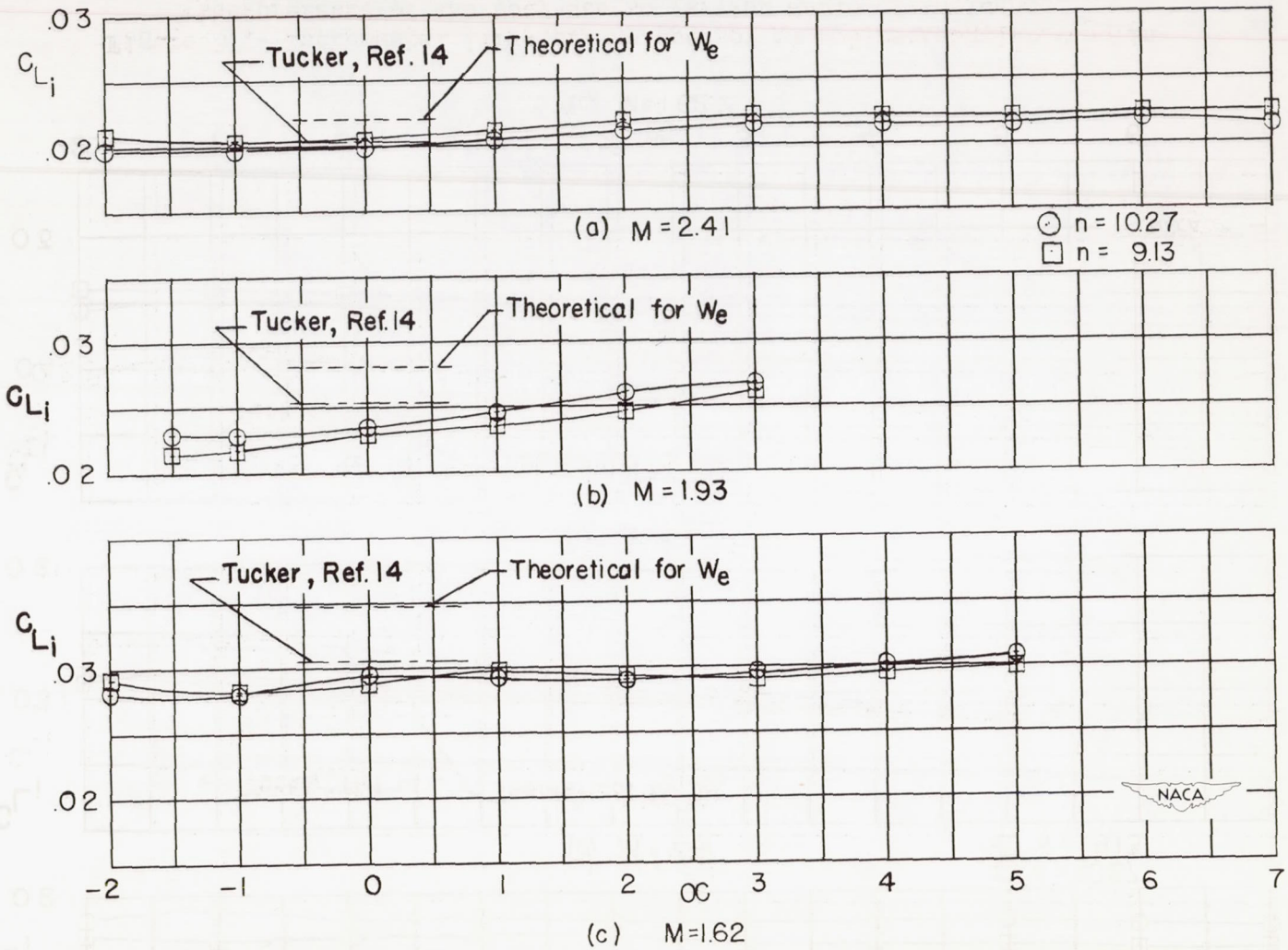

Figure 36.- Incremental lift-curve slopes of A = 3 rectangular wing in the presence of the body due to varying angle of incidence.

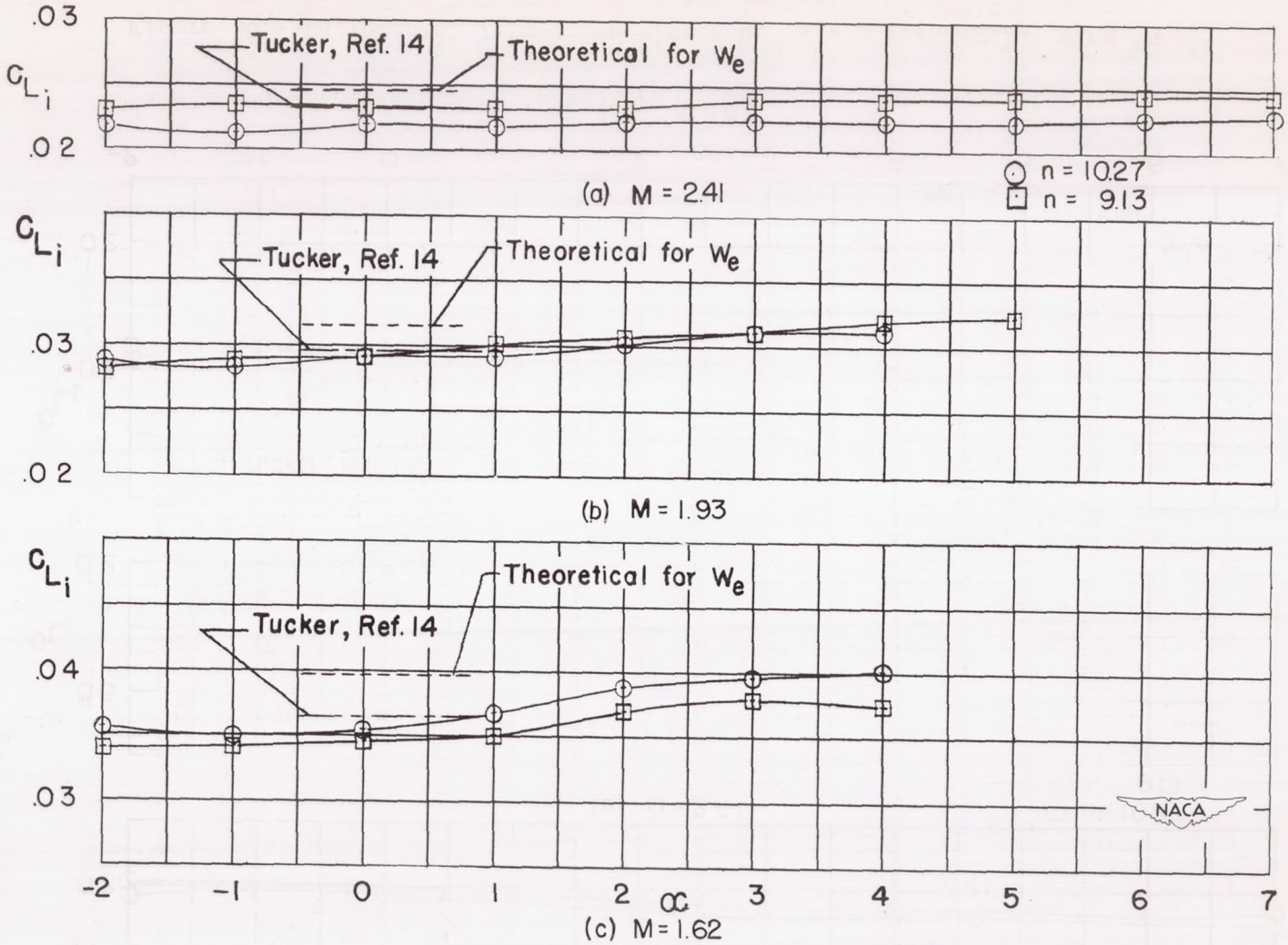

Figure 37.- Incremental lift-curve slopes of A = 4 rectangular wing in the presence of the body due to varying angle of incidence.

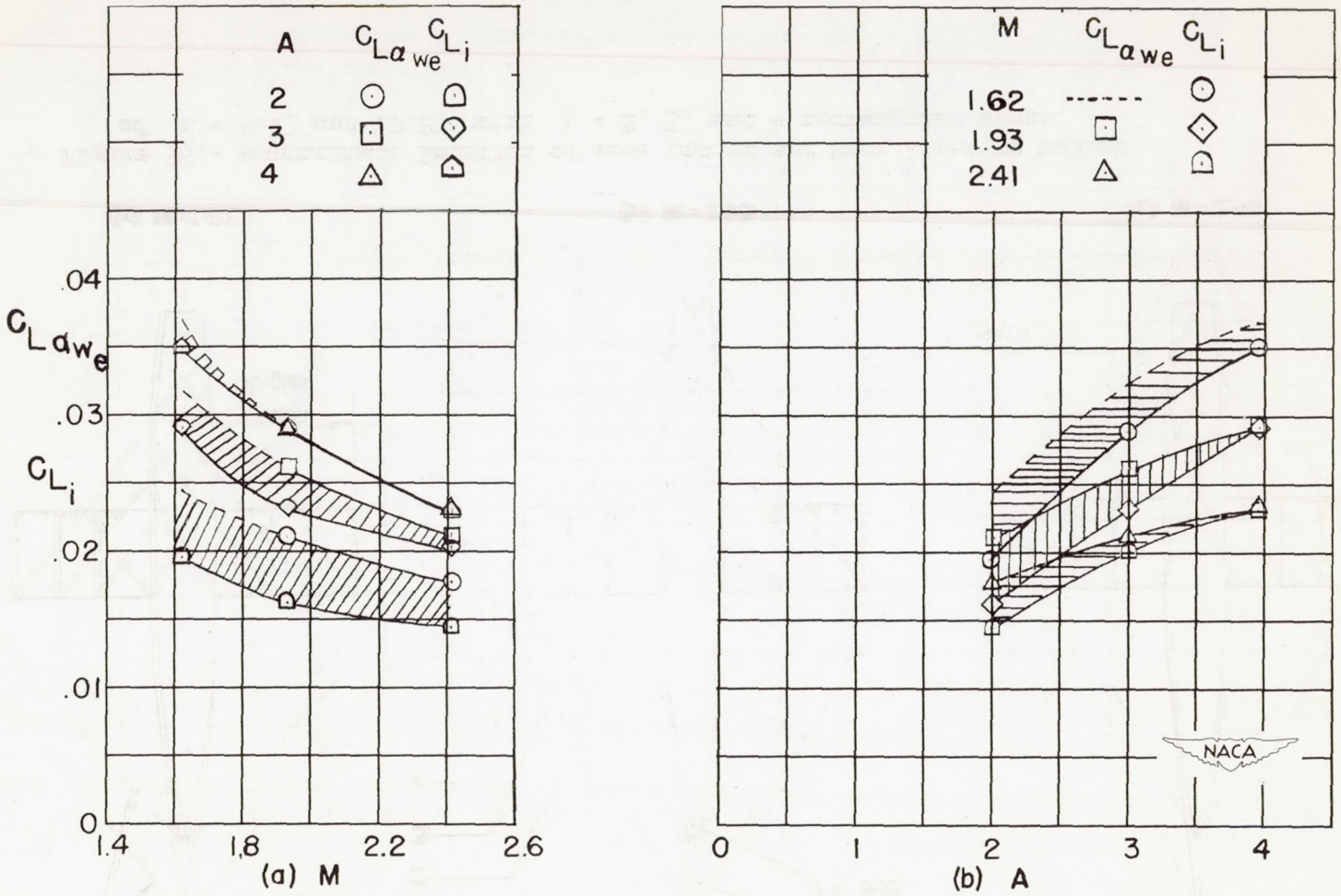

Figure 38.- Comparison of lift-curve slopes of the exposed wings alone due to varying angle of attack, $C_{L_{\alpha_{we}}}$, and wings due to varying angle of incidence, C_{L_i}, as a function of M and A.

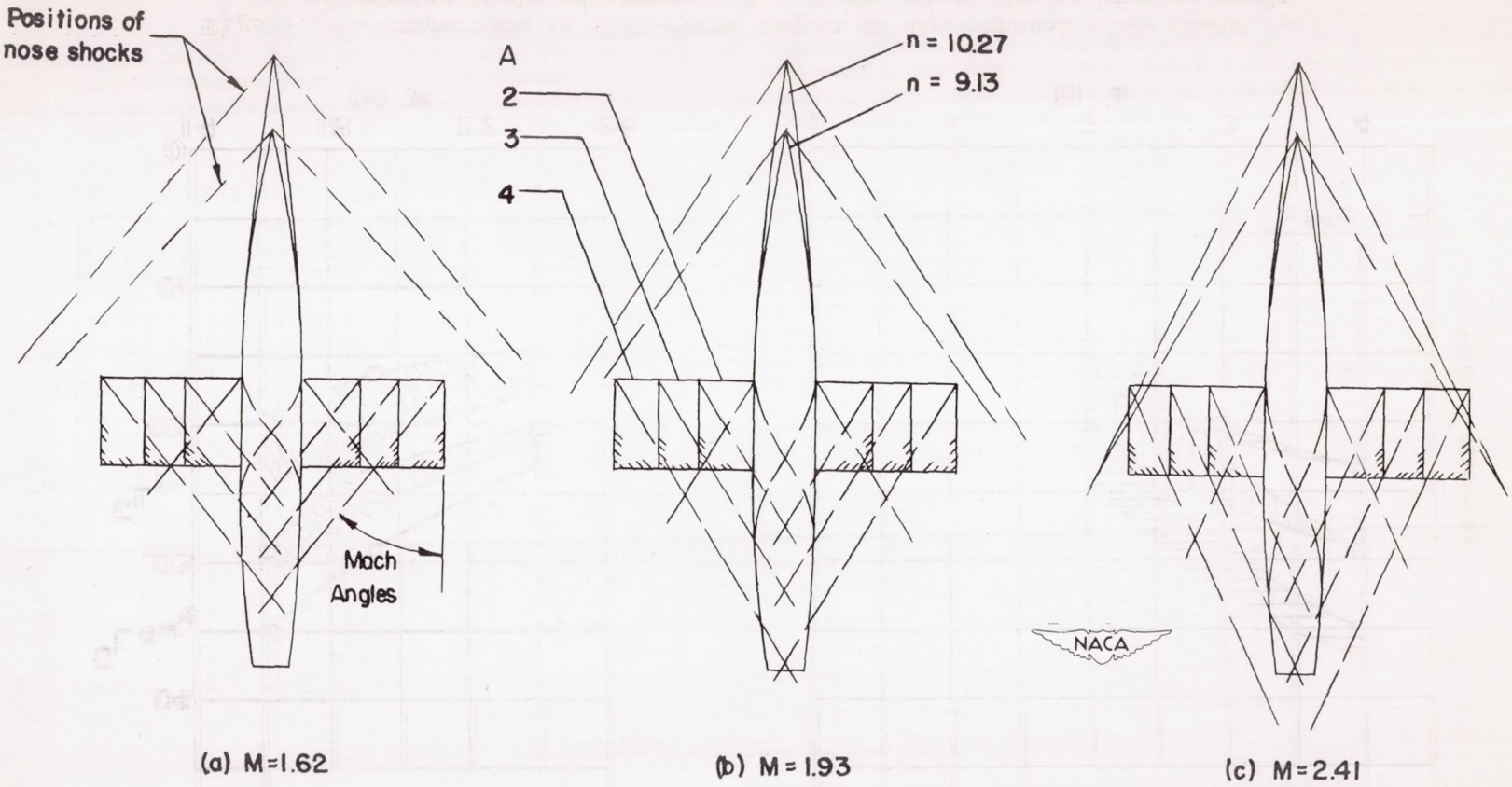

Figure 39.- Approximate location of nose shocks and Mach lines on bodies of $n = 9.13$ and 10.27 with $A = 2$, 3, and 4 rectangular wings.

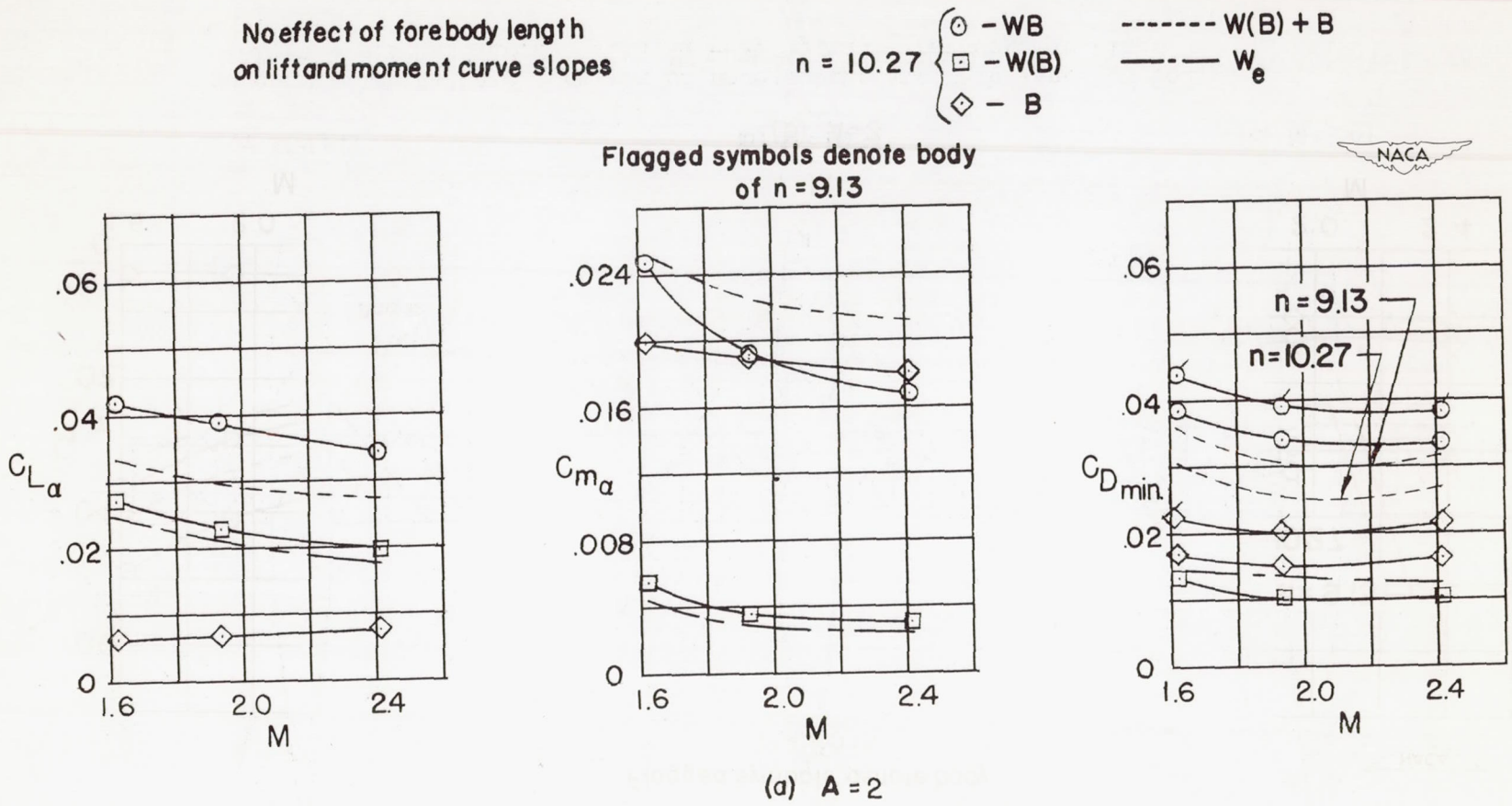

(a) A = 2

Figure 40.- Aerodynamic characteristics of WB, W(B), B, and W_e for bodies of n = 9.13 and 10.27 and wings at $i \cong 0^\circ$ and 3°.

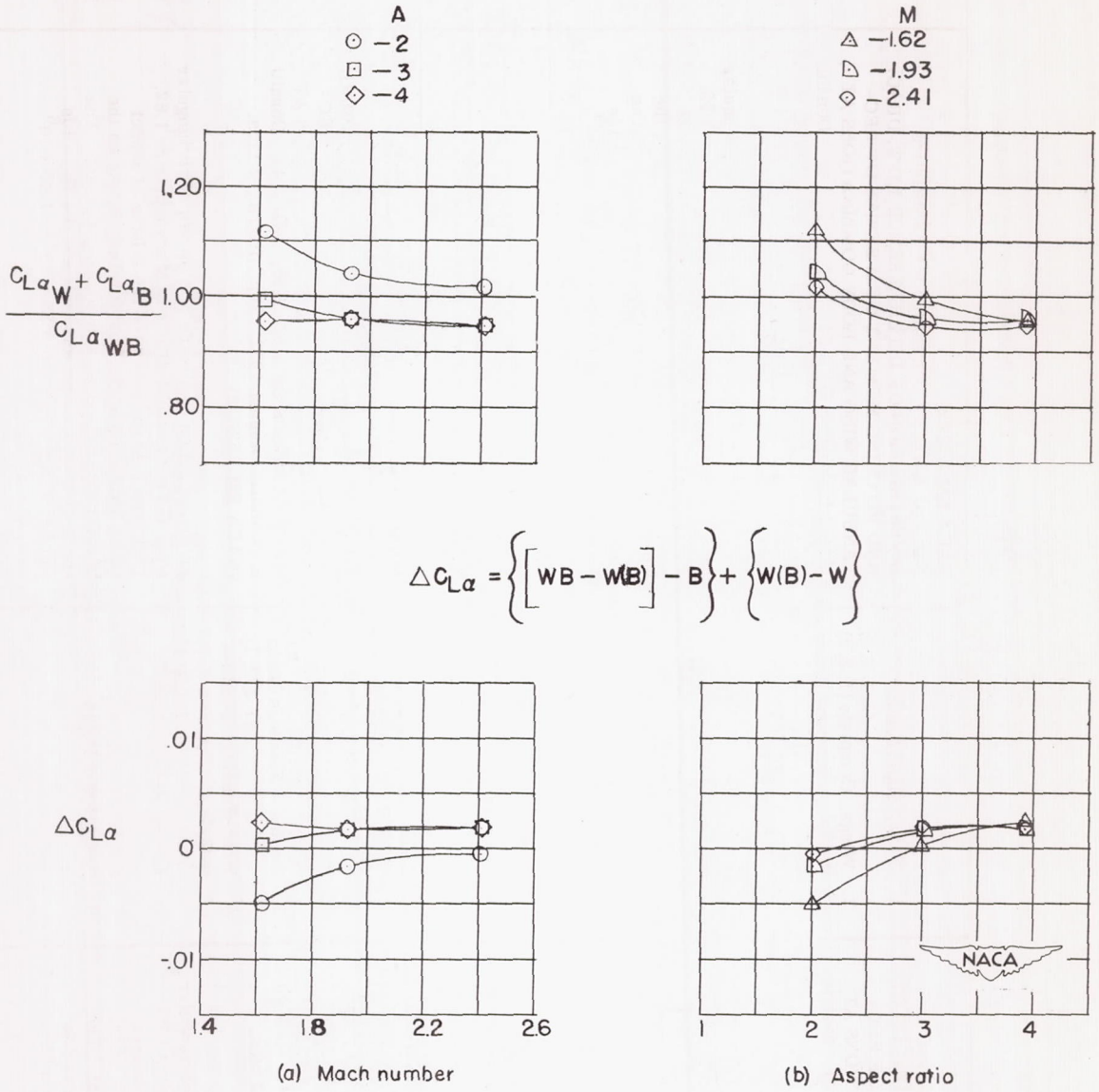

(a) Mach number

(b) Aspect ratio

Figure 46.- The validity of the concept of wing-lift carry-over as a function of Mach number and aspect ratio.

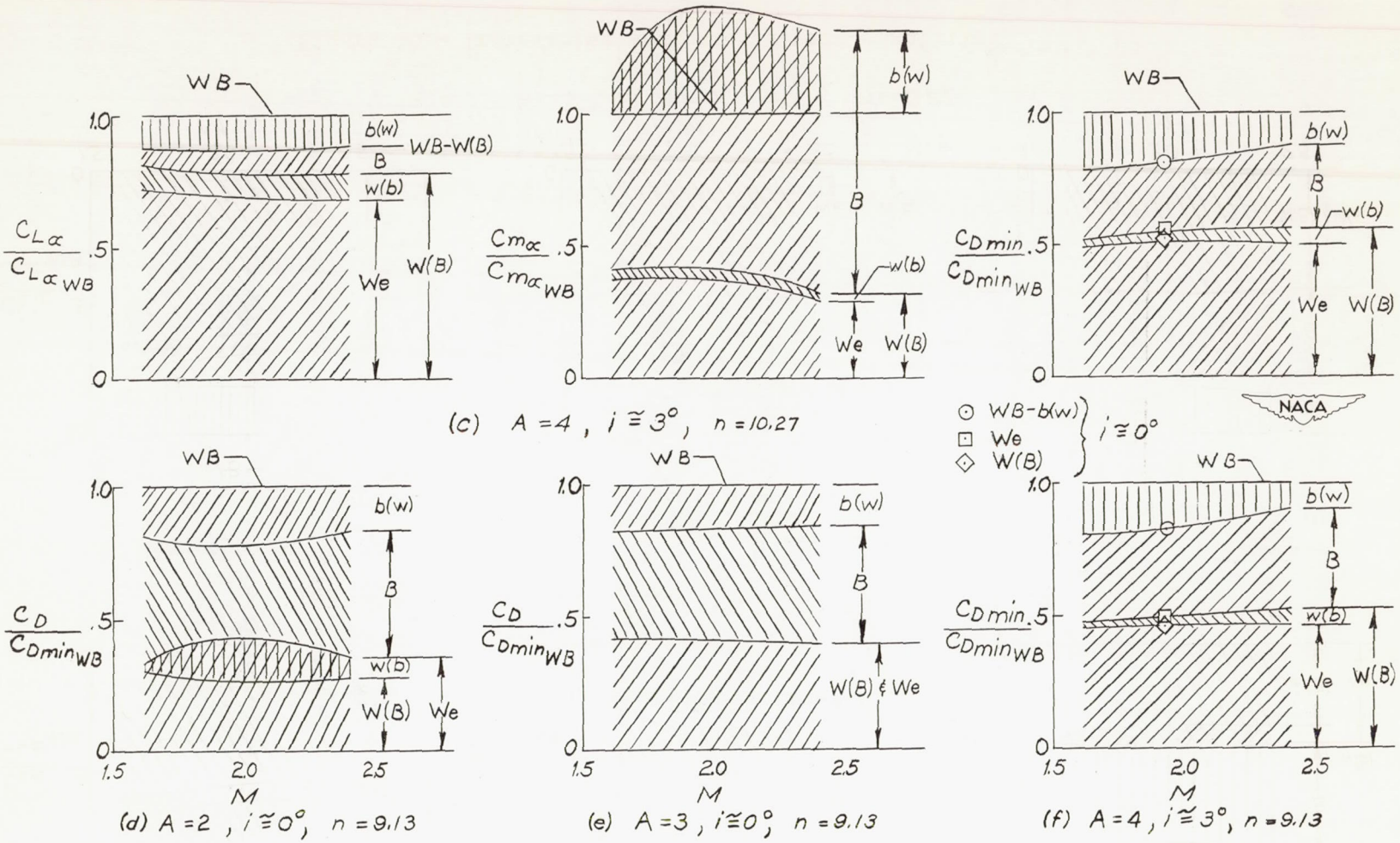

(c) A = 4, $i \cong 3°$, n = 10.27

(d) A = 2, $i \cong 0°$, n = 9.13

(e) A = 3, $i \cong 0°$, n = 9.13

(f) A = 4, $i \cong 3°$, n = 9.13

Figure 45.- Concluded.

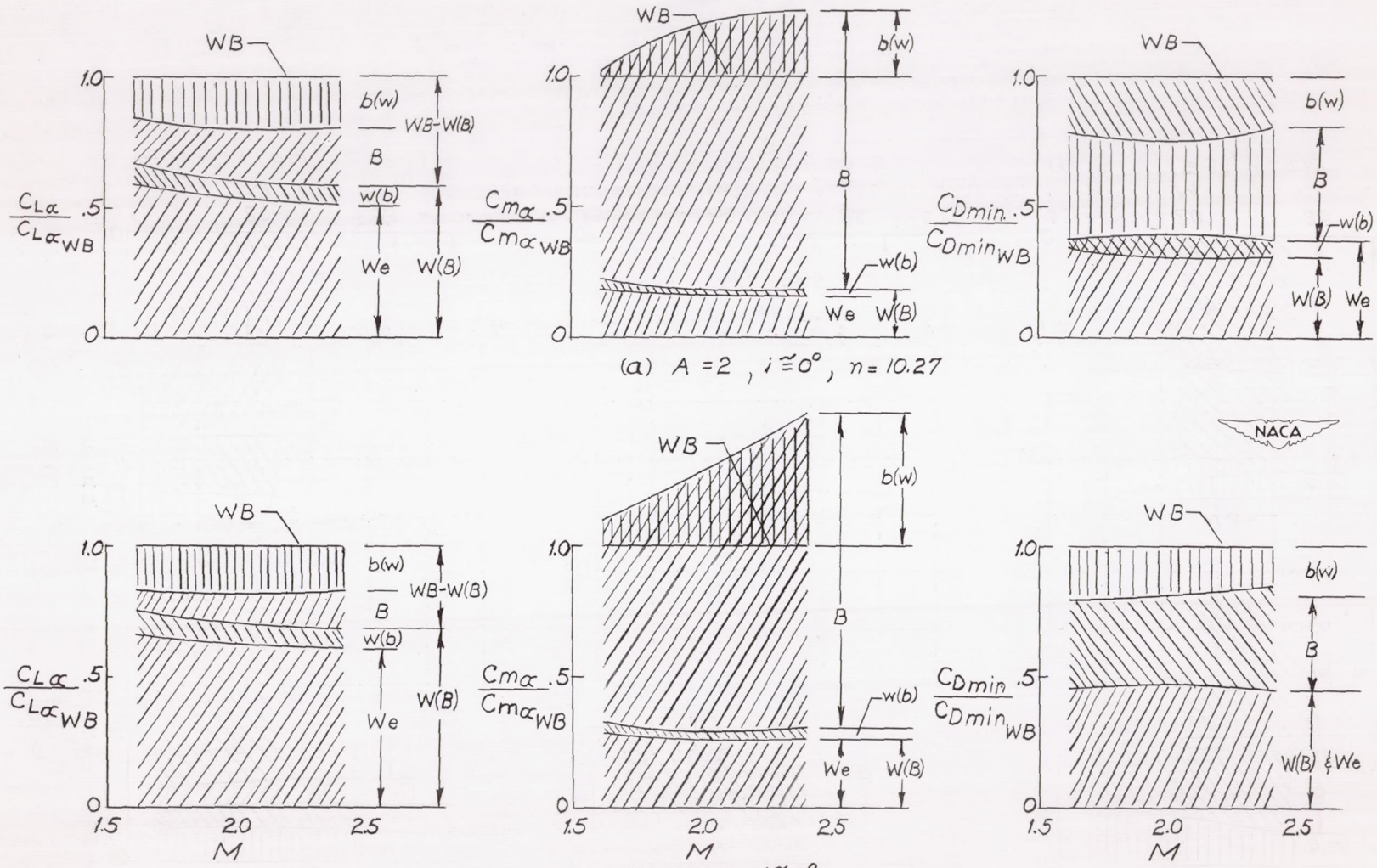

(a) $A = 2$, $i \cong 0°$, $n = 10.27$

(b) $A = 3$, $i \cong 0°$, $n = 10.27$

Figure 45.- Incremental and interference quantities.

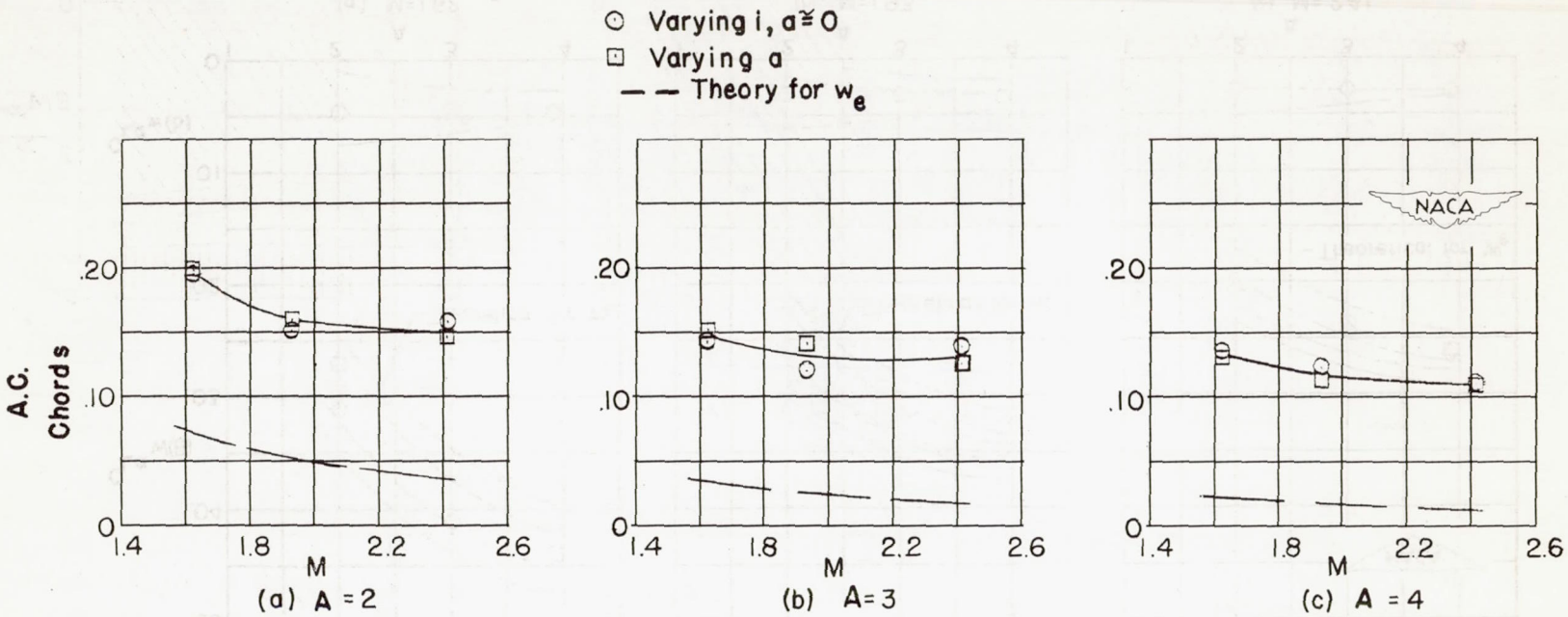

Figure 44.- Location of aerodynamic center of W(B) due to varying incidence angle and varying angle of attack.

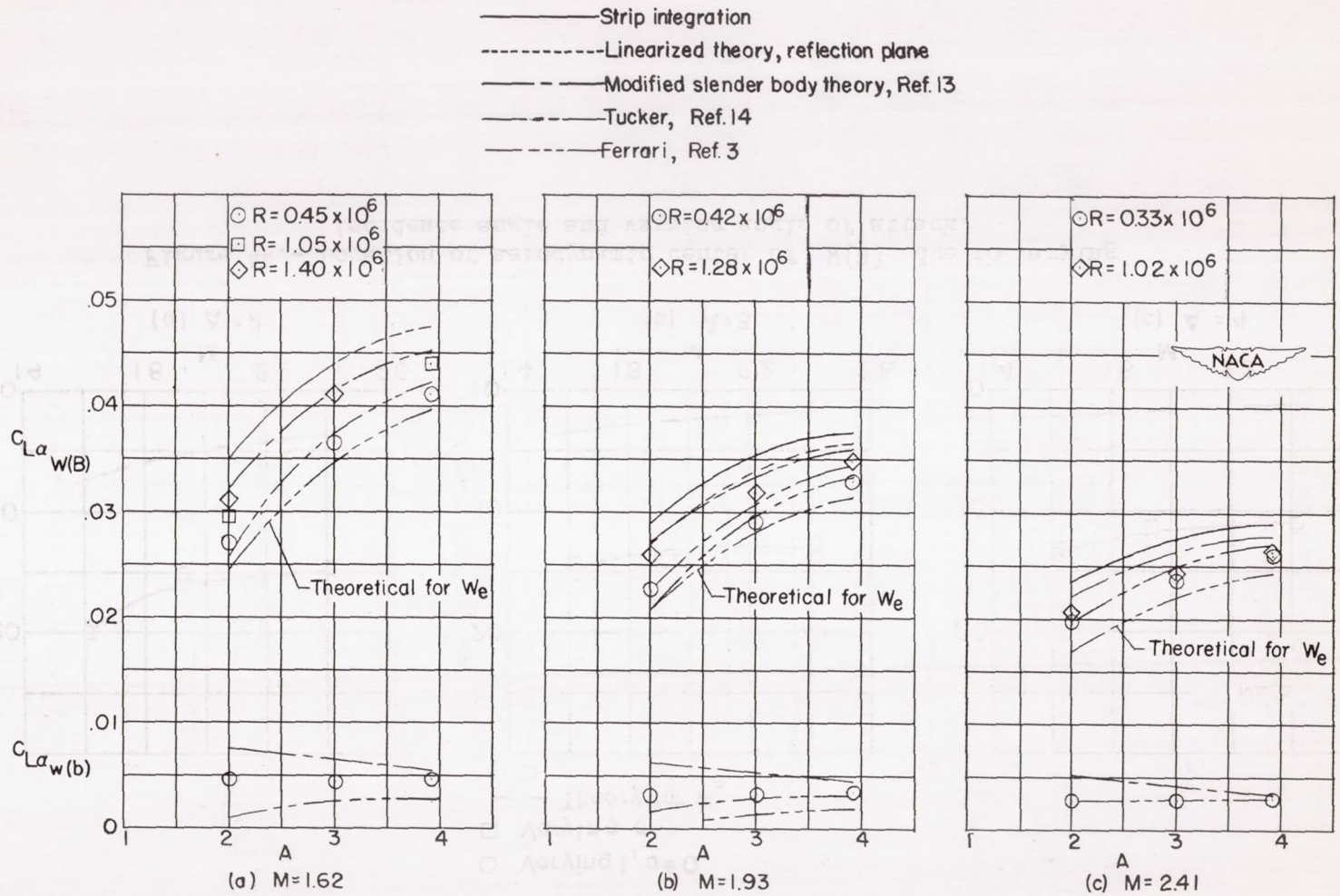

Figure 43.- Comparison of the lifts of the wing in the presence of the body, $C_{L_{\alpha_{W(B)}}}$, and wing due to the body, $C_{L_{\alpha_{W(b)}}}$, with various theories as a function of aspect ratio.

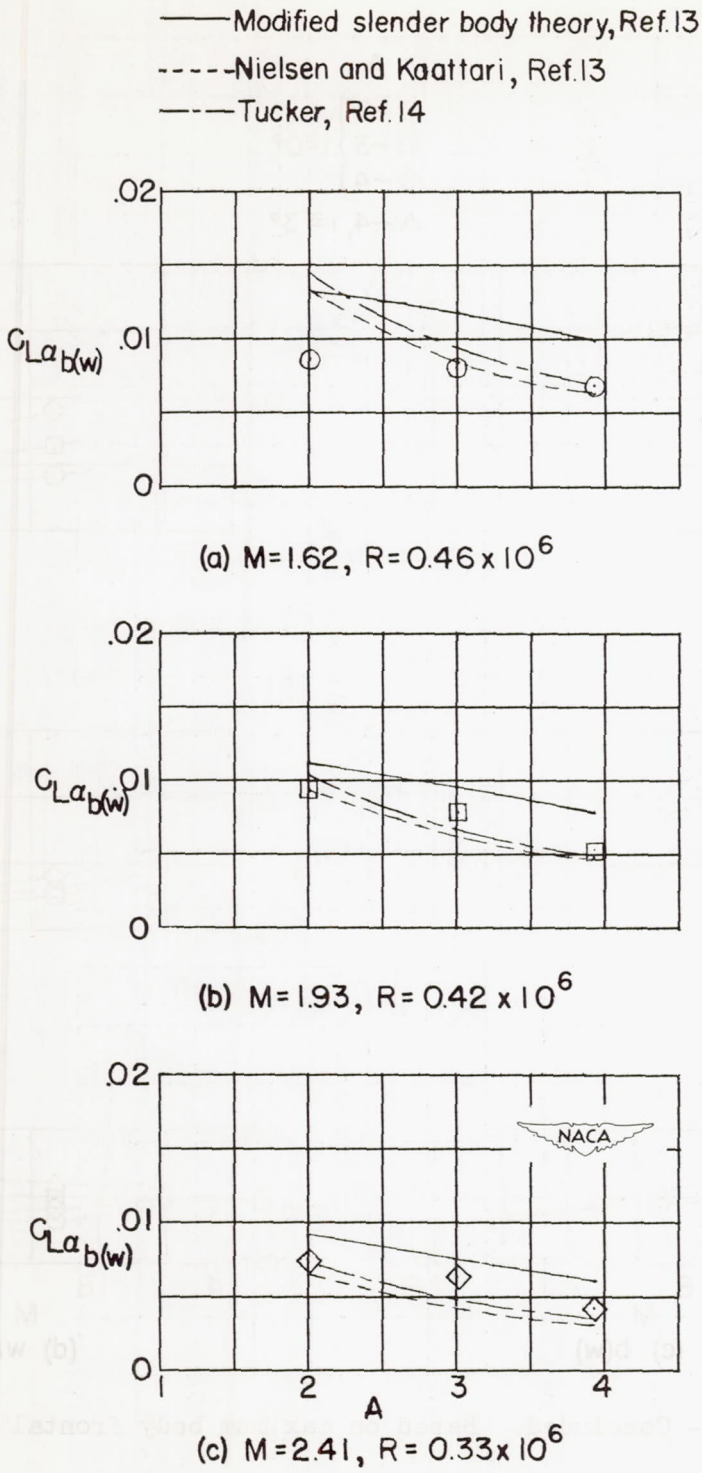

Figure 42.- Comparison of the lift of the body due to the wing, $C_{L_{\alpha_{b(w)}}}$, with various theories as a function of aspect ratio.

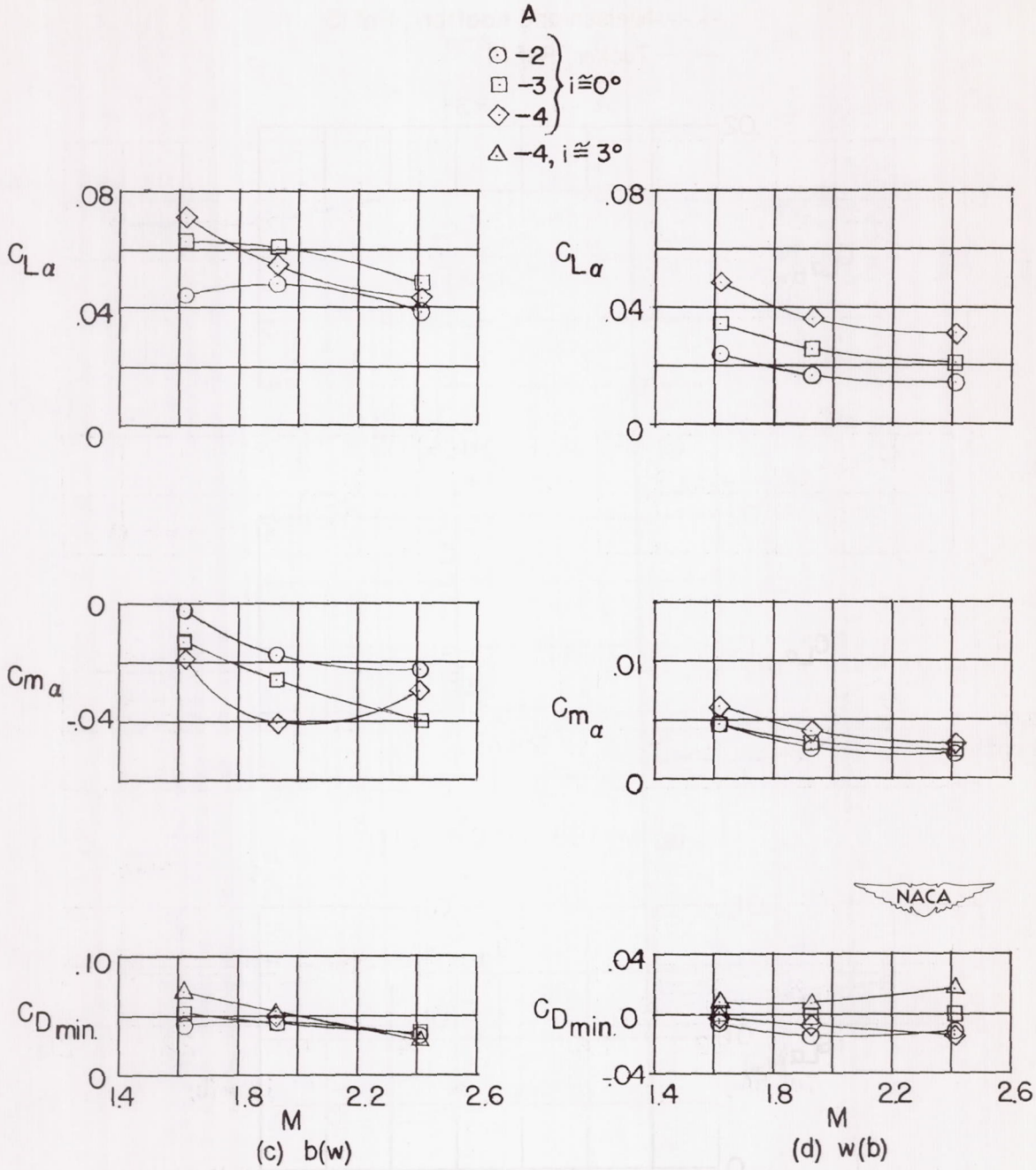

Figure 41.- Concluded. Based on maximum body frontal area.

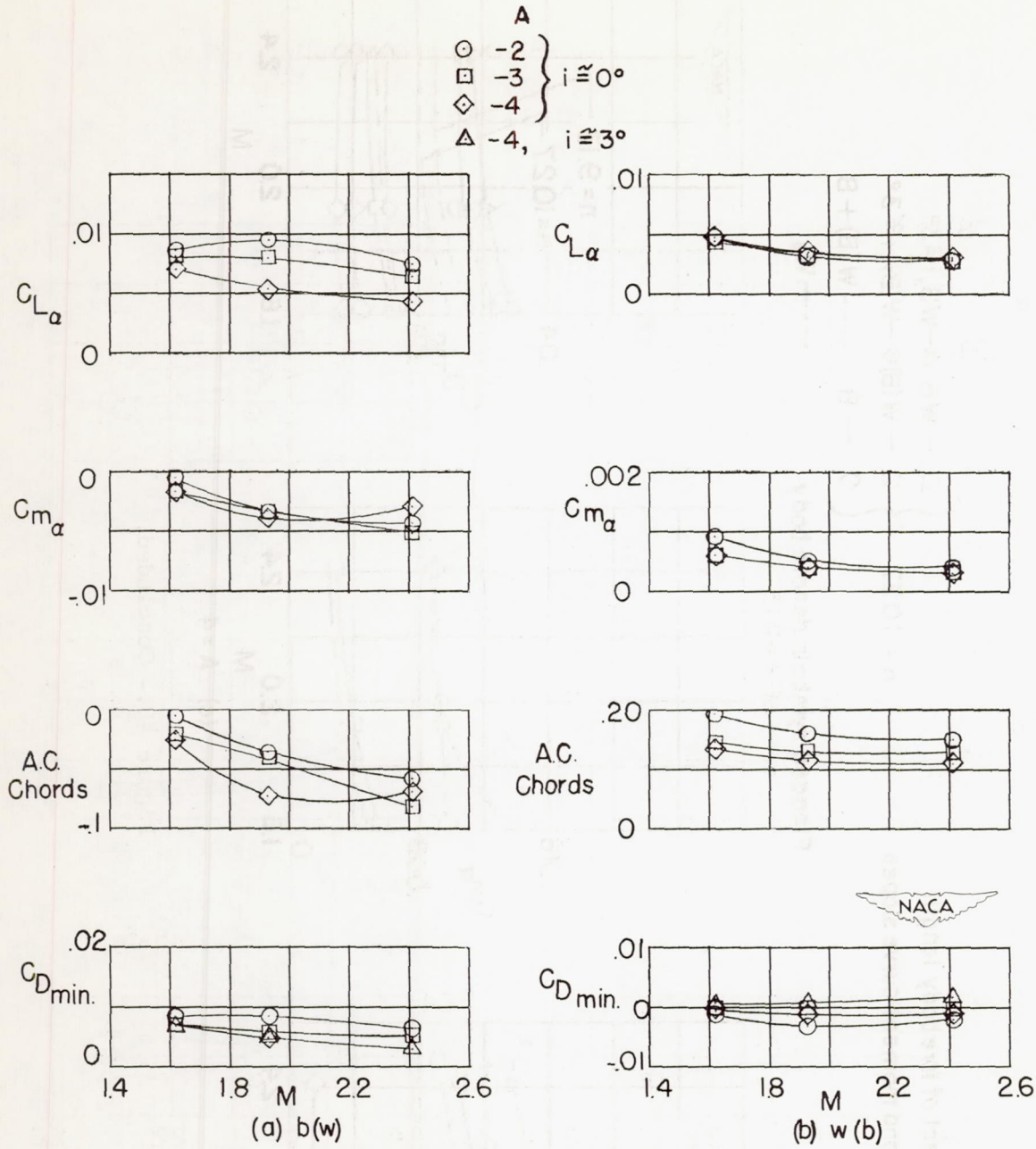

Figure 41.- Interference quantities as a function of Mach number for b(w) and w(b). Based on total wing area.

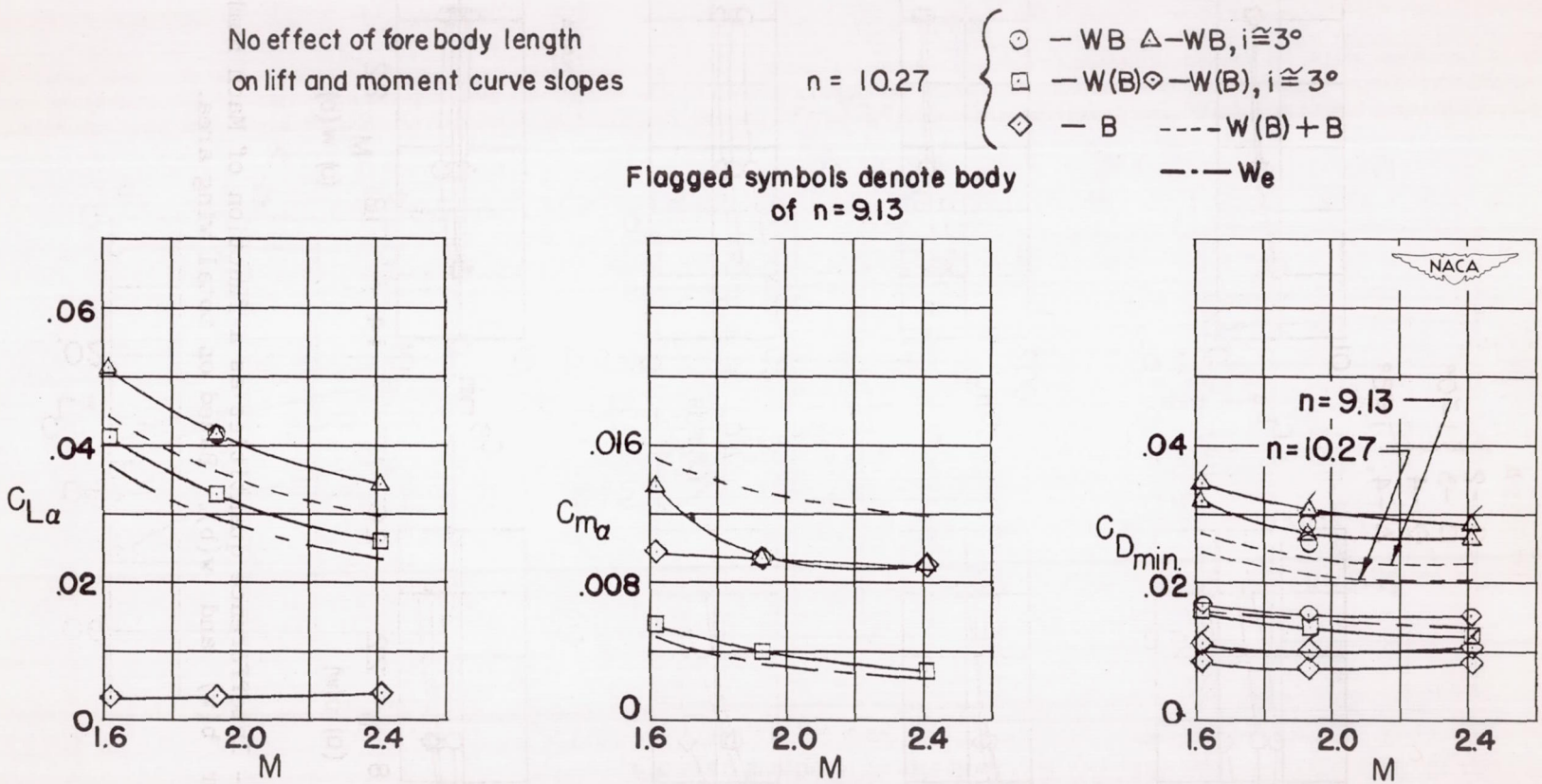

(c) A=4

Figure 40.- Concluded.

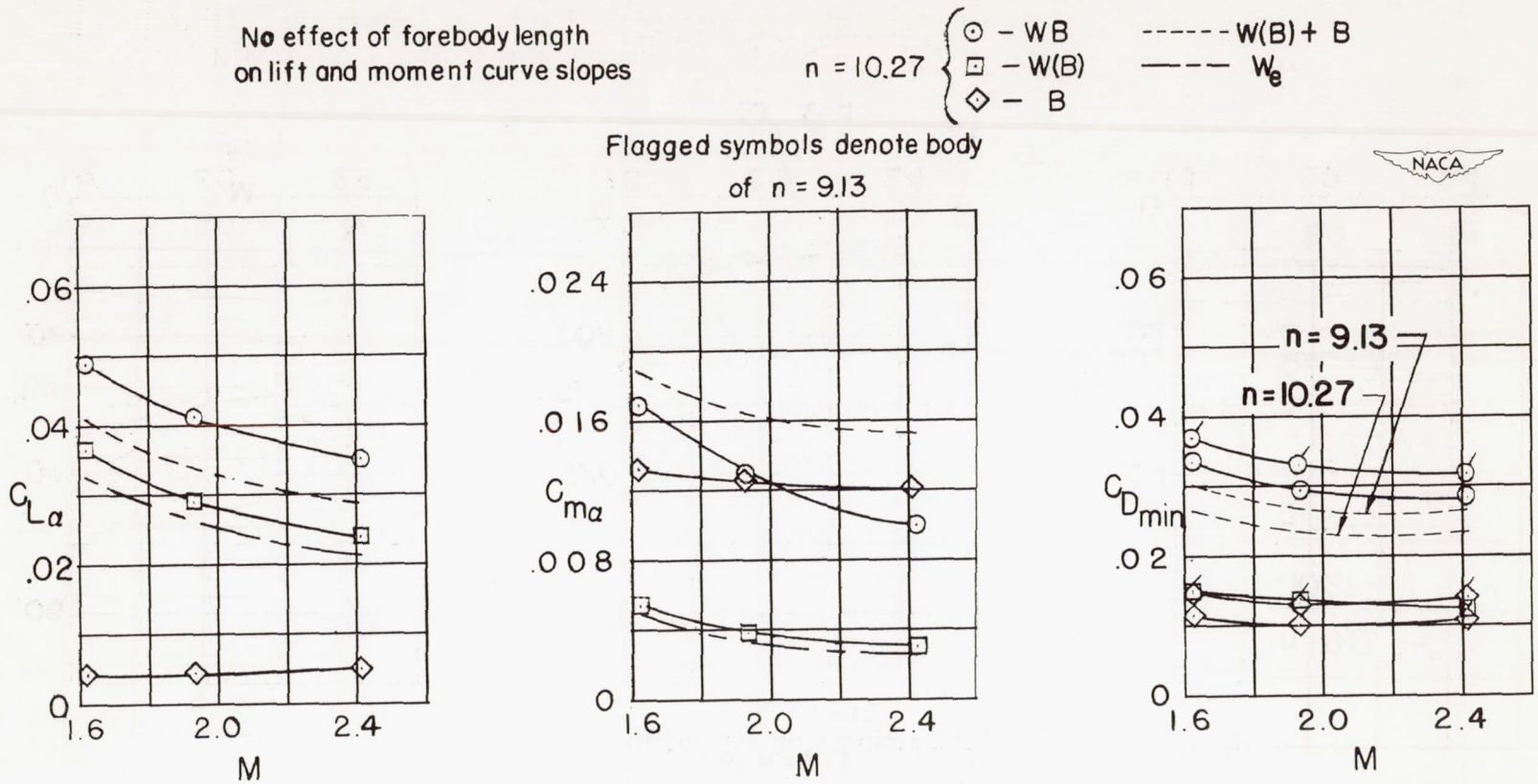

(b) A=3

Figure 40.- Continued.